QUANTIFYING AND CHARACTERIZING MICROPLASTICS IN DEEP-SEA SEDIMENT

Catherine Evelyn Wardinski

A Thesis submitted in partial satisfaction of the requirements
for the degree Master of Science

in

Marine Science

College of Natural and Computational Sciences

Hawai‘i Pacific University

May 2024

Honolulu, Hawaii

Advisory Committee:

Jennifer Lynch, Chair
Katherine Shaw
Meredith Seeley
Brenda Jensen

ABSTRACT

The ultimate fate and transport of plastics once they reach the environment are not well known, making it difficult to understand their impacts on marine ecosystems. The application of standardized and accurate methods to measure microplastics in deep-sea sediments is vital to comparing samples across oceans; gaining a more holistic understanding of the problem. This thesis reviews 16 past studies of microplastic analysis in sediment cores and found the studies to vary quite substantially in both methods used and reporting metrics, making it difficult to compare between studies. These recommendations served as guidelines for a sediment core analysis along an almost 800 km transect in the North Pacific. Using density separation and Py-GC/MS to identify polymers, there was a difference between the different sites, with locations closer to shore having more polymers detected than those offshore. These results allow us to start to understand how plastic moves through the marine ecosystem.

ACKNOWLEDGEMENTS

I would first like to thank my advisor, Dr. Jennifer Lynch, and my committee members Dr. Katherine Shaw, Dr. Meredith Seeley, and Dr. Brenda Jensen for their wonderful guidance and mentorship throughout this entire process. I have learned so much about becoming a great scientist thanks to you all. I also want to acknowledge the American Chemistry Council for funding this project. I want to thank Scripps Institute of Oceanography for giving me a once in a lifetime opportunity to sail in the Pacific Ocean and especially Dr. Richard Norris for his help and expertise while sampling out at sea. I also want to thank the University College of London for radiometric dating our samples. A special shout out also goes to the past and current members of the Center for Marine Debris Research who helped with both lab work and moral support throughout my entire project. I want to thank my fellow MSMS students who have encouraged me and supported my research every step of the way. Lastly, I want to acknowledge my friends and family back on the mainland, whose support I could feel halfway across the world.

TABLE OF CONTENTS

CHAPTER 1

A Review of Sediment Core Analyses for Microplastic Quantities and Types

1. INTRODUCTION

As plastic production and subsequent environmental pollution continue to increase, so will its effect on the environment. Plastic production has increased exponentially since the 1950s, reaching 359 million tons worldwide in 2019 (Brandon et al., 2019; PlasticsEurope, 2019). Since acknowledged as a problem in the 1970s, the effects of plastic pollution have been seen across all aspects of the marine environment in beaches, surface waters, and sediments ranging from the shore to the deep sea (Jambeck et al., 2015; Martin et al., 2022; Van Cauwenberghe et al., 2013). However, there is a disconnect between the amount of plastic produced and therefore estimated to enter the environment and the amount of plastic actually seen floating on the surface, highlighting a missing piece in our understanding of the fate of plastics in the environment (Andrady, 2011; Eriksen et al., 2014). And while there is also research into whether or not there is a missing sink of plastic, plastic pollution abundance is severely underestimated by only looking at what is floating on the surface of the water, with scientists predicting that only 0.2% of the plastic stock in the ocean can be accounted for by floating debris (Martin et al., 2022; Weiss et al., 2021). It is estimated that plastics sink because of differences in density or biological and physical processes. Some plastic polymers have a greater density than seawater, for example, polyvinyl chloride (PVC), and will sink due to these differences in densities (Table 1) (Andrady, 2011). However, even buoyant plastic polymers can sink through processes such as biofouling, degradation, ingestion/excretion by organisms, marine snow, and other physical methods of transport (Brignac et al., 2019; Galgani et al., 2022; Lebreton et al., 2019; Martin et al., 2022).

Table 1: Densities of common plastic polymers & density-separation chemicals. Density separation chemicals are highlighted gray and seawater is highlighted blue. Original concept based on a table from Brignac et al., 2019.

Polymer/Chemical	Density (g/mL or g/cm^3)	Reference
Polypropylene (PP)	0.83-0.90	(Andrady, 2011; Scientific Polymer Products, n.d.)
Canola Oil	0.914-0.917	(Eskin & Przybylski, 2003)
Low-density polyethylene (LDPE)	0.91-0.93	(Andrady, 2011; Scientific Polymer Products, n.d.)
High-density polyethylene (HDPE)	0.94-0.95	(Andrady, 2011; Scientific Polymer Products, n.d.)
Seawater	1.025	(Andrady, 2011)
Acrylonitrile Butadiene Styrene (ABS)	1.04-1.08	(Enders et al., 2015)
Polystyrene (PS)	1.05	(Andrady, 2011; Scientific Polymer Products, n.d.)
Polyester (PEST)	1.10-1.40	(Enders et al., 2015)
Nylon/Polyamide (PA)	1.12-1.15	(Enders et al., 2015)
Crumb Rubber (CR)	1.13-1.16	(Rhodes et al., 2012)
Polymethylmethacrylate (PMMA)	1.16-1.20	(Enders et al., 2015)
Polyacrylonitrile (PAN)	1.18	(Scientific Polymer Products, n.d.)
Saturated Sodium Chloride	1.2	(Zhang et al., 2020)
Polycarbonate (PC)	1.20-1.22	(Enders et al., 2015; Scientific Polymer Products, n.d.)
Polyurethane (PUR)	1.20-1.26	(Enders et al., 2015)
Cellulose Acetate (CA)	1.31	(Scientific Polymer Products, n.d.)
Zinc Chloride	1.37	(Kukkola et al., 2022)
Polyethylene Terephthalate (PET)	1.37-1.41	(Andrady, 2011; Enders et al., 2015; Scientific Polymer Products, n.d.)
Polyvinyl Chloride (PVC)	1.38-1.40	(Andrady, 2011; Scientific Polymer Products, n.d.)
Calcium Chloride	1.40	(Li et al., 2020)
Sodium Iodide	1.6-1.8	(Matsuguma et al., 2017; Willis et al., 2017)
Sodium Polytungstate	1.6-2.0	(Cunningham et al., 2020; Shaw et al., 2023)
Potassium Iodide	1.7	(Zhang et al., 2020)

One major theory for solving this potential missing piece is that the sinking plastics are concentrated in sediments, which serve as an environmental sink (Martin et al., 2022; Olivelli et

al., 2020; Woodall et al., 2014). This would not be uncommon, as sediments serve as sinks for other compounds in the ocean (Chiaia-Hernández et al., 2022). Typically this concept involves microplastics, defined as plastics smaller than 5 mm along the longest dimension, which pose a unique set of issues due to their small size (Andrady, 2011). Benthic organisms, including filter feeders and other lower trophic level organisms, inhabit these sediments and interact with the accumulated plastic (Graham & Thompson, 2009). Increasing our understanding of this vertical mode of plastic transport is incredibly important in determining the fate and biological impacts of plastic pollution. To date, studies quantifying microplastics in sediments vary widely in approach and analysis methods leading to difficulties in comparing results.

Previously, sediment studies have focused on the presence/absence of plastics by only looking at the top sections of sediments or homogenizing the entire sample. While these observations provide important information about the spatial distribution and current quantities of marine plastics in sediments, they do not address the larger trend over time or take into account seasonal variability. Researchers are now shifting to the collection of sediment cores because of the potential to see the vertical distribution of plastics with sediment depth. By combining the vertical measurements with known sedimentation rates for the area, scientists are now able to describe both the spatial distribution (by collecting cores across sites) and the rate of plastic deposition over time.

The goal of this literature review is to compare studies of microplastics in marine sediments, with a focus on the vertical distribution in sediment cores, and examine the implications for plastic transport. Based on the outcomes, recommendations for sediment analysis projects will be included to increase standardization in the future.

2. REVIEW OF SEDIMENT CORES STUDIES

This review covers 16 studies that used sediment cores for microplastic analysis, which can be collected at any ocean depth, to sample a variety of habitats from the shoreline to the deep ocean (Figure 1; Table 2). Sediment cores hollow out a section of the sediment, and can be subdivided to sample a range of depths. By using a dating method or calculating the average sedimentation rate researchers can determine the ages of the sediment throughout the core. Once the cores are separated horizontally into different sections by depth, scientists can determine how plastic concentrations change over time. Below are the locations, methods, and results from the studies included in this literature review and provide recommendations for future research.

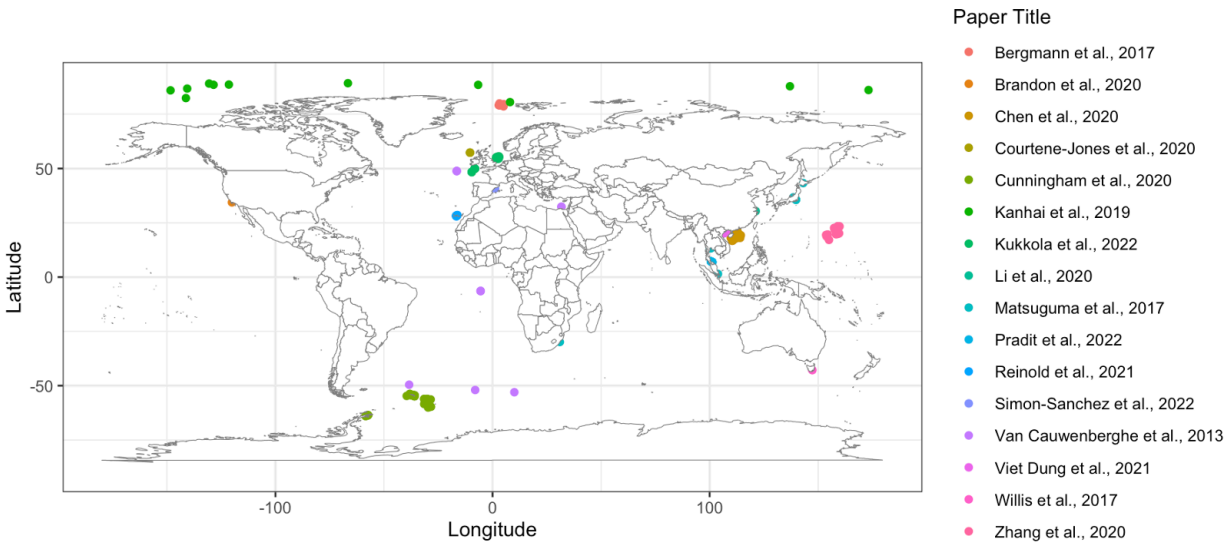

Figure 1: A world map depicting the sediment core locations from 16 studies reviewed in this chapter.

2.1 Study Locations

There was a wide range of locations within this group of studies as sediment cores were collected from inland canals (Matsuguma et al., 2017) to the Arctic deep sea (Bergmann et al., 2017). The most common area of study was the open ocean which accounted for 33% (6/18) of

the studies, followed by the coastal environments 28% (5/18), which included the continental shelf. The remaining locations had typically only 1-2 studies per environment type (Table 2).

Table 2: The environment types from the 16 sediment core studies that were analyzed for this review. The sum of the number of studies column does not equal 16, because some studies included multiple environment types.

Environment Type	Number of Studies	Reference
Open Ocean	6	Bergmann et al., 2017; Courtene-Jones et al., 2020; Cunningham et al., 2020; Kanhai et al., 2019; Van Cauwenberghe et al., 2013; Zhang et al., 2020
Coastal Waters	5	Brandon et al., 2019; Chen et al., 2020; Kukkola et al., 2022; Matsuguma et al., 2017; Simon-Sánchez et al., 2022
Salt Marsh/Estuary	2	Li et al., 2020; Willis et al., 2017
Mangroves	2	Pradit et al., 2022; Viet Dung et al., 2021
Beach	1	Reinold et al., 2021
Lake	1	Matsuguma et al., 2017
Canal/Moat	1	Matsuguma et al., 2017

2.2 Study Methods

When analyzing microplastics in sediment cores, the methodology usually involves four major steps: Collection, Cutting & Dating, Isolating Plastics, and Analysis. There is quite a variety of approaches within each step of the process, with some studies skipping steps altogether. This review will address these four different steps sequentially, mirroring the research flow pictured in Figure 2.

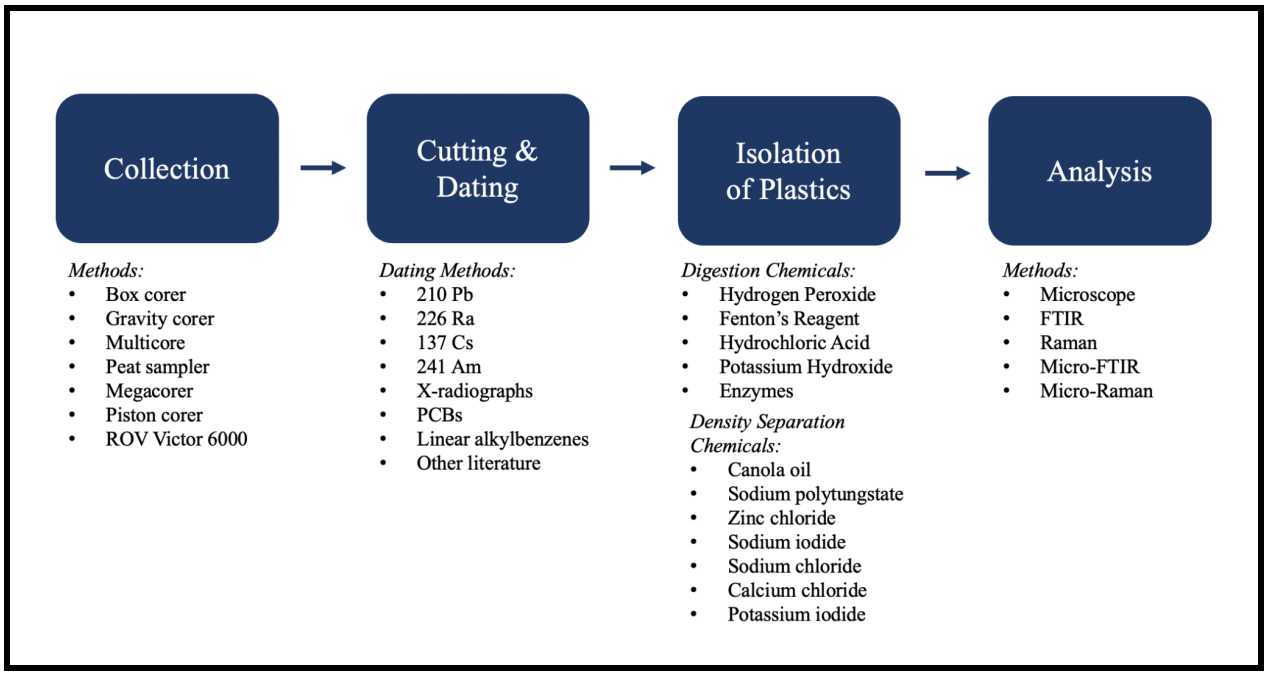

Figure 2: A flowchart listing the four major steps in sediment core analysis and illustrating the diverse methods used in each step

The first step in analyzing sediment cores for plastics is to collect the core itself using a variety of corer types including a gravity corer, a multicorer, or even a peat sampler. The goal of using these devices is to extract a column of sediment from the sampling location. No comparison among devices has suggested that a certain type of corer works better than another, in terms of sample collection, rather the type of material comprising the corer is more important. Many of the corer types listed above are made out of or use a liner made with plastic such as PVC, which can end up contaminating the core sample. To avoid a contamination issue, it is essential that modifications be made or extra precautions are used. For example, Viet Dung et al. 2021, sliced off the outer layer (0.5 cm) of each of their cores to eliminate potential contamination from their PVC peat corer. Brandon et al., 2019 also documented that they believed there was contamination of their samples from their core liner based on the fact that they detected plastic in layers that predated the mass production of plastics (pre-1950s). Chen et al. 2020 used a PVC pushcorer but found no evidence of contamination from the corer in their

samples. Although the exact amount of contamination from using a plastic corer is up for debate, the best solution is to avoid using any type of plastic. Alterations can be made to prevent contamination, for example using metal core tubes, but typically this can be at the expense of the sample collected (Tsuchiya et al., 2019).

Once the sediment cores have been collected, the second major step of the process is to separate the sediment core into manageable sections and to determine the relative date of the sediment being sampled. By separating the core into smaller sections, it becomes easier for scientists to extract plastics because the amount of organic material has decreased. The studies reviewed here sliced the cores in many different ways ranging from every 0.5 cm to every 15 cm (Brandon et al., 2019; Viet Dung et al., 2021). The key to slicing the cores is to maintain the original layers from the column, typically by keeping the core upright when slicing. The smaller the sections, the higher the resolution is for sediment aging because the smaller intervals allow for more precision. Studies have used different methods to calculate the age of the sediment, which aids in understanding the trend over time.

Sediment dating is a process that has been used outside of this context for many years and is now being applied to plastics research for scientists to understand how deposition rates change over time (Uddin et al., 2021). Methods can range from using past sedimentation rates found in the literature to using radioactive half-lives to determine the age of the sediment. By using an established dating technique, scientists can account for the variability in sedimentation rates that a constant calculated rate would not be able to do. Out of the studies mentioned above, ^{210}Pb is the most common and recommended method, but other studies suggest using multiple methods to acquire a more accurate concept of how the layers are dated (Uddin et al., 2021).

After the cores have been sectioned, the third major step in sediment core analysis is to isolate the plastics from the sediments themselves. Isolation of plastics can either be done using chemical or enzymatic digestion to get rid of the organic material or using the density difference between the sediment and the plastics to separate the two. Some of the studies reviewed here used both of these methods in conjunction (Bergmann et al., 2017; Cunningham et al., 2020; Li et al., 2020; Matsuguma et al., 2017; Reinold et al., 2021; Simon-Sánchez et al., 2022; Viet Dung et al., 2021; Willis et al., 2017; Zhang et al., 2020) while others just chose to do one or the other. Overall, there was a wide range of chemicals chosen for this step, with combinations varying greatly across studies (Figure 2). When selecting a chemical for digestion, it is important to avoid using a chemical that can degrade the plastics themselves along with the organic material (Prata et al., 2019). When choosing a chemical for density separation, it is extremely important to select a chemical that has a higher density than all types of plastics potentially being observed so that the plastic polymers will float to the surface (Prata et al., 2019)(Table 1).

Finally, the last step in sediment core analysis is to analyze the plastics and identify the polymers found. Almost all (94%, 15/16) studies used some sort of polymer identification method for at least a subset of their findings. Polymer identification is important as it validates the number of pieces predicted to be plastics based on preliminary analysis. Many studies began by looking at the samples under the microscope which leads to bias in particles separated as potential plastics, as well as forcing a size detection limit on the study. FTIR and Raman, the two most common methods used in these studies, identify polymer types based on the spectra that are produced from shooting a laser at the potential plastic particle. There are slight differences between FTIR and Raman spectroscopy in how they analyze potential plastic particles, and it is best when scientists can use both in conjunction (Cabernard et al., 2018). However, the latter is

quite expensive and time-consuming, so it is highly encouraged for scientists to have at least one polymer identification method.

Overall, the methodology for measuring plastic pollution in sediment cores is extremely variable and inconsistent. This makes it extremely difficult to compare the number of plastics found in different studies. While all the studies reviewed here follow the four general steps, there can be unique ways of getting there. This is further highlighted in Figure 3, which demonstrates how even studies that sample a similar sediment type (open ocean) can have widely different methodologies. Step 1 (Collection) and Step 4 (Analysis) seem to be the most consistent steps across the studies, while Step 2 (Slicing & Dating) and Step 3 (Isolation of Plastic) tend to be the most variable. A key step for future research is to work on creating a standardized protocol which will then allow for future comparisons across studies. This will be further explored in the Recommendations section of this review.

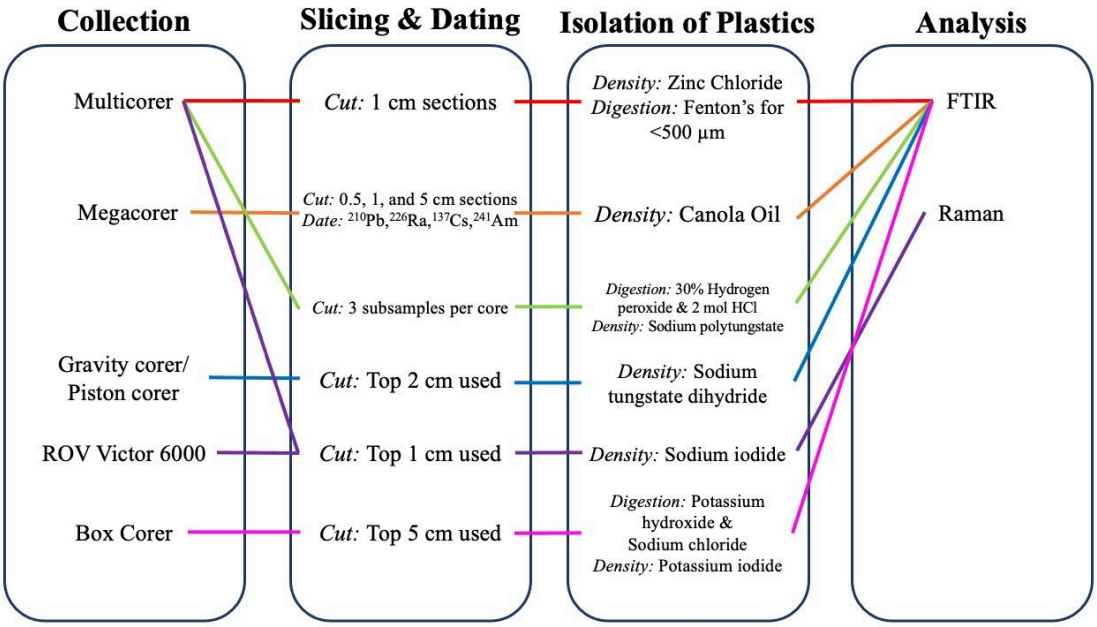

Figure 3: The six open ocean study methodologies compared across the four major steps, highlighting the variety in sampling methodology

Study Results

The results of the 16 studies varied greatly in terms of reporting units and values found in the respective environments (Table 3). While not every single sediment core had plastic, all studies reviewed found evidence of microplastics in at least one of their samples. Table 3 shows the microplastics found as described in the paper: sometimes it was the range of particles seen across multiple sediment cores or sometimes it was the mean plus or minus the standard deviation. The average of particles also tended to have a range which was reported here if applicable. Reporting units ranged from particle number (per sediment weight or volume), particle mass (per sediment weight), and particle deposition rate (per area * year). While sediment weight was the most common denominator, not all studies specified if the sediment weight used was wet or dry. Some studies did include other information about the sediment

including grain size, however this was not common. The most common reporting unit was the number of particles divided by kg of dry sediment. The only study to report both particle number and mass of particles per dry weight of sediment was Simon-Sánchez et al., 2022. This range of reporting units as well as the varying size classes makes it difficult to compare studies against one another. While all the studies were chosen for this review because they targeted microplastics, some upper size limits went beyond the commonly used definition of a microplastic (less than 5 mm) (Andrady, 2011). Again, methods aside, the lack of consistent size classes makes it impossible to compare one against another. Most studies also separated their plastics into separate size classes, but again the ranges included also varied widely and some were very specific to the study at hand. Almost 94% (15/16, 93.7%) specified what types of plastics were looked at in their respective studies, with all studies including fragments (some broke it up into even smaller groups such as foams & films), but not all including fibers. A few of the many polymers reported throughout the studies included: PE, PP, PS, PVC, PET, PUR, PEST, Nylon, ABS, PAN, rayon, nitrile rubber, and acrylic.

Table 3: Results from the Sediment Core Studies

Reference	Location	Microplastics	Reported Units	Types of Plastic Included	Plastic Size Range
Bergmann et al., 2017	Hausgarten Observatory	total avg. 4,356 ± 675	particles/kg sediment	All but NO Fibers	11 µm - 500 um AND > 500 µm
Brandon et al., 2019	Santa Barbara Basin	NA, rate over time	particles/100cm^2 *yr	Fibers, Fragments, Films, Quasi-Spherical	104 µm - > 9000 µm
Chen et al., 2020	South China Sea	avg. 34 - 224	pieces/kg dry weight	Didn't report	Didn't report
Courtene-Jones et al., 2020	Rockall Trough	avg. 0.197 ± 0.129 (top 0.5 cm, highest rate overall)	MP/g dry weight	Fibers, Fragments, Films	0.06 mm - > 12 mm
Cunningham et al., 2020	Antarctica & Southern Ocean	avg. 1.04 ± 0.39 - 1.30 ± 0.51	MP/g sediment	Fibers, Fragments, Films	Didn't report
Kanhai et al., 2019	Arctic Central Basin	total: 9	particles from all samples	Fibers & Fragments	> 100 µm
Kukkola et al., 2022	UK Continental Shelf & Slope	avg. 1050 - 2700	microplastics/g dry weight	All (Including Fibers)	> 10 µm
Li et al., 2020	Andong Salt Marsh, China	avg. 13.2 ± 6.0	items/50 g dry weight of sediment	Fibers, Fragments, Films, Pellets	100 µm - 5 mm
Matsuguma et al., 2017	Asia & Africa	range: 100 - 1900 (surface sediment)	pieces/kg dry sediment	Fibers, Fragments, Films, Beads	315 µm - 5 mm
Pradit et al., 2022	Thailand Mangrove Forests	range 106 - 413	items/kg dry weight	Fibers, Fragments, Films	< 5 mm
Reinold et al., 2021	Canary Island, Spain	avg: 1.30 - 130.64	items/L	Fibers, Fragments, Films, Lines, Pellets	25 µm - 2 cm
Simon-Sánchez et al., 2022	Balearic Sea	range: 706-6939 range: 0.05-1.43	items/kg dry weight mg/kg dry weight	Fibers & Fragments	11 - 1,000 µm
Van Cauwenberghe et al., 2013	Atlantic Ocean & Mediterranean Sea	avg. 0.5	microplastics/25 cm^2	No Fibers	75 - 161 µm (length), 44 - 137 µm (width)
Viet Dung et al., 2021	Vietnam Mangrove Forests	range: 0 - 4941	particles/kg	Fibers, Fragments, Films, Foams	0.3 - 5 mm
Willis et al., 2017	Derwent Estuary, Australia	avg. 2.43 - 4.2	fragments/g	Fibers, Fragments, Sheets, Beads	< 63 µm - > 4 mm
Zhang et al., 2020	Western Pacific Ocean	total avg. 240	items/kg dry weight sediment	Fibers, Fragments, Films	100.1 µm - 4930.1 µm

3. RECOMMENDATIONS

Based on the studies reviewed here we can conclude that ocean sediments contain plastic debris. However, due to the lack of consistency in the methods & reporting standards, it is extremely difficult to determine which ocean areas sampled contain more plastic than others. It is of utmost importance to develop a standard methodology protocol and reporting guidelines for the research community to follow.

When deciding on methodology four main factors should be taken into consideration: (1) reduction of contamination overall, especially on the sampling vessel and with the corer chosen, (2) slicing & dating the cores with the highest resolution possible, (3) selecting a proper digestion or density-separation chemical that will not harm the plastics or be too light (density-wise), and (4) using a polymer identification method (FTIR or Raman or both) for all samples rather than merely analyzing a subset selected by the researcher. Ensuring that each of these steps is completed will allow for better cross-study comparisons. To this end, method sections should contain all of the information listed in the checklist from Cowger et al., 2020. We can only start comparing sediment plastic concentrations worldwide once we have established methods following these recommendations.

Having consistent methods will not be effective unless we establish consistent reporting guidelines, which was emphasized by two previous review papers as well (Harris, 2020; Uddin et al., 2021). Results are displayed as both particles/sediment weight or weight of plastics/sediment weight in recent literature. Both ways provide different perspectives on the data; for example, the number of particles can be altered during the analysis process, while the total weight can be skewed by having large or small pieces. It is also vital that studies provide dry weights of sediments in order to create more standardization across the field. When analyzing sediment

cores two major questions can be answered: the total amount of plastic in the core and the trend in plastic over time. As studies shift to chronologically documenting trends over time, it is important to maintain a consistent reporting guideline on how these plastics are measured over time. Dating becomes extremely important since, without knowledge of sediment age, we cannot understand how plastic deposition rates change over time. Moreover, it is recommended that studies analyze the entire core they collect, rather than specific sections, to ensure that a long time scale is being accounted for. This is also important when determining the resolution of the data if looking at the abundance of plastics in the entire core. A sediment core with a depth of 5 cm has a much different amount of plastic per gram compared to a 25 cm core, which may underestimate plastic density by including pre-plastic age sediments. It is also essential to describe the full-size range of plastics (both upper and lower limits) that were included. It has been documented in previous literature that a majority of the plastics in sediment cores tend to be quite small. For example, Zhang et al., 2020 determined that 90% of the plastics they found were less than 1 mm. Different methodologies can lead to different lower detection limits, and readers need to understand the detection limit used in the study to compare it against their work. This limitation also applies to the types of plastics accounted for, as many studies chose to eliminate fibers from their study and only report fragments. Fibers have been proven to be difficult to analyze due to their odd shape and size, however have been reported in deep-sea sediment (Woodall et al., 2014). Thus, only publishing the numbers without providing the proper context of the types sampled and how they were sampled leaves gaps for comparisons across the board.

Revisiting the goal of this review, it can be concluded that the questions scientists can answer by using sediment cores are extremely important in understanding the fate and transport of plastic in the ocean. While we can't make cross-ocean comparisons yet due to the variable

methods, we can focus on maintaining consistency in both our methods and reporting guidelines to facilitate future comparisons across space and time. Sediment cores allow us to create a record of plastic pollution in the marine environment from pre-1950 (before the mass production of plastics) to the present and by using the recommendations provided in this review, scientists will be able to understand how plastic deposition rates change through time in a variety of ocean environments.

REFERENCES

Andrady, A. L. (2011). Microplastics in the marine environment. *Marine Pollution Bulletin*, *62*(8), 1596–1605. https://doi.org/10.1016/j.marpolbul.2011.05.030

Bergmann, M., Wirzberger, V., Krumpen, T., Lorenz, C., Primpke, S., Tekman, M. B., & Gerdts, G. (2017). High Quantities of Microplastic in Arctic Deep-Sea Sediments from the HAUSGARTEN Observatory. *Environmental Science & Technology*, *51*(19), 11000–11010. https://doi.org/10.1021/acs.est.7b03331

Brandon, J. A., Jones, W., & Ohman, M. D. (2019). Multidecadal increase in plastic particles in coastal ocean sediments. *Science Advances*, *5*(9), eaax0587. https://doi.org/10.1126/sciadv.aax0587

Brignac, K. C., Jung, M. R., King, C., Royer, S.-J., Blickley, L., Lamson, M. R., Potemra, J. T., & Lynch, J. M. (2019). Marine Debris Polymers on Main Hawaiian Island Beaches, Sea Surface, and Seafloor. *Environmental Science & Technology*, *53*(21), 12218–12226. https://doi.org/10.1021/acs.est.9b03561

Cabernard, L., Roscher, L., Lorenz, C., Gerdts, G., & Primpke, S. (2018). Comparison of Raman and Fourier Transform Infrared Spectroscopy for the Quantification of Microplastics in the Aquatic Environment. *Environmental Science & Technology*, *52*(22), 13279–13288. https://doi.org/10.1021/acs.est.8b03438

Chiaia-Hernández, A. C., Casado-Martinez, C., Lara-Martin, P., & Bucheli, T. D. (2022). Sediments: Sink, archive, and source of contaminants. *Environmental Science and Pollution Research*, *29*(57), 85761–85765. https://doi.org/10.1007/s11356-022-24041-1

Chen, M., Du, M., Jin, A., Chen, S., Dasgupta, S., Li, J., Xu, H., Ta, K., & Peng, X. (2020). Forty-year pollution history of microplastics in the largest marginal sea of the western Pacific. *Geochemical Perspectives Letters*, 42–47. https://doi.org/10.7185/geochemlet.2012

Courtene-Jones, W., Quinn, B., Ewins, C., Gary, S. F., & Narayanaswamy, B. E. (2020). Microplastic accumulation in deep-sea sediments from the Rockall Trough. *Marine Pollution Bulletin*, *154*, 111092. https://doi.org/10.1016/j.marpolbul.2020.111092

Cowger, W., Booth, A. M., Hamilton, B. M., Thaysen, C., Primpke, S., Munno, K., Lusher, A. L., Dehaut, A., Vaz, V. P., Liboiron, M., Devriese, L. I., Hermabessiere, L., Rochman, C., Athey, S. N., Lynch, J. M., De Frond, H., Gray, A., Jones, O. A. H., Brander, S., … Nel, H. (2020). Reporting Guidelines to Increase the Reproducibility and Comparability of Research on Microplastics. *Applied Spectroscopy*, *74*(9), 1066–1077. https://doi.org/10.1177/0003702820930292

Cunningham, E. M., Ehlers, S. M., Dick, J. T. A., Sigwart, J. D., Linse, K., Dick, J. J., & Kiriakoulakis, K. (2020). High Abundances of Microplastic Pollution in Deep-Sea Sediments: Evidence from Antarctica and the Southern Ocean. *Environmental Science & Technology*, *54*(21), 13661–13671. https://doi.org/10.1021/acs.est.0c03441

Enders, K., Lenz, R., Stedmon, C. A., & Nielsen, T. G. (2015). Abundance, size and polymer composition of marine microplastics ≥ 10 μm in the Atlantic Ocean and their modelled vertical distribution. *Marine Pollution Bulletin*, *100*(1), 70–81. https://doi.org/10.1016/j.marpolbul.2015.09.027

Eskin, N. A. M., & Przybylski, R. (2003). RAPE SEED OIL/CANOLA. In B. Caballero (Ed.), *Encyclopedia of Food Sciences and Nutrition (Second Edition)* (pp. 4911–4916). Academic Press. https://doi.org/10.1016/B0-12-227055-X/01349-3

Galgani, L., Goßmann, I., Scholz-Böttcher, B., Jiang, X., Liu, Z., Scheidemann, L., Schlundt, C., & Engel, A. (2022). Hitchhiking into the Deep: How Microplastic Particles are Exported through the Biological Carbon Pump in the North Atlantic Ocean. *Environmental Science & Technology*, *56*(22), 15638–15649. https://doi.org/10.1021/acs.est.2c04712

Graham, E. R., & Thompson, J. T. (2009). Deposit- and suspension-feeding sea cucumbers (Echinodermata) ingest plastic fragments. *Journal of Experimental Marine Biology and Ecology*, *368*(1), 22–29. https://doi.org/10.1016/j.jembe.2008.09.007

Harris, P. T. (2020). The fate of microplastic in marine sedimentary environments: A review and synthesis. *Marine Pollution Bulletin*, *158*, 111398. https://doi.org/10.1016/j.marpolbul.2020.111398

Jambeck, J. R., Geyer, R., Wilcox, C., Siegler, T. R., Perryman, M., Andrady, A., Narayan, R., & Law, K. L. (2015). Plastic waste inputs from land into the ocean. *Science*, *347*(6223), 768–771. https://doi.org/10.1126/science.1260352

Kanhai, L. D. K., Johansson, C., Frias, J. P. G. L., Gardfeldt, K., Thompson, R. C., & O'Connor, I. (2019). Deep sea sediments of the Arctic Central Basin: A potential sink for microplastics. *Deep Sea Research Part I: Oceanographic Research Papers*, *145*, 137–142. https://doi.org/10.1016/j.dsr.2019.03.003

Kukkola, A. T., Senior, G., Maes, T., Silburn, B., Bakir, A., Kröger, S., & Mayes, A. G. (2022). A large-scale study of microplastic abundance in sediment cores from the UK continental shelf and slope. *Marine Pollution Bulletin*, *178*, 113554. https://doi.org/10.1016/j.marpolbul.2022.113554

Lebreton, L., Egger, M., & Slat, B. (2019). A global mass budget for positively buoyant macroplastic debris in the ocean. *Scientific Reports*, *9*(1), 12922. https://doi.org/10.1038/s41598-019-49413-5

Li, J., Huang, W., Xu, Y., Jin, A., Zhang, D., & Zhang, C. (2020). Microplastics in sediment cores as indicators of temporal trends in microplastic pollution in Andong salt marsh, Hangzhou Bay, China. *Regional Studies in Marine Science*, *35*, 101149. https://doi.org/10.1016/j.rsma.2020.101149

Martin, C., Young, C. A., Valluzzi, L., & Duarte, C. M. (2022). Ocean sediments as the global sink for marine micro‐ and mesoplastics. *Limnology and Oceanography Letters*, *7*(3), 235–243. https://doi.org/10.1002/lol2.10257

Matsuguma, Y., Takada, H., Kumata, H., Kanke, H., Sakurai, S., Suzuki, T., Itoh, M., Okazaki, Y., Boonyatumanond, R., Zakaria, M. P., Weerts, S., & Newman, B. (2017). Microplastics in Sediment Cores from Asia and Africa as Indicators of Temporal Trends in Plastic Pollution. *Archives of Environmental Contamination and Toxicology*, *73*(2), 230–239. https://doi.org/10.1007/s00244-017-0414-9

Olivelli, A., Hardesty, B. D., & Wilcox, C. (2020). Coastal margins and backshores represent a major sink for marine debris: Insights from a continental-scale analysis. *Environmental Research Letters*, *15*(7), 074037. https://doi.org/10.1088/1748-9326/ab7836

PlasticsEurope. (2019). *Plastics- the facts 2019*.

Pradit, S., Noppradit, P., Loh, P.-S., Nitiratsuwan, T., Le, T. P. Q., Oeurng, C., Mohamed, C. A. R., Lee, C. W., Lu, X., Anshari, G. Z., Kandasamy, S., & Wang, J. (2022). The Occurrence of Microplastics in Sediment Cores from Two Mangrove Areas in Southern Thailand. *Journal of Marine Science and Engineering*, *10*(3), 418. https://doi.org/10.3390/jmse10030418

Prata, J. C., da Costa, J. P., Duarte, A. C., & Rocha-Santos, T. (2019). Methods for sampling and detection of microplastics in water and sediment: A critical review. *TrAC Trends in Analytical Chemistry*, *110*, 150–159. https://doi.org/10.1016/j.trac.2018.10.029

Reinold, S., Herrera, A., Stile, N., Saliu, F., Hernández-González, C., Martinez, I., Ortega, Z., Marrero, M. D., Lasagni, M., & Gómez, M. (2021). An annual study on plastic accumulation in surface water and sediment cores from the coastline of Tenerife (Canary Island, Spain). *Marine Pollution Bulletin*, *173*, 113072. https://doi.org/10.1016/j.marpolbul.2021.113072

Rhodes, E. P., Ren, Z., & Mays, D. C. (2012). Zinc Leaching from Tire Crumb Rubber. *Environmental Science & Technology*, *46*(23), 12856–12863. https://doi.org/10.1021/es3024379

Scientific Polymer Products. (n.d.). *Density of Polymers (By Density)*. Scientific Polymer Products Inc. http://scipoly.com/density-of-polymers-by-density/

Shaw, K., Sandquist, R., & Lynch, J. M. (2023). *Report of Analysis: Separation of microplastics from sediment using a novel density separation device*.

Simon-Sánchez, L., Grelaud, M., Lorenz, C., Garcia-Orellana, J., Vianello, A., Liu, F., Vollertsen, J., & Ziveri, P. (2022). Can a Sediment Core Reveal the Plastic Age? Microplastic Preservation in a Coastal Sedimentary Record. *Environmental Science & Technology*, *56*(23), 16780–16788. https://doi.org/10.1021/acs.est.2c04264

Tsuchiya, M., Nomaki, H., Kitahashi, T., Nakajima, R., & Fujikura, K. (2019). Sediment sampling with a core sampler equipped with aluminum tubes and an onboard processing protocol to avoid plastic contamination. *MethodsX*, *6*, 2662–2668. https://doi.org/10.1016/j.mex.2019.10.027

Uddin, S., Fowler, S. W., Uddin, Mohd. F., Behbehani, M., & Naji, A. (2021). A review of microplastic distribution in sediment profiles. *Marine Pollution Bulletin*, *163*, 111973. https://doi.org/10.1016/j.marpolbul.2021.111973

Van Cauwenberghe, L., Vanreusel, A., Mees, J., & Janssen, C. R. (2013). Microplastic pollution in deep-sea sediments. *Environmental Pollution*, *182*, 495–499. https://doi.org/10.1016/j.envpol.2013.08.013

Viet Dung, L., Huu Duc, T., Thi Khanh Linh, L., Thi Dieu Ly, T., Anh Duong, H., & Thi My Hao, N. (2021). Depth Profiles of Microplastics in Sediment Cores from Two Mangrove Forests in Northern Vietnam. *Journal of Marine Science and Engineering*, *9*(12), 1381. https://doi.org/10.3390/jmse9121381

Weiss, L., Ludwig, W., Heussner, S., Canals, M., Ghiglione, J.-F., Estournel, C., Constant, M., & Kerhervé, P. (2021). The missing ocean plastic sink: Gone with the rivers. *Science*, *373*(6550), 107–111. https://doi.org/10.1126/science.abe0290

Willis, K. A., Eriksen, R., Wilcox, C., & Hardesty, B. D. (2017). Microplastic Distribution at Different Sediment Depths in an Urban Estuary. *Frontiers in Marine Science*, *4*, 419. https://doi.org/10.3389/fmars.2017.00419

Woodall, L. C., Sanchez-Vidal, A., Canals, M., Paterson, G. L. J., Coppock, R., Sleight, V., Calafat, A., Rogers, A. D., Narayanaswamy, B. E., & Thompson, R. C. (2014). The deep sea is a major sink for microplastic debris. *Royal Society Open Science*, *1*(4), 140317. https://doi.org/10.1098/rsos.140317

Zhang, D., Liu, X., Huang, W., Li, J., Wang, C., Zhang, D., & Zhang, C. (2020). Microplastic pollution in deep-sea sediments and organisms of the Western Pacific Ocean. *Environmental Pollution*, *259*, 113948. https://doi.org/10.1016/j.envpol.2020.113948

CHAPTER 2

Quantifying Microplastic Mass in Deep-Sea Sediment Along a Transect in the North Pacific

1. INTRODUCTION

Plastic pollution is an ongoing and pervasive problem in the marine environment that continues to increase with the exponential production rates. Since the 1950s, worldwide production has continued to increase, reaching 359 million tons in 2019, leading to mismanaged waste which can end up in the environment (Jambeck et al., 2015; Plastics Europe, 2019). While many of the initial impacts of plastic pollution are reported in the literature, there lacks an overall understanding of the long-term fate of plastic once it enters the marine environment, which is vital in determining its prolonged effects.

Multiple models that calculated a global estimate for floating plastics have found that the North Pacific Ocean has the largest mass of floating plastic compared to the other oceans in the world (Cózar et al., 2014; Eriksen et al., 2014; van Sebille et al., 2015). Floating plastics accumulate in subtropical gyres, which for the North Pacific is commonly known as the Great Pacific Garbage Patch (GPGP) (Figure 1, Cózar et al., 2014; Lebreton et al., 2018) However, these worldwide plastic abundance estimates have found that the amount of plastic modeled to be floating on the surface is less than what is predicted based on production and input projections, which has led to the concept of finding the 'missing plastic' (Andrady, 2011; Eriksen et al., 2014; Martin et al., 2022; Thompson et al., 2004).

Sediments have been regarded as one of the final reservoirs for plastics (Eriksen et al., 2014; Martin et al., 2022; Olivelli et al., 2020; Thompson et al., 2004; Woodall et al., 2014; Zhu et al., 2024). Both physical and biological mechanisms can drive plastic particles to the seafloor via processes such as density, biofouling, degradation, ingestion/excretion by organisms, marine snow, and physical processes (Brignac et al., 2019; Galgani et al., 2022; Kooi et al., 2017; Lebreton et al., 2019; Martin et al., 2022). Many studies have looked at microplastics in

sediments ranging from beaches, estuaries, and subtidal sediments from the continental shelf to the deep sea, with results ranging over multiple orders of magnitude (Harris et al., 2020). It is difficult to compare results between studies due to the wide differences in methods and reporting metrics, however, there is an indication that the type of benthic environment plays a role in plastic deposition rate (Harris et al., 2020). While nobody has looked at microplastic concentrations in the seafloor directly underneath the GPGP, there has been reported evidence of fallout in the water column below (Egger et al., 2020).

Recent studies tried to estimate the total amount of plastic in these global sediment sinks and have come up with slightly differing results. A study based on remotely operated vehicle (ROV) data predicted that 3-11 million metric tonnes (MMT) of macroplastic (>5 mm) rested on the ocean floor as of 2020 (Zhu et al., 2024). A separate study looked at non-fibrous micro- & mesoplastic concentrations (10 µm - 25 mm) in global ocean bulk sediment and estimated 25-900 Teragrams had accumulated in sediments from 1950-2010 (Martin et al., 2022). Based on results from their sediment core analysis, a third study predicted 14.4 million tonnes of plastic in the top nine cm of the ocean floor (Barrett et al., 2020). While these papers have quite a range in their estimates, all of them are greater than what is estimated to be floating at the surface: 268,940 tons (Eriksen et al., 2014), 7,000 - 35,000 tons (Cózar et al., 2014), and 93,000-236,000 tons (van Sebille et al., 2015), supporting the notion of sediments serving as a long term sink.

Sediment cores hollow out a section of sediment, sampling a range of depths, which serve as a way to study plastic deposition rates over time. Specifically, they can be used to understand the time scale in which sediments serve as a sink. Like the review of plastics in sediment, a review of 16 papers that looked at microplastic concentrations in sediment cores across the world, found that the methodology and reporting metrics varied greatly between studies.

Methods typically followed four main steps: Collection, Cutting & Dating, Isolating Plastics, and Analysis, but there were great differences between them, making it difficult to compare across studies, with some studies skipping steps altogether. Results were typically displayed as both particles/sediment weight or weight of plastics/sediment weight but the units chosen varied greatly. Only one study reviewed reported both count and mass (Simon-Sánchez et al., 2022), which allows the most opportunity to compare against other studies. All sediment core studies reviewed reported the presence of microplastics, with concentrations ranging by orders of magnitude.

There are two main objectives of this study: 1) Trial the density-separation device created by members of the Hawaii Pacific University Center for Marine Debris Research (CMDR) and Coastal Ocean Vision on environmental samples (Shaw et al., in review) as well as become the first study completed at CMDR using Pyrolysis Gas Chromatography/Mass Spectrometry (Py-GC/MS) to test for multiple plastic polymers in an environmental matrix and 2) Analyze the top section from sediment cores across an east/west transect of approximately 800 km from the coast of California, USA offshore into the North Pacific Ocean to look at differences in microplastic concentration from nearshore to offshore. By trialing the density-separation method with environmental samples, we will be one step closer to creating more standardization across the field. We hypothesize that cores further offshore will have smaller concentrations of plastic compared to the ones closer to shore. This study will display an effective way to extract microplastics from sediments using density separation, identify polymers using Py-GC/MS, and provide a larger geographic region of study compared to previous literature. The results from this study will guide our understanding of how the vertical transport of plastic changes across different benthic environments, ranging from the continental shelf to the deep sea. Understanding

how plastics settle in the environment will allow scientists and policymakers to create better management policies to protect the benthic environment and the organisms that live within it as well as increase plastic clean-up effort efficiency.

2. METHODS

2.1 Sediment Core Collection

Sediment cores were collected on board the R/V Sally Ride during a cruise with the Scripps Institute of Oceanography from December 20-27, 2022 (Cruise 2215). The cruise followed an east-to-west transect from San Diego to approximately 800 km offshore. Five sites were selected equidistant along the transect, with a sixth site added onboard closer to the coast (Figure 1, Table 1).

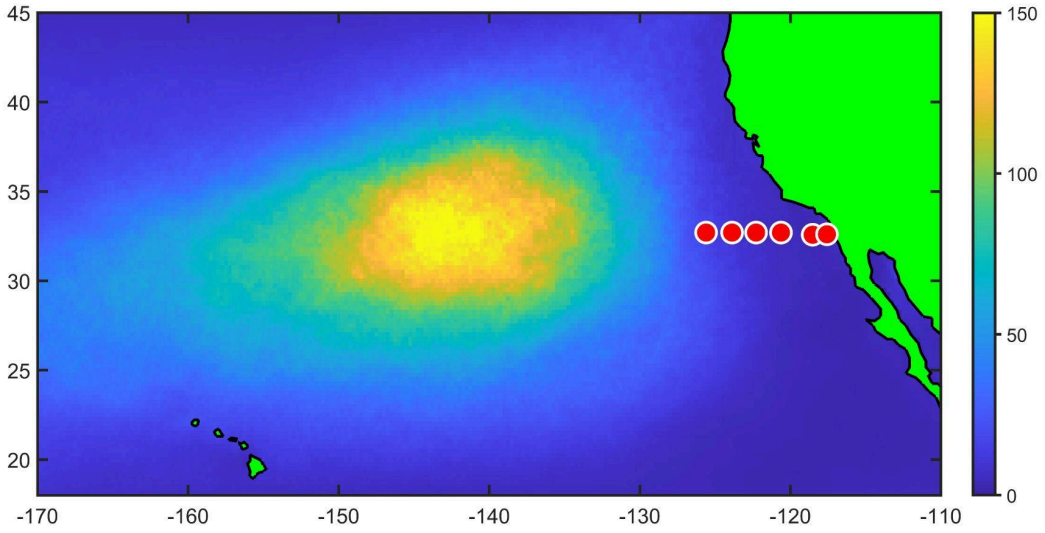

Figure 1: A map showing the locations of the six sampling sites (in red) in relation to the GPGP. Latitude and longitude are shown on axes.The GPGP model was created by Maximenko & Hafner, 2010: "Colors show model solution, simulating debris accumulation in the North Pacific garbage patch, averaged over 1994-2024. The model is forced by weak sources, distributed along the global coastline. Experiments start from the "no debris" state and the model is looped over a 30-year period until its solution saturates. Model is the next generation of the SCUD model (Maximenko and Hafner, 2009), with coefficients optimized during the FloatEco project (www.floateco.org). Concentration units are conventional model units."

Table 1: The coordinates & maximum water depths of the six sampling locations on the S2215 cruise from December 20-27, 2022. Cruise coordinates and water depths were taken on board and the distance to San Diego was calculated using ArcGIS. Total distance was calculated using Pythagorean theorem = $a^2 + b^2 = c^2$, solving for c.

Date	Station	Lat	Long	Water Depth (km)	Distance from Shore (km)	Total Distance (km)
12/23/22	1	32.700117 N	125.599967 W	4.516	786.48	786.49
12/23-12/24/22	2	32.699933 N	123.874117 W	4.347	624.66	624.68
12/24/22	3	32.700033 N	122.280033 W	4.170	473.47	473.49
12/25/22	4	32.700233 N	120.625017 W	3.803	319.39	319.41
12/26/22	5	32.57885 N	118.521283 W	1.138	120.42	120.43
12/26/22	6	32.603383 N	117.573017 W	1.204	31.34	31.36

The sediment cores were collected using a multicorer (Ocean Instruments, Deep-Sea Multi-Corer MC-800, Fall City, WA) which can collect eight cores per deployment (polycarbonate core tube dimensions: inner diameter: 9.53 cm, length: 69.85 cm, actual core lengths depended on site). Before the deployment at each site, three of the eight polycarbonate tubes were cleaned with LiquiNox soap and rinsed with 0.2 μm filtered Milli-Q water. This cleaning process was done to ensure particles from previous deployments were washed away. The three cleaned tubes were placed randomly around the rosette to prevent any bias in sampling and give a higher chance of core collection in case the multicorer landed awkwardly. The tubes were wrapped with electrical tape around the outside so they could be identified post-deployment. After each deployment, the two best-looking cores were selected for analysis. Good cores were assessed by observing the overall length of the cores compared to the others as well as if the water looked 'clean', suggesting that it didn't jostle around too much on the way up. The 1 L of water directly above the sediment was siphoned off using a glass pipet and stored in glass bottles (pre-baked in a Thermo Fisher Scientific Thermolyne F30438CM oven, Waltham, MA at 450 ºC for 4 h before use) for a separate project. Once the water was extracted the cores were placed on the extruder device (Figure 2). Sediment layers of 1 cm in depth were sliced off using a clean, pre-baked metal spatula into clean, pre-baked glass jars for the top 10 cm of the core. For all sites except Site 3, the next 5 cm layer was also collected, which serves as control sediment since it should contain no plastic based on estimated sedimentation rates and plastic production beginning in the 1950s. The deep sea can have an extremely low sedimentation rate ranging from 0.001-0.1 mm/yr (Diesing, 2020; Seibold, 1975). All of the core sampling was completed outside on the ship deck. Sediment samples were kept at room

temperature on the boat and while being shipped back to Hawai‘i. Once they arrived back in O‘ahu, they were inventoried and placed in the freezer at -20 ºC.

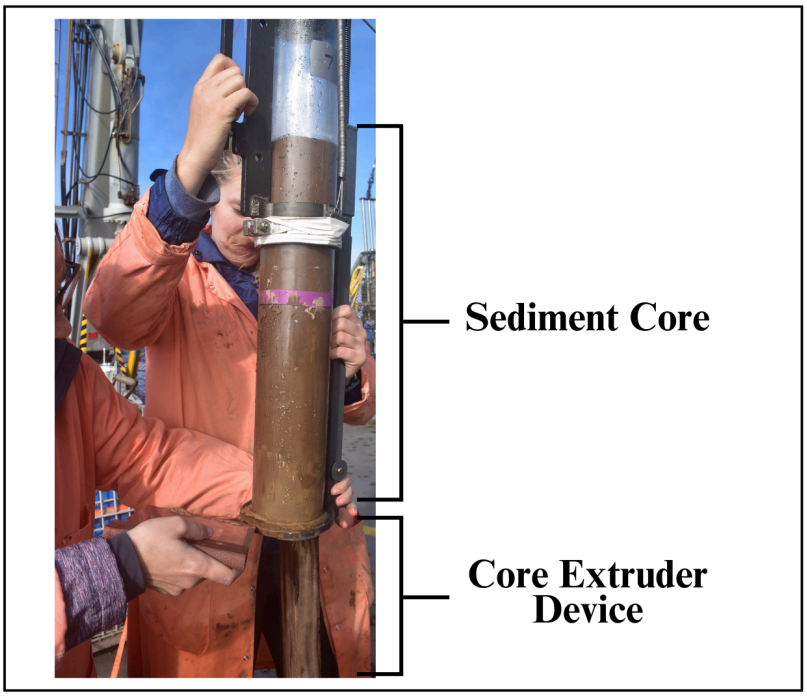

Figure 2: A photo from the SR2215 cruise documenting the process of transferring the core to the extruder device.

2.2 Sediment Analysis for Microplastics

Because method development was a key goal of this project, the samples underwent a few method changes throughout the study. The entire method workflow can be seen in Figure 3.

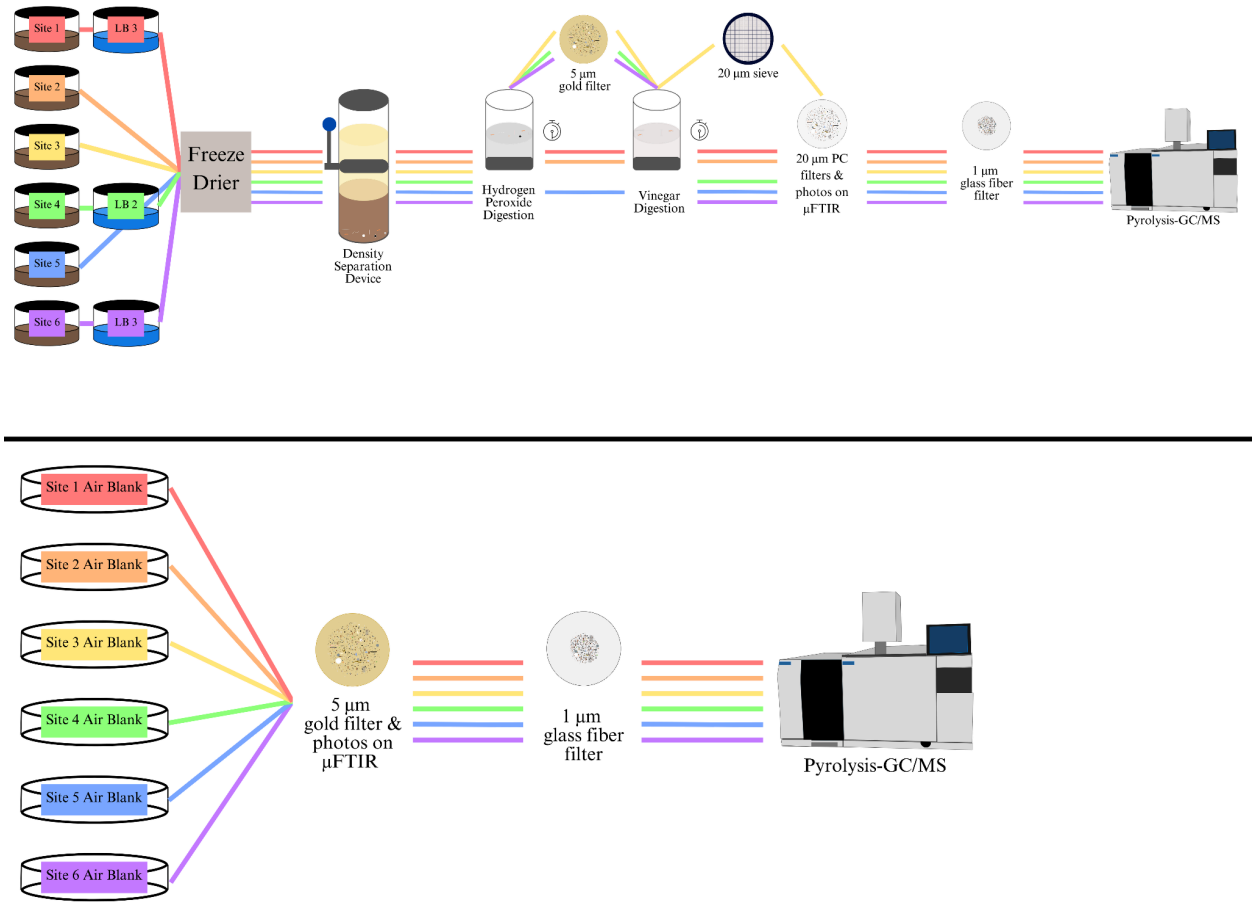

Figure 3: The method workflow that the different samples went through. LB = lab blank.

2.2.1 Density-Separation of Sediment Samples

The first step was to dry the sediment before density separation. Sediment jars were taken out of the freezer and placed in a drying oven set to 40 °C to start to evaporate the water; however, this process proved to be extremely time-consuming. Sediment samples were then freeze-dried before density separation. To freeze-dry the samples, sediments were spread onto the metal freeze-dryer trays. Before use, the metal trays were cleaned with LiquiNox and rinsed with Milli-Q water. The sediment jars were rinsed thoroughly with Milli-Q water to make sure all particles were transferred to the trays. Trays were covered with muffled foil and placed in the

freeze-dryer (Harvest Right, HRFD-PLrg-BK, Salt Lake City, Utah) until dry. The dry sediment was transferred into a tared, clean density separation device (DSD) chamber, and a dry weight was recorded. The DSD consisted of a metal end cap on each side, two sight glasses, and a ball valve in the middle that could separate the two chambers (Shaw et al., in review). All the parts from the DSD were purchased from Amazon and are listed in the Supplementary Information (Table S1). Once a dry weight was taken, the metal freeze-dry tray was rinsed with Milli-Q water to transfer any last particles into the DSD.

Once the sediment was inside the bottom chamber of the DSD, the process followed what was developed by researchers at CMDR and Coastal Ocean Vision (Shaw et al. in prep.). The reason for choosing density separation was because it yields a high amount of plastics from complex organic matrices, especially sediment, as well as its effectiveness in extracting very small particles. Collecting the small particles was important since the literature states that 90 % of plastics recorded in sediment are less than 0.1 mm (Martin et al., 2022). Milli-Q water (70 mL) was added to the bottom sight glass containing sediment and a vacuum was pulled for 30 minutes with the top vacuum adapter and pump (pressure: 8-23 in. Hg) (GAST, DOA-P704-AA 115V / 2.4A / 60Hz, Benton Harbor, MI) to remove gas bubbles from all particles and increase separation (Steucek & Hill, 1985). After the vacuum, the rest of the DSD was assembled by attaching the ball valve and the second sight glass on top. After assembly, 180 mL of sodium polytungstate was added. Sodium polytungstate (SPT) (sodium metatungstate monohydride, ThermoScientific, Waltham, MA) was chosen as it can be made to be extremely dense, is non-toxic, and will allow all types of plastic polymers to become buoyant (Chapter 1: Table 1). Sodium polytungstate was brought up to a density greater than 2.0 g/mL (target 2.39 g/mL) so that when it was mixed with the water in the DSD, it would reach a final density of at least 2.0

g/mL (Equation 1). Once the entire DSD was built, the apparatus was shaken with the ball valve open to allow all particles to mix. Once a day for the next two days the entire DSD apparatus was shaken with the ball valve closed, and then opened again, allowing the material to settle in between shakes. After three total shakes, the top chamber (buoyant particles) was isolated by closing the ball valve, and the SPT was drained out through a 20 µm top screen sieve attachment. This step determined the lower size limit of particles analyzed in the study (20 µm).

Formula (cited by Skipp & Brownfield 1993 as written communication w/ Don Cheney 1988

$$(Vd)\ (pm - pd) = (Vl)\ (pl - pm)$$

Vd = volume of the diluent (water)
Vl = volume of the liquid (liquid SPT)
pl = density of the liquid at hand (liquid SPT)
pm = density of the mixture (final density we want = 2g/mL)
pd = density of the diluent (water = 1g/mL)

(Vd)(pm- pd) = (Vl)(pl-pm)
(70)(2.0 - 1.0) = (180)(pl - 2.0)
140 - 70 = 180(pl) - 360
70 = 180(pl) - 360
430 = 180(pl)
2.39 = pl

Equation 1: The formula used to calculate the target density for the SPT before adding it to the DSD (Skipp & Brownfield, 1993).

2.2.2 Chemical Digestion of Sediment Samples

For Sites 3, 4, and 6 as well as Lab Blanks 2 & 3, the chamber containing the buoyant particles then underwent chemical digestion with 30 mL of 30 % hydrogen peroxide on a shaker table for 24 hours to digest the residual organic material. After the digestion, the chamber was filtered onto a 25 mm diameter 5 µm pore gold filter (Sterlitech, Auburn, WA, Cat # 1300037) to be analyzed on the iN10 MX µFTIR (Thermo Fisher Scientific, Waltham, MA) in reflectance

mode. However, the filters proved to be too overloaded and could not be properly analyzed under the iN10 MX microscope μFTIR, so a new plan was created.

After further review of our methods so far, it was decided to conduct a second chemical digestion and run the filters on the Pyrolysis-Gas Chromatography/Mass Spectroscopy (Py-GC/MS). Vinegar was chosen as the second digestion chemical because of its acidic properties which dissolve the calcium carbonate, removing interfering pieces of organisms' calcium carbonate skeletons that have trapped bubbles and floated to the top of our DSD. Py-GC/MS was selected due to its ability to detect extremely small amounts of plastic, even with large amounts of organic material. The samples that were already on gold filters (Sites 3,4,6 & Lab Blanks 2 & 3), were sonicated (VWR, Ultrasonic Cleaner 97043-984, Radnor, PA) twice for 10 seconds each time in vinegar. In the beginning, the first two filters were observed under the microscope to confirm that particles were not left behind and then the double sonication protocol became the standard moving forward. The solution was placed on the shaker table (130 RPM, 40℃) for 24 hours.

The other half of the samples (Sites 2, 3, 5 & Lab Blank 1) were run through the DSD, hydrogen peroxide digestion, and straight into the vinegar digestion. This was completed by sieving out the excess hydrogen peroxide through the 20 μm sieve and rinsing the particles off the sieve back into the chamber. After 24 hours on the shaker table, the samples were filtered onto polycarbonate filters the same way as above.

2.2.3 Particle Analysis via Imagery

Post vinegar digestion, particles were then transferred out of the density-separation chamber. The first sample (Site 3) remained on the 20 μm sieve and was analyzed with a camera

under the microscope (Amscope, MU1603, Irvine, CA; Nikon, Eclipse E400, Melville, NY) for fibers. It proved to be quite difficult to analyze this way for fibers so every other sample was filtered onto a 47 mm diameter 20 µm polycarbonate filter (Sterlitech, Auburn, WA, Part #1270175). These filters were then placed on the iN10 MX microscope µFTIR to capture visual images, which could be stitched together into mosaics, using the computer program Canva, to create a magnified image of the sample. These images could then be used to observe the presence/absence of fibers in the samples before being run on the Py-GC/MS.

2.2.4 Polymer Quantification via Pyrolysis-GC/MS

2.2.4.1 Sample Set Up

Once photos were taken of all samples and lab blanks, the samples were sonicated back into Milli-Q water (following the same sonication procedure as mentioned above). This liquid mixture was then filtered onto 1 µm binderless glass fiber filters (Osmonics Inc., 25 mm diameter with the 13 mm filtration cup opening, Cat #G40WP02505). Immediately after filtering each sample, the corresponding glass fiber filter was trimmed around the edge, rolled up, and placed inside a stainless steel pyrolysis cup (Frontier Labs, Eco-Cup LF-V4, Fukushima, Japan) pre-loaded with 20 µL of deuterated polystyrene (D_8-PS) (Cambridge Isotope Laboratories, Poly(styrene) (Styrene-D8, 98%) 1 mg/mL in toluene, Andover, MA, Item #DLM-221-1.2, Lot #SEBI-015) to serve as the internal standard. Filters were trimmed to a diameter of 13 mm so that they would fit inside the cup easier. The cups were loaded with D_8-PS via a Hamilton syringe and left to dry loosely covered in the fume hood overnight before the addition of the filters. The samples were run with the double-shot program detailed in Table 2, at a 20:1 split ratio (Frontier Laboratories EGA/PY-3030, affixed to an Agilent 8890 GC / 5977 MSD). The

thermal desorption chromatograms were collected, but the analysis of them remained out of the scope of the thesis.

Table 2 Pyrolysis-GC/MS Methods

Microfurnace Pyrolysis	**Frontier Labs EGA/PY-3030**
Carrier gas	Helium
Upper interface temperature	300 °C
Single-Shot	
Temperature	600 °C
Pyrolysis time	0.2 min
Double Shot	
Thermal desorption temperature	100-200 °C
Thermal desorption program	Ramping at 20 °C min^{-1}, holding for 2 min
Pyrolysis temperature	600 °C
Pyrolysis time	0.2 min
Gas Chromatograph	**Agilent 8890**
Injection mode	Split; 20:1
Inlet temperature	300 °C
Oven temperature program	40 °C (2 min) -> 320 °C at 20 °C min^{-1} (14 min)
Run time	30 min
Carrier gas flow and split ratio	1 ml min^{-1} in Helium
Column	Frontier UA5: 30 m x 250 µm x 0.25 µm
Mass Spectrometer	**Agilent MSD 5977**
MS source temperature	230 °C
MS Quadruple temperature	150 °C
Detection type	Scanning ion mode
Scan range	30-600 m/z
Scan rate	2.6 scans sec^{-1}
Ionization energy	70 eV

2.2.4.2 Quantification

Nine different plastic polymers were chosen for quantification: Nylon-6, polyacrylonitrile (PAN), polycarbonate (PC), polyethylene (PE), polyethylene terephthalate (PET), polymethyl-methacrylate (PMMA), polypropylene (PP), polystyrene (PS), and polyvinyl chloride (PVC) (Supplementary Information Table S3). During initial tests, the polymers were also run individually using the same double-shot program mentioned earlier (Table 2). Agilent MassHunter Qualitative software program and the National Institute of Standards & Technology

(NIST) mass spectral library (MS Search 23) were used in the initial tests to confirm marker compound peaks before the polymer standard was used in the calibration curves.

Known masses of each of the reference polymers were weighed and placed into pyrolysis cups to create an external calibration curve (Mettler Toledo, XPR6U, Columbus, OH). Exact weights (Table S2) and commercial sources of the polymer standards (Table S3) can be found in the Supplementary Information. Three of the nine polymers targeted were mixed into the same cup: Mix 1 (HDPE, PAN, PVC), Mix 2 (PP, PC, PET), and Mix 3 (Nylon-6, PMMA, PS) (Table S2). Mixing polymers allows for the influence of polymer interaction to be accounted for when assessing peak areas (Ishimura et al., 2021; Seeley & Lynch, 2023). Calibration cups were also filled with a piece of the glass fiber filter to account for any interference it may cause. Marker compounds were chosen based on previous literature (Table 3) (Coralli et al., 2022; Seeley & Lynch, 2023; Tsuge et al., 2011). Multiple marker compounds were selected for each polymer (when applicable) to confirm the presence of the polymer qualitatively. Some marker compounds were also selected for compounds not chosen for quantification to potentially determine the presence/absence of that polymer. We chose to use the 110 ion for our marker compound styrene from our D_8-PS, because it did not overlap as much with other compounds we were looking at compared to the 84 ion. Calibration mixes were run using the same double-shot program mentioned above, at a 20:1 split ratio (Table 2).

The Agilent MassHunter Quantitative software program was used for peak integration. Calibration curves were created by comparing the mass ratio (mass of the polymer in the sample/mass of the D_8-PS) to the area ratio (peak area for the marker compound/peak area of styrene D_8-PS) and fitted with a polynomial line (Table 4). The left (negative) side of the

polynomial equation was used for quantification. All calibration calculations were completed in Google Sheets and Excel.

Peak area ratios (peak area of sample/area of styrene from D_8-PS) of the targeted polymer marker compounds from the Py-GC/MS were analyzed using the following workflow to determine if the polymer mass fractions were above the limit of detection (LOD) or limit of quantification (LOQ) (Figure 4). Briefly, the peak areas were compared against the average instrument blank (a sample run with no cup) plus 3 standard deviations to determine if they were above the limit of detection (LOD). Next, the chromatograms were viewed to see if they passed the qualification rules set prior (Table 5). If they did not pass the qualitative test, they were determined to be below the LOD. If the peak areas passed the qualitative test, the micrograms were calculated on a per sample basis using the calibration curves to determine if the polymer mass was above the lowest detectable calibration point mass. If samples had a polymer mass greater than the lowest detectable calibration point, they underwent a blank subtraction. These masses were divided by the dry sediment weight before the final mass was reported as mass of the polymer/g sediment. The polycarbonate (what the multicorer tube was made out of) from the scrape blank was also subtracted out of the samples. Due to the fact that one of the boat air contamination blanks was destroyed in analysis, an average of the five remaining blanks were divided by the estimated time it took to collect the top layer (4.5%). If their per sample mass was below the lowest detectable calibration point mass, the samples were reported as below the limit of quantification (LOQ).

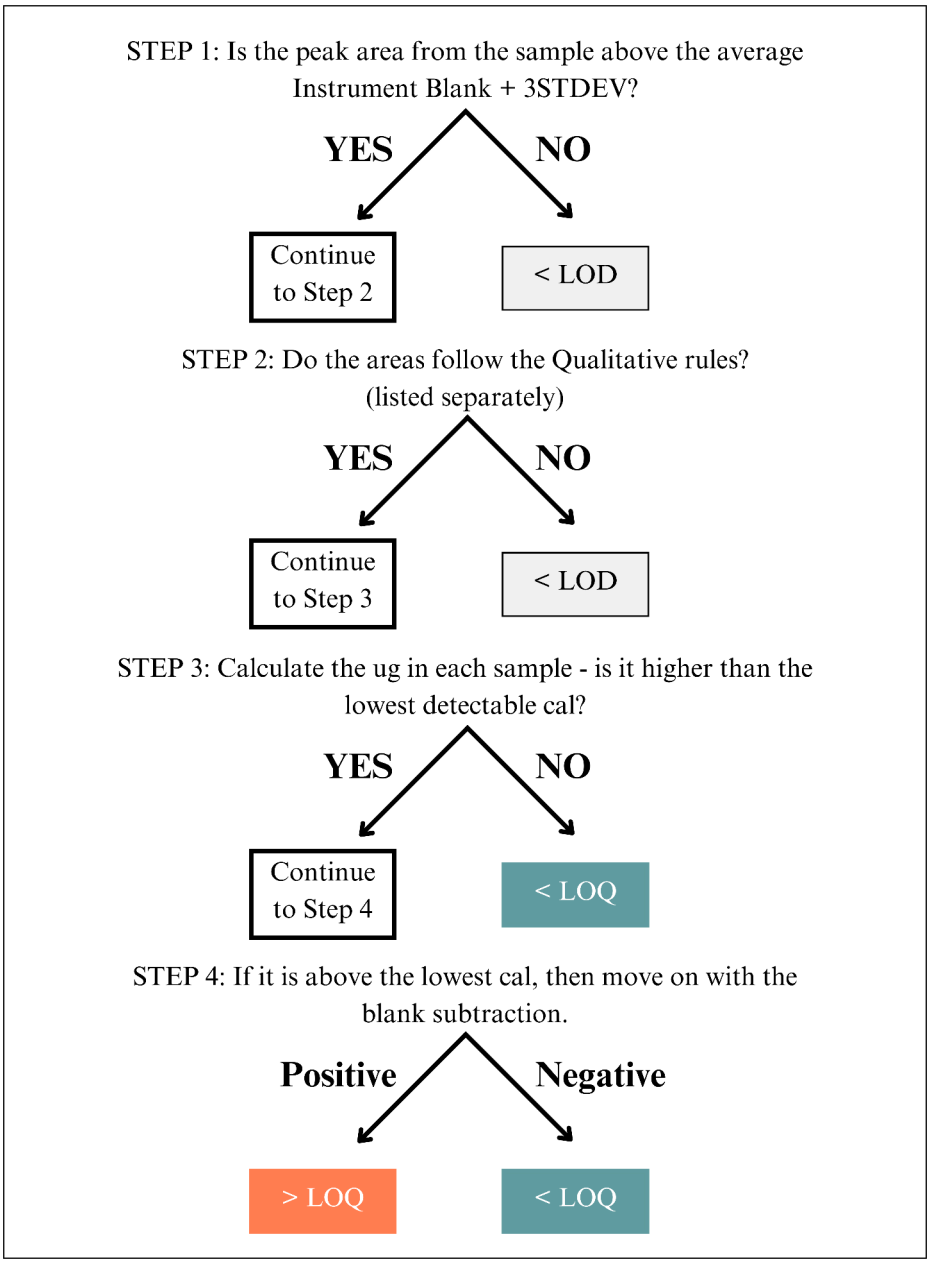

Figure 4: The Py-GC/MS workflow to assess the presence/absence and quantity of microplastics present in a sample.

Table 3: The pyrolyzates (“marker compounds") used in qualifying the presence/absence of polymers chosen in this study. **Boldface** denotes the mass ion, the compounds with * signify the ones chosen for quantification (when applicable), and marker compounds for polymers not chosen for quantification are denoted with a ^.

Polymer	Marker Compound	Retention Time	Quantifying Ion	Qualifying Ion (Relative %)
Polyethylene (PE)	C15 alkadiene	10.36	81	55 (120); **208** (5)
Polyethylene (PE)	C15 alkene	10.41	83	55 (95); **210** (5)
Polyethylene (PE)	C15 alkane	10.45	85	57 (160); **212** (10)
Polypropylene (PP)	2,4-dimethyl-1-heptene*	5.10	70	43 (85); **126** (30)
Polystyrene (PS)	Styrene dimer*	11.91	91	**208** (40); 130 (30)
Polystyrene (PS)	Styrene trimer	15.38	91	117 (40); 207 (35); **312** (10)
Polyvinyl-Chloride (PVC)	HCl	1.72	**36**	38 (40)
Polyvinyl-Chloride (PVC)	benzene	2.98	**78**	77 (30); 51 (25)
Polyvinyl-Chloride (PVC)	toluene	4.17	91	**92** (60); 65 (15)
Polyvinyl-Chloride (PVC)	indene*	7.17	**116**	115 (95); 89 (15)
Polyvinyl-Chloride (PVC)	naphthalene*	8.37	**128**	127 (15); 102 (10)
Polyvinyl-Chloride (PVC)	2-methylnaphthalene*	9.21	**142**	141 (90); 115 (40)
Polyvinyl-Chloride (PVC)	1-methylnaphthalene*	9.34	**142**	141 (90); 115 (40)
Polyethylene Terephthalate (PET)	vinyl benzoate	7.92	105	77 (50); **148** (5)
Polyethylene Terephthalate (PET)	benzoic acid*	8.28	105	**122** (85); 77 (65)
Nylon-6	5-cyano-1-pentene*	5.26	55	41 (50); **95** (10)
Nylon-6	hexanenitrile	5.44	41	55 (90); 54 (85); 97 (5)
Nylon-6	caprolactam*	8.92	**113**	55 (80); 85 (60)
Polymethylmethacrylate (PMMA)	methyl methacrylate*	3.62	69	41 (95); **100** (65)
Polyacrylonitrile (PAN)	2-methylenepentanedinitrile*	7.45	66	91 (35); **106** (35)
Polyacrylonitrile (PAN)	hexane-1,3,5-tricarbonitrile (trimer)*	10.93	106	119 (60), 66 (55); 161 (1)
Polyurethane(MDI-PU)^	diphenylmethane diisocyanate	13.83	**250**	208 (50); 221 (40)
Polycarbonate (PC)	p-cresol*	7.36	107	**108** (90); 77 (30)
Polycarbonate (PC)	p-tert-butylphenol	9.10	135	107 (35); **150** (25)
Polycarbonate (PC)	4-isopropenylphenol*	9.14	**134**	119 (75); 91 (35)
Polycarbonate (PC)	bisphenol a	14.16	213	**228** (25); 119 (20)
Polyurethane (TDI-PU)^	2,4- or 2,6-tolylene diisocyanate	9.53	**174**	145 (70)
Tire & Road-Wear Particles (TRWP)^	Isoprene	1.99	67	**68** (80); 53 (70)
Tire & Road-Wear Particles (TRWP)^	1,4-Vinylcyclohexene	5.02	79	54 (90); **108** (20)
Tire & Road-Wear Particles (TRWP)^	Dipentene	7.07	68	93 (85); **136** (40)
Nylon-6,6^	1,8-Diazacyclotetradecane-2,7-dione	14.55	**226**	152 (100); 55 (200); 97 (200); 112 (200)
Nylon-11^	1, 13-diazacyclotetracosane-2,14-dione	19.55	**366**	184 (100)
Nylon-12^	1,14-diazacyclohexacosane-2,15-dione	21.2	**394**	198 (100)
d8-PS	d8-Styrene*	5.64	**110**	
d8-PS	d8-Styrene Dimer	11.9	98	

Table 4: The polynomial equations created from the calibration curves and used for quantification of plastic polymers in our samples.

Polymer - Marker Compound	Equation	R-squared
Nylon 6 - 5-cyano-1-pentene	$y = -0.0013x^2 + 0.2109x + 0.0284$	0.999
Nylon 6 - caprolactam	$y = -0.0244x^2 + 0.7735x + 0.2121$	0.984
PAN - 2-methylenepentanedinitrile	$y = -0.1091x^2 + 1.0873x + 0.0612$	0.987
PAN - hexane-1,3,5-tricarbonitrile (trimer)	$y = -0.0688x^2 + 0.7123x + 0.0265$	0.932
PC - p-cresol	$y = -0.0182x^2 + 0.2581x + 0.0628$	0.965
PC - 4-isopropenylphenol	$y = -0.0401x^2 + 0.474x + 0.1291$	0.966
PET - benzoic acid	$y = -0.0487x^2 + 0.8509x - 0.3344$	0.975
PMMA - methyl methacrylate	$y = 0.0135x^2 + 0.7634x + 0.4227$	1
PP - 2,4-dimethyl-1-heptene	$y = -0.007x^2 + 0.1849x + 0.1748$	0.994
PS - Styrene dimer	$y = 0.0074x^2 + 0.2008x + 0.4807$	0.983

Table 5: Qualitative Rules to Determine Presence/Absence of Polymers. **PVC was eventually thrown out from analysis due to the fact that samples that should contain no PVC were passing these rules**

Polymer	Rule
PE	Presence of the triplicate pattern (alkadiene, alkene, alkane) multiple times sequentially between carbon8 and carbon20, would need to confirm in MassHunter Qual (use Extracted Ion Chromatogram)
PP	Presence of 2,4-dimethyl-1-heptene
PS	Presence of styrene and styrene dimer
PVC**	Presence of benzene, toluene, indene, naphthalene, 2-methylnaphthalene, 1-methylnaphthalene; ideally also HCl but proves to be quite difficult to find in samples
PET	Presence of benzoic acid, ideally confirm vinyl benzoate (has proven to diminish in low concentrations)
PC	Presence of 4-isopropylphenol, p-cresol, p-tert-butylphenol, bisphenol-A (if able to find)
PMMA	Presence of methyl methacrylate
PAN	Presence of both 2-methylenepentanedinitrile and hexane-1,3,5-tricarbonitrile (trimer)
Nylon-6	Presence of caprolactam & one other marker (hexanenitrile or 5-cyano-1-pentene)
Nylon-6,6	Presence of 1,8-Diazacyclotetradecane-2,7-dione (can check for others if it is present to confirm)
Nylon-11	Presence of 1,13-diazacyclotetracosane-2,14-dione (can check for others if it is present to confirm)
Nylon-12	Presence of 1,14-diazacyclohexacosane-2,15-dione (can check for others if it is present to confirm)
MDI-PU	Presence of diphenylmethane diisocyanate
TDI-PU	Presence of 2,4 or 2,6-tolylene diisocyanate

2.2.5 Water Sample Trial

In order to prepare for future analysis of the water samples, a small trial was completed. About half (480 mL) of the water sample from Site 6 from the core that was not used for

microplastic analysis was directly filtered onto four different glass fiber filters and run with the rest of the samples according to the Py-GC/MS methods listed above. The purpose of this trial was to determine if microplastics could be detected without completing any clean up processes.

2.3 Experimental Design: QA/QC

All glassware and materials used in the sediment collection process were sonicated with warm soapy water, rinsed thoroughly with tap and Milli-Q water, and baked in an oven (Thermo Fisher Scientific Thermolyne F30438CM oven, Waltham, MA) at 450 ºC for 4 h before use (when applicable) before the cruise and laboratory processes. Orange lab coats were also worn when possible on board during the extrusion process to distinguish fibers from the sample vs. fibers from onboard contamination. During each core extrusion process, a petri dish with a diameter roughly the same size as the coring tube was opened to collect airborne contamination that was present at the time of sampling ("air blank"). These samples were filtered onto gold filters, sonicated, and re-filtered onto glass fiber filters (to account for the analysis method change) and run with the rest of the samples on the Py-GC/MS. Potential sources of contamination were noted during the cruise and samples from these sources, such as the plastic tops used to cover water samples, paint from the inside of the metal sediment jar tops, silicone stoppers, and carpet from the bottom of the multicorer apparatus were collected when possible and analyzed on the iN10 MX microscope μFTIR to be added to the spectral library. A "core blank" was also collected by adding 0.2 μm filtered Milli-Q water to the multicorer apparatus and shaking to collect any contamination inside the tube, particularly the carpet that lined the bottom of the apparatus, before being stored in a glass bottle. This sample ended up not being analyzed since the top layer did not come in contact with the carpet and we felt it did not

represent the samples we were analyzing so it did not undergo the Py-GC/MS analysis. Finally, a clean, baked spatula was used to scrape across the top of a clean multicorer tube three times and rinsed into a glass jar in the same manner as sediment slicing to account for any contamination from the polycarbonate tube ("scrape blank"). Three lab blanks were also taken to account for contamination through the laboratory process. All blanks underwent the same processes as the samples (including the method-switch). In the lab, orange lab coats were used during all laboratory processes and all sample processing was completed under the laminar flow hood when possible to prevent fiber contamination. A previous study was completed to determine the recovery of extracting different microplastic polymers using the same density-separation equipment used in this study (% recovered: Polystyrene (PS): 86.9 % ± 25.7 %, Polyvinyl Chloride (PVC): 100.0 % ± 12.4 %, Nylon-6 (PA6): 106.3 ± 76.1 %, High Density Polyethylene (HDPE): 96.9 % ± 11.9 %, Polypropylene (PP): 78.4 % ± 34.0 %, Crumb Rubber (CR): 92.7 % ± 30.8 %, Cellulose Acetate (CA): 25.9 % ± 17.3 %, Polyester (PEST): 20.7 % ± 18.4 %)(Shaw et al., in review).

For the Py-GC/MS analysis, the samples were prepped on muffled foil or stone to prevent contamination. All tools used were either muffled or rinsed with 70% isopropanol between uses. Before the samples were run on the Py-GC/MS, a few different tests were completed. A part of the sediment from the bottom of a DSD chamber from two of the six sites was dried and saved. Later, it was run on the Py-GC/MS to confirm that there would not be peaks interfering with our samples. The sediment was also run with a piece of HDPE (HPU CMDR Polymer Kit 1.0) to confirm that we would be able to detect plastic in the matrix. The glass fiber filters were also run by themselves to understand the noise level they would contribute to the samples. The results of these tests can be seen in the Supplementary Information (Figures S1, S2, and S3).

2.4 ^{210}Pb Dating

To prepare samples for dating, an initial wet density was calculated by filling and weighing a 3 mL glass test tube with wet sediment. From this same batch of sediment (and more if needed) was placed in a crucible and weighed. The samples were placed in the drying oven at a temperature of ~100°C overnight and a dry weight was taken after. This allows us to calculate a dry density using the ratio of wet sediment weight to dry sediment weight and the wet density. Once dry, the dry sediment layers were sent to University College London where they were ^{210}Pb dated. A detailed protocol can be found in the Supplementary Material.

2.5 Statistical Analysis

Prior to any statistical analysis the data were tested for normality. To test the spatial gradient hypothesis, both the number and concentration of polymers (µg polymer per g dry sediment) found at each site were compared to the distance from shore. Distance from shore was calculated using ArcGIS, drawing a line between the site and the port the ship left from (San Diego, California, USA) and recording the distance (Table 1). To test the water depth hypothesis, both the number and concentration of polymers (µg polymer per g dry sediment) were compared to the water depth calculated on board. The Spearman rank test was used to calculate correlation between the number of polymers detected, mass, water depth, and distance from shore respectively. A Spearman rank test was also completed to determine if the water depth and distance from shore were co-correlated. A Wilcoxon test was performed to compare the polymers detected between the lab blanks and the samples. All tests were completed in R (R Core Team, 2023).

3. RESULTS

3.1 Qualitative Detection of Plastic Polymers

The number of polymers below the LOD or LOQ and the µg/g dry sediment of polymers greater than the LOQ can be seen in Figure 5. Although PVC was detected in all samples and lab blanks, it was eliminated from all analyses due to the presence of PVC marker compounds found in the calibration cups which contained no PVC, so we did not trust the accuracy of our quantification results (Figure 6, Supplementary Information Figure S7). Table 6 shows what the concentrations of PVC would have been if we trusted the marker compounds and kept it in the analysis following the equations in the Supplementary Information (Table S5). This is not the first time PVC has been eliminated from Py-GC/MS analysis results. Galgani et al., 2022 eliminated PVC from their Py-GC/MS data, due to a larger PVC noise in their blanks compared to their samples. Marker compounds for PU, TRWP, and three nylon variants were selected (Table 3) to potentially screen the samples for presence of these polymers. These polymers were not included in any calibration curve. None of the compounds for PU and the nylons were above the instrument noise + 3 STDEV (LOQ). The remaining focus of this thesis is on the targeted analysis of polymers and future studies could assess the pyrograms for TRWP and other polymers. The LOQ per sample was calculated as the mass of the lowest detectable calibration point divided by the sediment weight.

According to a Shapiro-Wilk test, the number of polymers detected at each site was found to be normally distributed across sites ($W = 0.94957$, p-value = 0.7368). The number of polymers detected increased as the site moved closer to shore. At Site 1, the deepest water and furthest offshore, only one of the potential eight polymers were observed. While at Site 6, the closest to shore and the second shallowest, six of the eight potential polymers were observed

(Figure 5; Figure 7). Due to the lack of replicate samples, no statistical test could be performed to test for differences among sites.

	Site 1	Site 2	Site 3	Site 4	Site 5	Site 6
N6	< LOD	< LOD	< LOD	< LOD	0.326	< LOD
PAN	< LOD	< LOD	< LOD	< LOD	< LOD	< 0.192
PC	< 0.0669	< 0.123	< 0.121	1.33	0.484	0.283
PE	< LOD	< LOD	< LOD	< LOD	< LOD	< LOD
PET	< LOD	< LOD	0.0316	0.280	0.361	0.424
PMMA	< LOD	< 0.317	< LOD	< LOD	< LOD	< 0.220
PP	<LOD	<LOD	< 0.282	< 0.272	0.650	< 0.200
PS	<LOD	<LOD	<LOD	<LOD	< 0.753	< 0.616

OFFSHORE ⟷ NEARSHORE

Figure 5: A heat-map depicting the outcomes of the different polymers at the respective sites. <LOD = below limit of detection, values in teal with a less than symbol = below limit of quantification, and values in orange are the detected and quantified concentration in µg/g dry sediment.

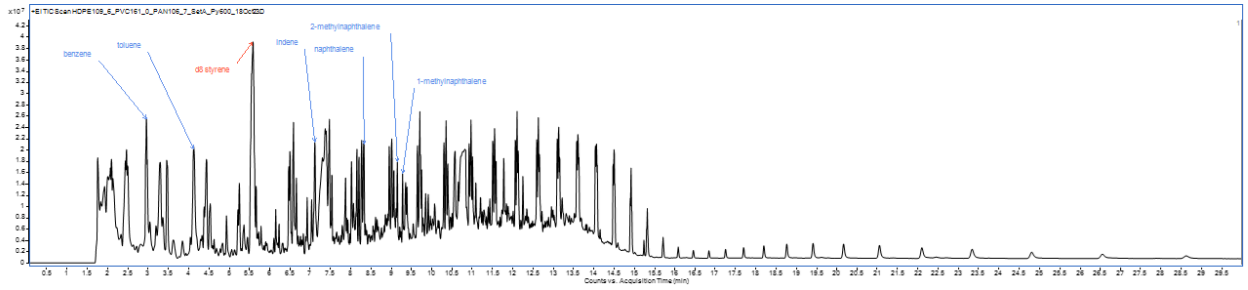
benzene
toluene
d8 styrene
Indene
naphthalene
2-methylnaphthalene
1-methylnaphthalene

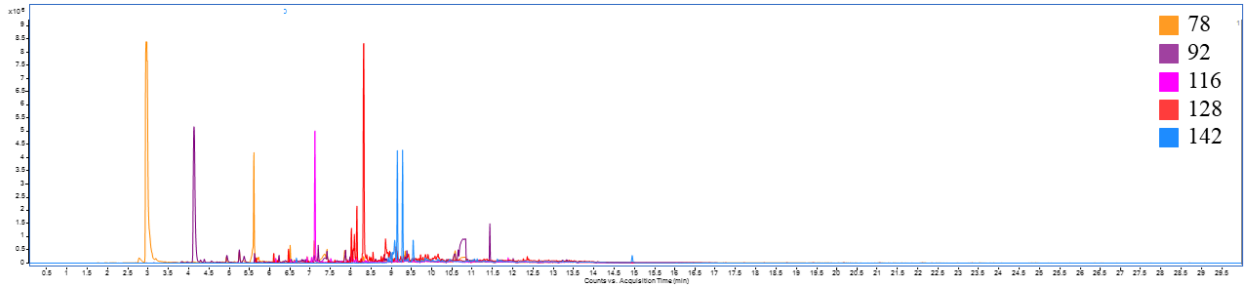
78
92
116
128
142

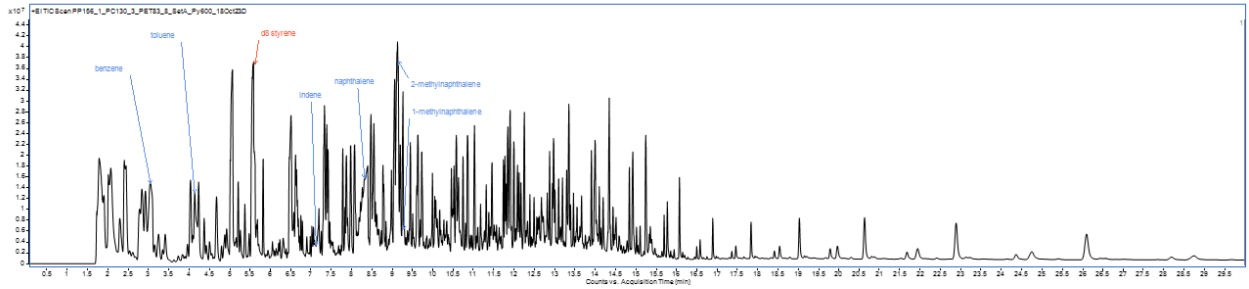
benzene
toluene
d8 styrene
Indene
naphthalene
2-methylnaphthalene
1-methylnaphthalene

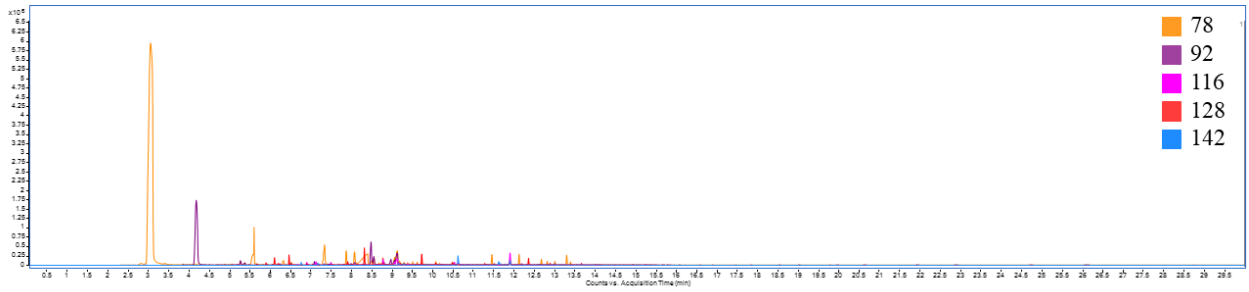
78
92
116
128
142

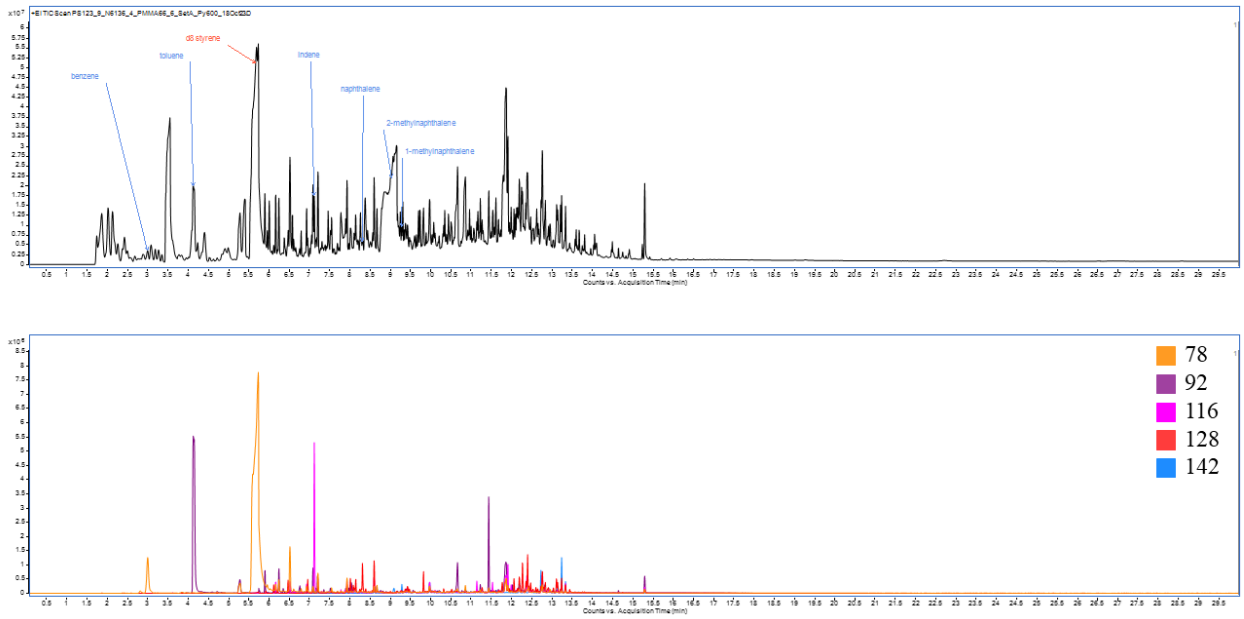

Figure 6: PVC marker compounds from Mix 1 (top) compared to the other cal mixes: Mix 2 (middle) and Mix 3 (bottom), which do not contain any PVC, demonstrating the marker compounds to be non-specific to PVC and unreliable.

Table 6: The concentrations of PVC (µg/g dry sediment) if we had kept it in the analysis.

Site Number	PVC (µg/g dry sediment)
1	0.936
2	2.17
3	0.396
4	1.50
5	3.42
6	0.981

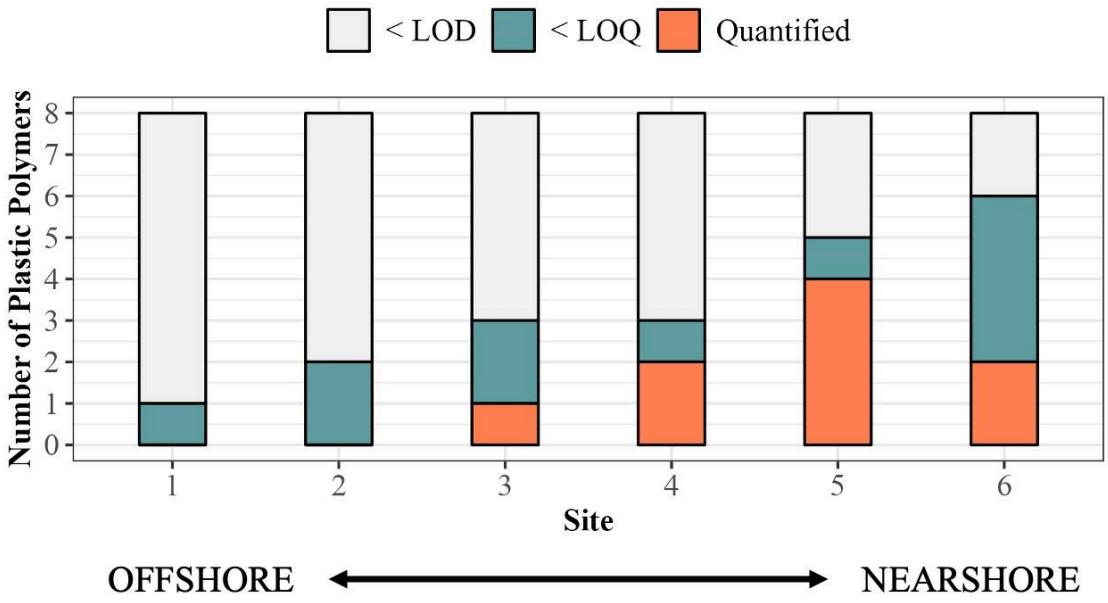

Figure 7: A bar chart depicting the outcomes of the 8 potential microplastic polymers at each site

3.2 Quantification of Plastic Polymers

We were able to derive a mass concentration (in µg/g dry sediment) for the polymers that were above the LOQ (Figure 5). With the removal of PVC, no polymers were able to be quantified from Site 1 or 2. The lowest concentration occurred at Site 3, while Site 5 had the

highest mass of polymers quantified (Figure 8). A Shapiro-Wilk test found the concentration of polymers above the LOQ to be just barely normally distributed across sites (W = 0.80618, p-value = 0.06676).

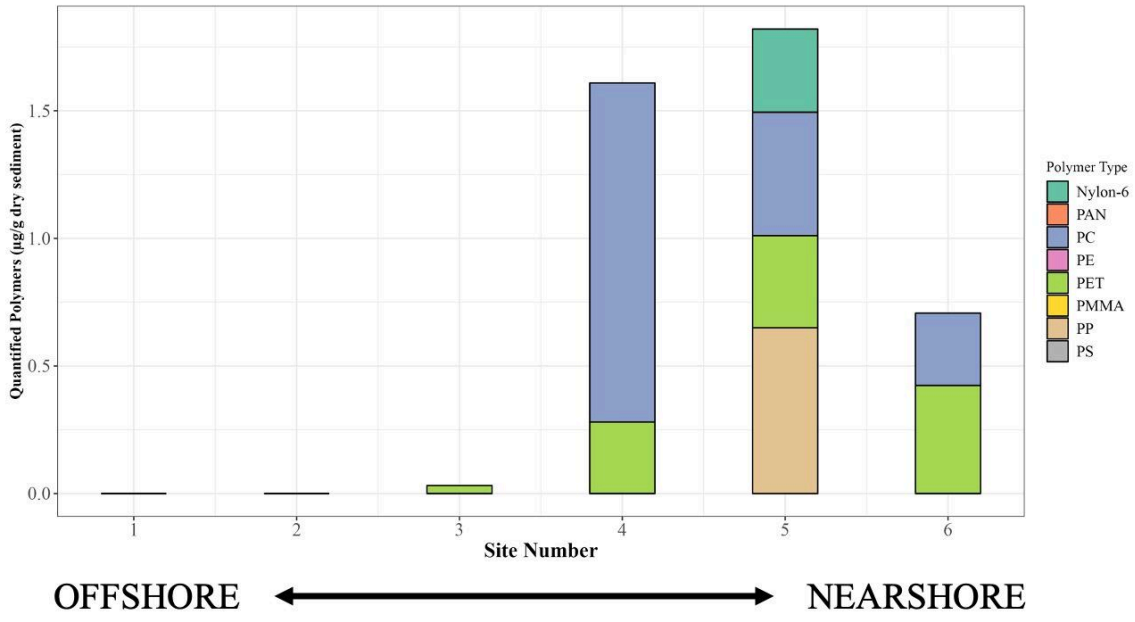

Figure 8: A bar chart depicting the plastics that were able to be quantified by site.

3.*3 Relationship with Water Depth and Distance from Shore*

There was a significant negative correlation between the number of polymers detected and both the water depth (Spearman correlation, rho = -0.9376337, p = 0.007666) and distance from shore (Spearman correlation, rho = -0.9856108, p = 0.0003091). There was a negative correlation between the concentration of polymers quantified and both water depth and distance from shore, but neither were significant (Spearman correlation, rho = -0.6, p = 0.2417 and rho = -0.4285714, p = 0.4194 respectively). However, it is important to note that water depth and distance from shore are significantly positively correlated with each other (Spearman correlation, rho = 0.9428571, p = 0.01667).

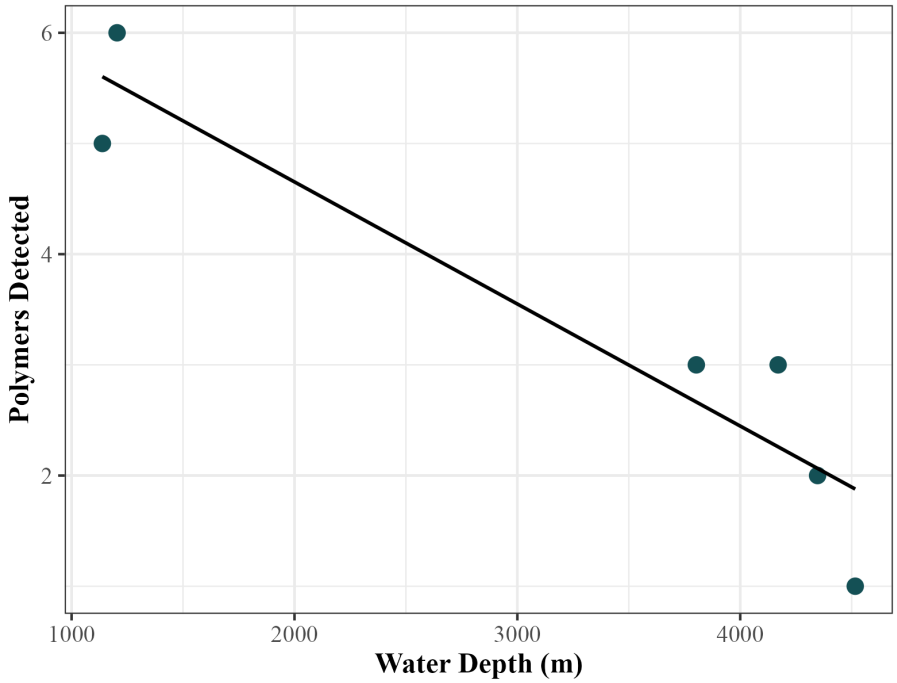

Figure 9: A scatter plot comparing total number of polymers detected compared to water depth, with the linear trend line added (equation: y = -0.0011030x + 7.8587302, adjusted R^2 = 0.8543, p-value = 0.005307).

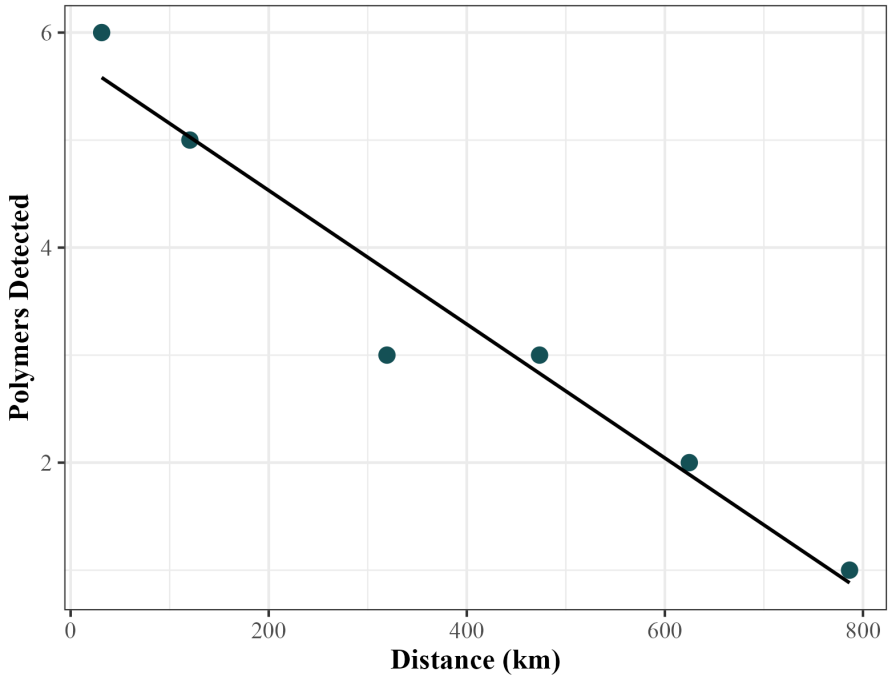

Figure 10: A scatter plot comparing total number of polymers detected compared to distance from shore, with the linear trend line added (equation: $y = -0.0062235x + 5.7768598$, adjusted $R^2 = 0.9385$, p-value = 0.0009242).

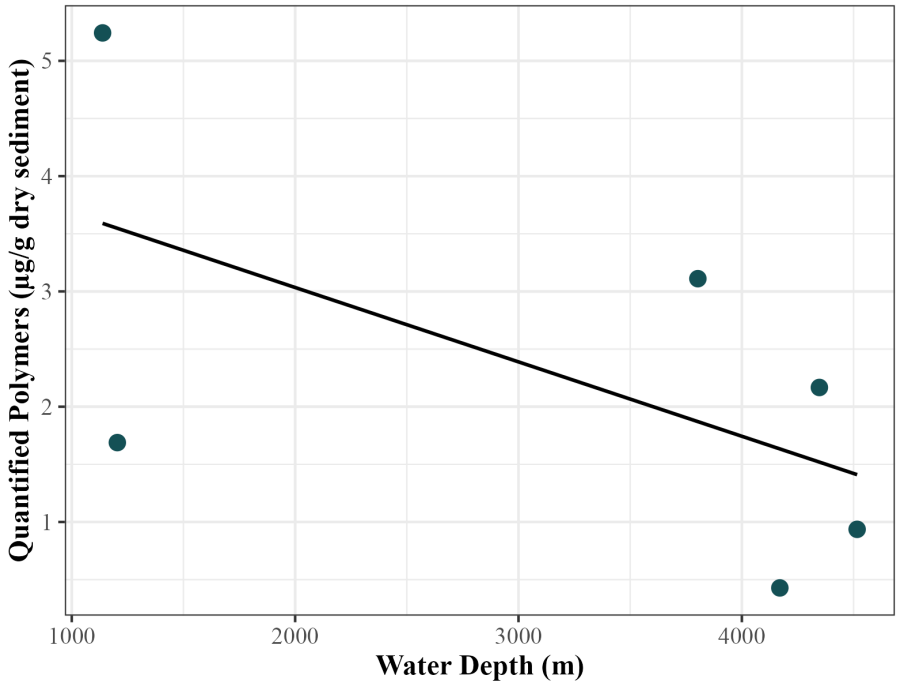

Figure 11: A scatter plot comparing total quantified polymers compared to water depth, with the linear trend line added (equation: y = -0.0006452x + 4.3244880, adjusted R^2 = 0.185, p-value = 0.2178).

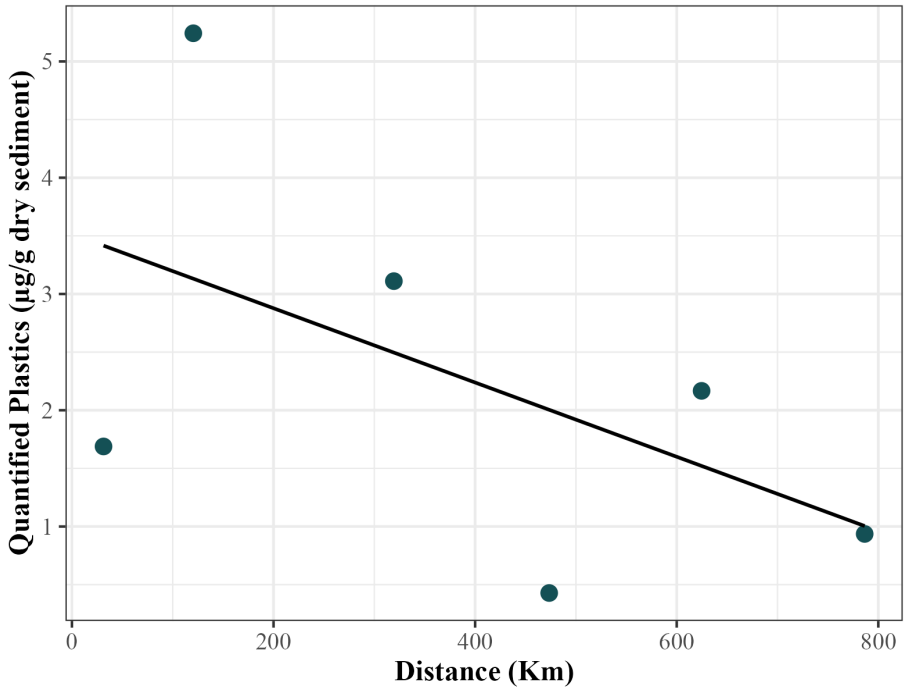

Figure 12: A scatter plot comparing total quantified polymers compared to distance from shore, with the linear trend line added (equation: y = -0.003193x + 3.515916, adjusted R^2 = 0.185, model = 0.2722).

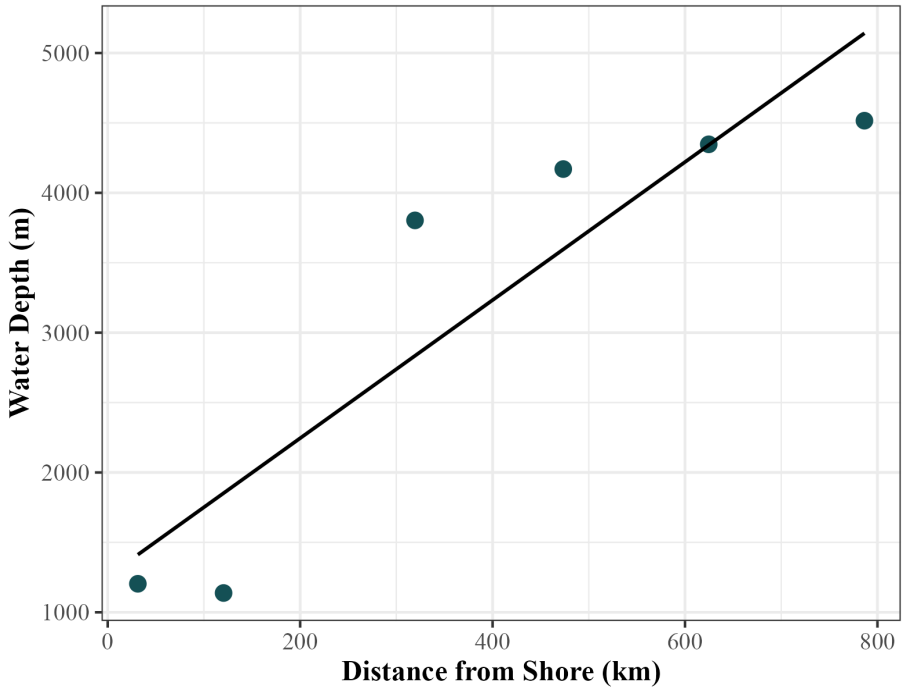

Figure 13: A scatter plot demonstrating the collinearity between water depth and distance from shore, with the linear trend line added (equation: $y = 4.938x + 1257.460$, adjusted $R^2 = 0.1101$, p-value = 0.0123).

3.4 Difference Between Lab Blanks & Samples

The average number of particles detected (on a per sample basis) was higher in the samples (n = 6, mean = 3.33, standard deviation = 1.86) compared to the lab blanks (n = 3, mean = 2, standard deviation = 0), however the results of the Wilcoxon test supported that there was no significant difference between the two groups (W = 4.5, p-value = 0.2785). The only polymers detected in the lab blanks were PC and PP, while the samples contained Nylon-6, PAN, PC, PET, PMMA, PP, and PS.

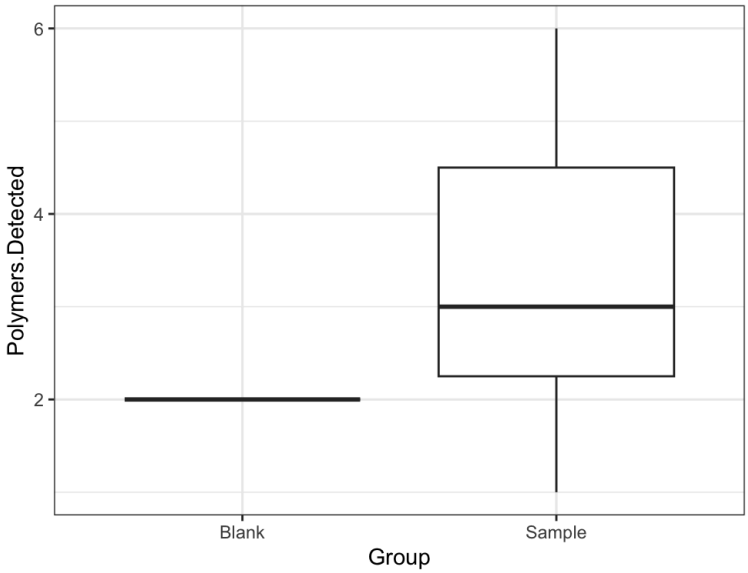

Figure 14: A box plot showing the number of polymers detected in the lab blanks vs. the samples.

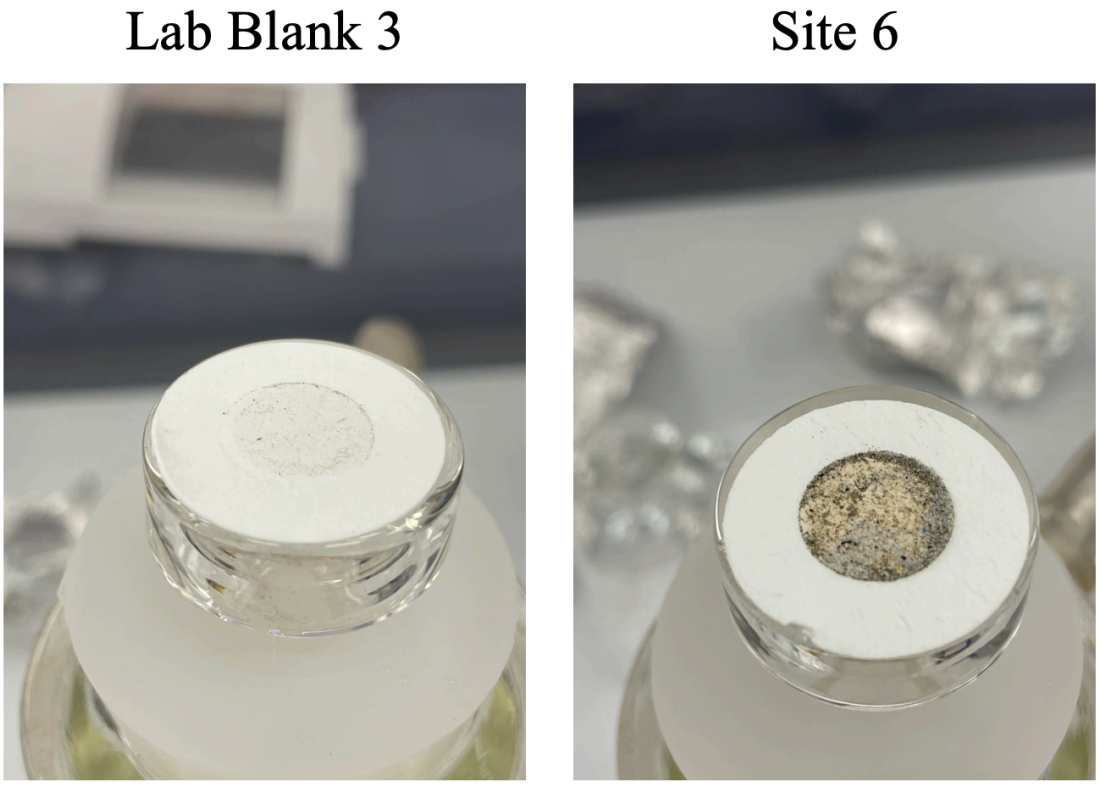

Figure 15: Photographs of both a lab blank (Lab Blank 3) and a sediment sample (Site 6).

3.5 Water Sample Trial

No marker compounds were detected in the water samples, suggesting that in the future they should be concentrated and cleaned up using the density separation device. The density separation device would be able to eliminate organic material which was accumulating on the filter and causing a filter switch every 100 mL. By only using one glass fiber filter for the entire water sample, we would have our best chance at detecting polymer presence.

3.6 ^{210}Pb Dating

The summarized results of the ^{210}Pb dating of the top layer of the sediment scores can be seen in Table 7, with the full report included in the Supplementary Information.

Table 7: The summarized results of the ^{210}Pb dating. Depth is in cm and years are listed in calendar years ± standard deviation. The color scheme is as follows: red = 2021-2022, orange = 2011-2020, yellow = 2001-2010, light green = 1991-2000, dark green = 1981-1990, light blue = 1971-1980, dark blue = 1961-1970, light purple = 1951-1960, and dark purple = pre 1950.

	Offshore		Site Number		Nearshore	
Depth	1	2	3	4	5	6
0	2022 ± 0	2022 ± 0	2022 ± 0	2022 ± 0	2022 ± 0	2022 ± 0
0.5	2015 ± 2	2019 ± 2	2019 ± 2	2013 ± 2	2010 ± 2	2014 ± 2
1.5	2003 ± 2	2012 ± 2	2014 ± 2	1991 ± 2	1993 ± 2	2001 ± 2
2.5	1995 ± 3	2004 ± 3	2011 ± 3	1951 ± 3	1986 ± 3	1990 ± 3
3.5	1989 ± 4	1997 ± 4	2008 ± 4	1863 ± 19	1979 ± 3	1982 ± 4
4.5	1983 ± 5	1993 ± 5	2005 ± 5		1962 ± 6	1974 ± 5
5.5	1979 ± 6	1990 ± 5	2002 ± 6		1936 ± 11	1967 ± 6
6.5	1974 ± 7	1985 ± 7	1998 ± 7		1924 ± 12	1959 ± 8
7.5	1966 ± 9	1979 ± 8	1994 ± 8		1920 ± 12	1952 ± 10
8.5	1951 ± 15	1966 ± 14	1990 ± 10		1913 ± 14	1948 ± 12
9.5			1989 ± 11		1898 ± 16	1938 ± 15

4. DISCUSSION

4.1 Microplastic Concentrations in Sediment

Our results demonstrated that not all sediment habitat is equal to one another in terms of microplastic concentration, with sites closer to shore bearing the burden of higher concentrations. This is not a new concept, and previous studies have looked at a variety of factors which could influence the concentrations. A few factors include: region sampled, year sampled, depth of ocean floor, slope of ocean floor, shipping intensity, fishing effort, distance to shore, and population density (Zhu et al., 2024). While the scope of this thesis was not to determine causes

of microplastic concentration distributions, we did collect data on both water depth and distance from shore and discuss findings here.

Two studies that looked at microplastic concentrations in the sea floor saw the highest concentrations in the coastal regions (Martin et al., 2022; Zhu et al., 2024). While they targeted slightly larger size classes than this study which targeted particles greater than 20 µm (Martin et al., 2022: 10 µm - 25 mm and Zhu et al., 2024: > 5 mm), it provides some insight into how our trends might fit into the global picture. A separate review paper of microplastics in sediments also concluded that plastics in sediments are concentrated in coastal environments (Harris et al., 2020). It is worth questioning: are the highest concentrations in coastal sediments due to physical or human effects? Coastal sediments are shallower in depth, requiring less time for plastics to sink. However, coastal communities can also be the source of plastics into the nearby oceans through mismanaged waste, river input, atmospheric deposition, runoff, and wastewater outflows which may affect sinking concentrations (Bao et al., 2023; Jambeck et al., 2015; Martin et al., 2020; Sutton et al., 2016; Wright et al., 2020). This again highlights how correlated water depth and distance from the coastlines are intertwined with one another.

Previous studies have examined how water depth influences microplastic deposition. One study estimated that out of their 25-900 Tg seafloor estimate of plastics between 10 µm - 25 mm in sediment, 60 % were accumulated in the slope region and only 0.1% in the abyssal plain region, even though it covers a much larger percent of the ocean floor. (Martin et al., 2022). They also concluded that plastic concentrations were at their lowest at water depths greater than 4,000 m, suggesting that the deep sea is not as large of a sink as it was once predicted (Martin et al., 2022). Looking at a larger size class than this study, Zhu et al., 2024 estimated that 46% of plastics > 5mm were found at depths shallower than 200 m. These findings are consistent with

the fact that we saw a greater diversity and concentration of polymers closer to shore. Additional studies have also determined the importance of bathymetry along with depth. Barrett et al., 2020 found a significant relationship between the slope of the seafloor and the amount of plastic found, with higher slope angle leading to more plastic on the ocean floor.

Particle size and water depth also prove to be important factors when looking at plastic concentrations. Kooi et al., 2017 looked at the sinking speeds of different sized PVC particles and found that a 10 mm particle would need only 1.6 minutes to sink to 4,000 m, whereas a 0.1 mm particle of the same polymer would take 10 days, and a 1 μm particle would need 278 years. This demonstrates that when the polymer is the same, size will drive sinking rates. This also suggests that there could potentially be a lag which affects concentrations in different benthic environments. Biofouling also alters the initial density of plastic particles, causing once buoyant particles to sink in the water column (Gaylarde et al., 2023; Li et al. 2023). However, there might be a limit as to how far biofouled particles can sink. At a certain depth, the algae is unable to continue growing and combined with remineralization, causes the plastic to rise in the water column until it reaches a shallow enough depth at which algae can grow on it again. This creates a cycle of plastic moving up and down in the water column, without reaching the bottom (Kooi et al., 2017).

When looking at polymer densities, we saw both “floaters” (polymers with densities less than seawater) and “sinkers” (polymers with densities greater than seawater). The only “floater” polymer we saw in the samples was PP which was detected at Sites 3 through 6. We did not see any PE in any of the samples. This was surprising because even though it is a “floater”, it has been recorded in the sediments previously (Simon-Sánchez et al., 2022) and we know PE is found in the GPGP, a potential offshore source of microplastics (Egger et al., 2020). The majority

of the polymers we detected in our samples were “sinkers”, and have a density greater than seawater, which can drive them to sink in the water column. These findings are similar to Brignac et al., 2019, which cataloged meso to macro-plastic marine debris found in four environmental compartments in the Hawaiian Islands and found > 75% of the polymers on the sea floor were “sinkers”. While distance from shore, depth, and size of plastics vary between their study and ours, the polymer stratification did not. While beyond the scope of this thesis, the buoyant polymers found in sediments were often biofouled causing them to sink (Brignac et al., 2019). We were unable to observe biofouling with our samples due to the small size of the microplastics and cannot draw any conclusions if biofouling caused the “floaters” to sink.

Future research must take into account what happens to plastic once it reaches the sediment. Depending on burial rates, bioturbation, natural or human-caused disturbance, plastics could be resuspended into the environment or moved around within the sediment profile (Kane et al., 2019). If so, sediment cores may not be as great of a time series as once thought. Continued sampling of the deeper layers of the sediment core will aid in understanding if this has an effect.

4.2 Application of the Density-Separation Method & Py-GC/MS

This study was able to extract an originally unknown amount of microplastic particles from sediment ranging from the continental shelf to the deep sea. This finding supports the advantages and utility of the DSD created by members of CMDR and Coastal Ocean Vision, as a useful tool in quantifying microplastics (Shaw et al., in review). Since the average number of particles in the samples was greater than the lab blanks, this demonstrates that the DSD can separate *in situ* plastics from the natural sediment matrix.

The pros of the DSD used in this project are that it is very accessible to any researcher due to its inexpensive price and ease of ordering through Amazon, a mainstream retailer. The entire cost (as of 2022) for one set-up is $167.32 (Table S1), which is relatively inexpensive compared to other methods. The device is not made out of plastic (except the silicone o-ring between the pieces) which is advantageous compared to other plastic devices made in the past. The entire protocol is fairly straightforward and the video created explaining its use will be helpful in implementation beyond CMDR (Shaw et al., in Review).

It is worth noting that sodium polytungstate is not a cheap chemical, making it potentially less accessible to all. However, it is less toxic compared to other density-separation chemicals. The DSD decreased the sample mass by 99.925 +/- 0.0756%, leaving the majority of the sediment and organic material in the bottom chamber of the DSD while floating plastic particles accumulated in the top chamber (Table S4). Unfortunately our initial gold filters were still too overloaded to acquire accurate spectra and particle counts, forcing the switch away from μFTIR to Py-GC/MS. Even on the larger diameter PC filters that were used for imagery, we still ran into issues of clumping and crowding of particles making it very difficult to visualize particles. Large clumps of particles make it difficult to focus on one plane, which leads to an underestimation of particles present. While unideal, if we had been forced to continue with μFTIR we would have needed to develop a way to subset the sample to have fewer particles on each filter. This assumes that the particles could act homogeneously in a solution, which is unlikely (Thaysen et al., 2020). Other attempts at CMDR have tried to subset samples with minimal success at accurately predicting the number of particles that will end up on each filter. This overloading of filters was the main reason for the switch to Py-GC/MS. Potential future studies could delve into the major components in different types of sediment to determine if there is more suitable chemical

digestion. Additionally, more research could be done regarding the time the sample spends in digestion. Shaw et al., added the vacuum step to help eliminate organic material, suggesting that there might be other aspects of the procedure that could improve decreasing organic material while still preserving plastics. The DSD also struggles with recovery of fibers (Athey & Erdle, 2021). A spike-recovery study, in which a known quantity of microplastics are added to a sample to determine the effectiveness of the method in recovering those microplastics, was used to develop the DSD. The DSD struggled to recover fibers compared to other polymers: 25.9% for cellulose acetate fibers and 20.7% for PEST fibers, where no fragment recovery fell below 78.4% (Shaw et al., in review). Overall, the DSD was able to separate out microplastics from the sediment, but because not all sediment is created equal, modifications for each study will be required to increase effectiveness.

We were also able to use the Py-GC/MS to quantify microplastic masses, supporting our original objective. Py-GC/MS is a newer approach to analyzing microplastics in a variety of matrices, and the methods can continue to be improved. More work is being done on determining the effects of organic matrices on polymers, including sediments (Bouzid et al., 2022). By understanding if there are interactions with the matrix, we will be able to take appropriate measures when creating reference curves. Due to the higher frequency of spectroscopic approaches, mass fraction estimates for polymers in sediments are lacking in the literature. Only one of the studies mentioned in the review of the sediment cores earlier, reported any type of mass measurement. This lack of established mass concentrations in previous studies forced us to "shoot in the dark" when choosing reference polymer weights for our calibration curve. Now after analyzing the top layer, which we predict to have the highest amount of plastic, we have a better understanding of how much is in our samples and how to improve our calibration curve

points. We can focus our efforts on including more points in the smaller range of our calibration curve to feel even more confident in our calculations. While weighing the standards can be quite cumbersome, our results demonstrate the importance of having those small values included in our curve. Rather than targeting one point under 10 µg, we could include multiple points, making sure at least one is smaller than 5 µg. However, there is not much more room to lower the mass of our first point. The approach of weighing polymers by hand is limited by the capabilities and accuracy of the balance (in our case: 0.1 ug). It is important to not extrapolate mass measurements beyond the calibration curve created, which is why weighing out the smallest mass we can actually obtain while feeling confident in the accuracy of our balance is so important. There are other options to create calibration curves that could create lower quantification limit, but they are inconsistent with the way our samples are processed, which is more important (Seeley & Lynch, 2023).

Py-GC/MS is a destructive sampling method, meaning that once the filters are run, there is no second chance at analysis. Py-GC/MS also does not give any detail about size, shape, and color like µFTIR can give. FTIR or other spectroscopy methods do not give a mass, rather it is typically calculated using the size measurements and the average density of the polymer. We combatted this lack of particle information by photographing the filters prior to the Py-GC/MS, but we still could not count particles, let alone fibers, in the overloaded organic material on the filters. This again highlights the importance of effective cleanup methods or the need to subsample in order to spread the particles out on the filters. The blank samples had almost no organic material so it was much easier to see fibers present. Although we could visually see fibers, we could not confirm if they were plastic or not, which decreases their usefulness in this study. However, potentially comparing our sample photos to the polymer quantification results

can provide some insight in the future analyses of filter photos. We are also still learning the capabilities of the Py-GC/MS. Py-GC/MS struggled with the identification of PVC in the samples due to the nonspecific marker compounds that have been chosen before in the literature, which can be found in other things beyond PVC. By continuing to explore the Py-GC/MS we will be able to improve our confidence in both detection and quantification of polymers.

While the methods were successful, there are always improvements that can be made. Because the samples were originally prepared for μFTIR, the lowest size limit possible for Py-GC/MS was not used in this study. Our μFTIR instrument can only accurately identify particles that are greater than 30 μm, so we used 20 μm sieves and filters in our processing. Py-GC/MS can detect any size particle as long as the mass is greater than the detection limit. This means that we limited our particle size range to anything larger than 20 μm, something we would do differently in the future. Swapping the 20 μm pore sieve for a 5 μm pore sieve unlocks an even smaller size class that is not often explored with microplastics.

Density separation is an effective method at separating plastic from an organic matrix and should be used in all studies looking at plastics in a complex organic matrix, like sediment. While every matrix will be different and require slight modifications, the overall process should become more standardized across the field. The device used in this study is cost effective and easy to acquire which makes it the prime candidate for use across the board. By using the same protocol, studies will be able to be compared easier than they are now. While sodium polytungstate is an expensive chemical, it is less toxic and can be brought to a density high enough to account for all polymer types of interest, which is vital for comparison. Density separation, combined with more useful reporting metrics such as size class analyzed, will foster future comparisons and allow scientists to gain a more holistic understanding.

Py-GC/MS is an effective tool at identifying polymers and quantifying plastic masses. It can be incredibly useful for analyzing smaller size classes and complex matrices. And it acquires a more accurate mass compared to spectroscopy, which relies on the average density calculations. It also has the opportunity to understand additives, which is important for future work. However, no method is perfect, and the lack of polymer color, shape, and size limits the understanding of the polymer prior to its analysis. The sampling method is destructive, leaving no opportunity for secondary analysis. Just like FTIR, it has some polymer limitations, especially PVC and even PET at smaller concentrations. Because of its newness in this aspect, more work is being done to understand interactions between polymers and interactions within the matrix. At this time, it is more important that studies confirm polymer type in their samples with whatever method they have access to compared to only focusing on recommending one polymer identification method that not everybody uses quite yet. When reporting polymer analysis, including the caveats of the method chosen is vital for readers to gain context about the results.

5. CONCLUSIONS

This study analyzed sediment cores from the North Pacific Ocean, spanning a transect of almost 800 km, making it one of the largest studies to date. We found that the number of polymers detected increased as sites moved from offshore to onshore. There was also a significant negative correlation between the number of polymers detected, water depth, and distance from shore. However, it is difficult to determine which is driving the trend we see due to their high correlation with one another. These results support previous hypotheses that not all benthic sediment is equal. This study also successfully trialed the density-separation device created by CMDR and collaborators on environmental samples, finding different polymers in our

samples compared to the lab blanks. By working to create more standardized methods across studies we will be able to make cross-ocean comparisons, which will be vital in filling in the knowledge gaps about plastic transport into sediments.

REFERENCES

Andrady, A. L. (2011). Microplastics in the marine environment. *Marine Pollution Bulletin*, *62*(8), 1596–1605. https://doi.org/10.1016/j.marpolbul.2011.05.030

Athey, S. N., & Erdle, L. M. (2022). Are We Underestimating Anthropogenic Microfiber Pollution? A Critical Review of Occurrence, Methods, and Reporting. *Environmental Toxicology and Chemistry*, *41*(4), 822–837. https://doi.org/10.1002/etc.5173

Barrett, J., Chase, Z., Zhang, J., Holl, M. M. B., Willis, K., Williams, A., Hardesty, B. D., & Wilcox, C. (2020). Microplastic Pollution in Deep-Sea Sediments From the Great Australian Bight. *Frontiers in Marine Science*, *7*, 576170. https://doi.org/10.3389/fmars.2020.576170

Bao, M., Xiang, X., Huang, J., Kong, L., Wu, J., & Cheng, S. (2023). Microplastics in the Atmosphere and Water Bodies of Coastal Agglomerations: A Mini-Review. *International Journal of Environmental Research and Public Health*, *20*(3), 2466. https://doi.org/10.3390/ijerph20032466

Bouzid, N., Anquetil, C., Dris, R., Gasperi, J., Tassin, B., & Derenne, S. (2022). Quantification of Microplastics by Pyrolysis Coupled with Gas Chromatography and Mass Spectrometry in Sediments: Challenges and Implications. *Microplastics*, *1*(2), 229–239. https://doi.org/10.3390/microplastics1020016

Brignac, K. C., Jung, M. R., King, C., Royer, S.-J., Blickley, L., Lamson, M. R., Potemra, J. T., & Lynch, J. M. (2019). Marine Debris Polymers on Main Hawaiian Island Beaches, Sea Surface, and Seafloor. *Environmental Science & Technology*, *53*(21), 12218–12226. https://doi.org/10.1021/acs.est.9b03561

Coralli, I., Goßmann, I., Fabbri, D., & Scholz-Böttcher, B. M. (2023). Determination of polyurethanes within microplastics in complex environmental samples by analytical pyrolysis. *Analytical and Bioanalytical Chemistry*, *415*(15), 2891–2905. https://doi.org/10.1007/s00216-023-04580-3

Cózar, A., Echevarría, F., González-Gordillo, J. I., Irigoien, X., Úbeda, B., Hernández-León, S., Palma, Á. T., Navarro, S., García-de-Lomas, J., Ruiz, A., Fernández-de-Puelles, M. L., & Duarte, C. M. (2014). Plastic debris in the open ocean. *Proceedings of the National Academy of Sciences*, *111*(28), 10239–10244. https://doi.org/10.1073/pnas.1314705111

Diesing, M. (2020). Deep-sea sediments of the global ocean. *Earth System Science Data*, *12*(4), 3367–3381. https://doi.org/10.5194/essd-12-3367-2020

Egger, M., Sulu-Gambari, F., & Lebreton, L. (2020). First evidence of plastic fallout from the North Pacific Garbage Patch. *Scientific Reports*, *10*(1), 7495. https://doi.org/10.1038/s41598-020-64465-8

Eriksen, M., Lebreton, L. C. M., Carson, H. S., Thiel, M., Moore, C. J., Borerro, J. C., Galgani, F., Ryan, P. G., & Reisser, J. (2014). Plastic Pollution in the World's Oceans: More than 5 Trillion Plastic Pieces Weighing over 250,000 Tons Afloat at Sea. *PLoS ONE*, *9*(12), e111913. https://doi.org/10.1371/journal.pone.0111913

Galgani, L., Goßmann, I., Scholz-Böttcher, B., Jiang, X., Liu, Z., Scheidemann, L., Schlundt, C., & Engel, A. (2022). Hitchhiking into the Deep: How Microplastic Particles are Exported through the Biological Carbon Pump in the North Atlantic Ocean. *Environmental Science & Technology*, *56*(22), 15638–15649. https://doi.org/10.1021/acs.est.2c04712

Gaylarde, C. C., De Almeida, M. P., Neves, C. V., Neto, J. A. B., & Da Fonseca, E. M. (2023). The Importance of Biofilms on Microplastic Particles in Their Sinking Behavior and the Transfer of Invasive Organisms between Ecosystems. *Micro*, *3*(1), 320–337. https://doi.org/10.3390/micro3010022

Harris, P. T. (2020). The fate of microplastic in marine sedimentary environments: A review and synthesis. *Marine Pollution Bulletin*, *158*, 111398. https://doi.org/10.1016/j.marpolbul.2020.111398

Ishimura, T., Iwai, I., Matsui, K., Mattonai, M., Watanabe, A., Robberson, W., Cook, A.-M., Allen, H. L., Pipkin, W., Teramae, N., Ohtani, H., & Watanabe, C. (2021). Qualitative and quantitative analysis of mixtures of microplastics in the presence of calcium carbonate by pyrolysis-GC/MS. *Journal of Analytical and Applied Pyrolysis*, *157*, 105188. https://doi.org/10.1016/j.jaap.2021.105188

Jambeck, J. R., Geyer, R., Wilcox, C., Siegler, T. R., Perryman, M., Andrady, A., Narayan, R., & Law, K. L. (2015). Plastic waste inputs from land into the ocean. *Science*, *347*(6223), 768–771. https://doi.org/10.1126/science.1260352

Kane, I. A., & Clare, M. A. (2019). Dispersion, Accumulation, and the Ultimate Fate of Microplastics in Deep-Marine Environments: A Review and Future Directions. *Frontiers in Earth Science*, *7*, 80. https://doi.org/10.3389/feart.2019.00080

Kooi, M., Nes, E. H. V., Scheffer, M., & Koelmans, A. A. (2017). Ups and Downs in the Ocean: Effects of Biofouling on Vertical Transport of Microplastics. *Environmental Science & Technology*, *51*(14), 7963–7971. https://doi.org/10.1021/acs.est.6b04702

Lebreton, L., Slat, B., Ferrari, F., Sainte-Rose, B., Aitken, J., Marthouse, R., Hajbane, S., Cunsolo, S., Schwarz, A., Levivier, A., Noble, K., Debeljak, P., Maral, H., Schoeneich-Argent, R., Brambini, R., & Reisser, J. (2018). Evidence that the Great Pacific Garbage Patch is rapidly accumulating plastic. *Scientific Reports*, *8*(1), 4666. https://doi.org/10.1038/s41598-018-22939-w

Lebreton, L., Egger, M., & Slat, B. (2019). A global mass budget for positively buoyant macroplastic debris in the ocean. *Scientific Reports*, *9*(1), 12922. https://doi.org/10.1038/s41598-019-49413-5

Li, J., Shan, E., Zhao, J., Teng, J., & Wang, Q. (2023). The factors influencing the vertical transport of microplastics in marine environment: A review. *Science of The Total Environment*, *870*, 161893. https://doi.org/10.1016/j.scitotenv.2023.161893

Martin, C., Baalkhuyur, F., Valluzzi, L., Saderne, V., Cusack, M., Almahasheer, H., Krishnakumar, P. K., Rabaoui, L., Qurban, M. A., Arias-Ortiz, A., Masqué, P., & Duarte, C. M. (2020). Exponential increase of plastic burial in mangrove sediments as a major plastic sink. *Science Advances*, *6*(44), eaaz5593. https://doi.org/10.1126/sciadv.aaz5593

Martin, C., Young, C. A., Valluzzi, L., & Duarte, C. M. (2022). Ocean sediments as the global sink for marine micro‐ and mesoplastics. *Limnology and Oceanography Letters*, *7*(3), 235–243. https://doi.org/10.1002/lol2.10257

Maximenko, N.A., and J. Hafner, 2010: *SCUD: Surface Currents from Diagnostic model*, IPRC Tech. Note 5, 17pp.

Olivelli, A., Hardesty, B. D., & Wilcox, C. (2020). Coastal margins and backshores represent a major sink for marine debris: Insights from a continental-scale analysis. *Environmental Research Letters*, *15*(7), 074037. https://doi.org/10.1088/1748-9326/ab7836

PlasticsEurope. (2019). *Plastics- the facts 2019*.

R Core Team (2023). _R: A Language and Environment for Statistical Computing_. R Foundation for Statistical Computing, Vienna, Austria. <https://www.R-project.org/>.

Seeley, M. E., & Lynch, J. M. (2023). Previous successes and untapped potential of pyrolysis–GC/MS for the analysis of plastic pollution. *Analytical and Bioanalytical Chemistry*, *415*(15), 2873–2890. https://doi.org/10.1007/s00216-023-04671-1

Seibold, E. (1975). Der Meeresboden Forschungsstand und Zukunftsaufgaben. *Die Naturwissenschaften*, *62*(7), 321–330. https://doi.org/10.1007/BF00608892

Shaw, K., Sandquist, R., Fairclough, C., Black, J., Fitzgerald, A., Gallager, S., & Lynch, J. (in Review). Separation of microplastics from deep-sea sediment using an affordable, simple to use, and easily accessible density separation device.

Simon-Sánchez, L., Grelaud, M., Lorenz, C., Garcia-Orellana, J., Vianello, A., Liu, F., Vollertsen, J., & Ziveri, P. (2022). Can a Sediment Core Reveal the Plastic Age? Microplastic Preservation in a Coastal Sedimentary Record. *Environmental Science & Technology*, *56*(23), 16780–16788. https://doi.org/10.1021/acs.est.2c04264

Sutton, R., Mason, S. A., Stanek, S. K., Willis-Norton, E., Wren, I. F., & Box, C. (2016). Microplastic contamination in the San Francisco Bay, California, USA. *Marine Pollution Bulletin*, *109*(1), 230–235. https://doi.org/10.1016/j.marpolbul.2016.05.077

Thaysen, C., Munno, K., Hermabessiere, L., & Rochman, C. M. (2020). Towards Raman Automation for Microplastics: Developing Strategies for Particle Adhesion and Filter Subsampling. *Applied Spectroscopy*, *74*(9), 976–988. https://doi.org/10.1177/0003702820922900

Thompson, R. C., Olsen, Y., Mitchell, R. P., Davis, A., Rowland, S. J., John, A. W. G., McGonigle, D., & Russell, A. E. (2004). Lost at Sea: Where Is All the Plastic? *Science*, *304*(5672), 838–838. https://doi.org/10.1126/science.1094559

Tsuge, S., Ohtani, H., & Watanabe, C. (2011). *Pyrolysis-GC/MS Data Book of Synthetic Polymers: Pyrograms, Thermograms and MS of Pyrolyzates*. Elsevier.

Van Sebille, E., Wilcox, C., Lebreton, L., Maximenko, N., Hardesty, B. D., Van Franeker, J. A., Eriksen, M., Siegel, D., Galgani, F., & Law, K. L. (2015). A global inventory of small floating plastic debris. *Environmental Research Letters*, *10*(12), 124006. https://doi.org/10.1088/1748-9326/10/12/124006

Woodall, L. C., Sanchez-Vidal, A., Canals, M., Paterson, G. L. J., Coppock, R., Sleight, V., Calafat, A., Rogers, A. D., Narayanaswamy, B. E., & Thompson, R. C. (2014). The deep sea is a major sink for microplastic debris. *Royal Society Open Science*, *1*(4), 140317. https://doi.org/10.1098/rsos.140317

Wright, S. L., Ulke, J., Font, A., Chan, K. L. A., & Kelly, F. J. (2020). Atmospheric microplastic deposition in an urban environment and an evaluation of transport. *Environment International*, *136*, 105411. https://doi.org/10.1016/j.envint.2019.105411

Zhu, X., Rochman, C. M., Hardesty, B. D., & Wilcox, C. (2024). Plastics in the deep sea – A global estimate of the ocean floor reservoir. *Deep Sea Research Part I: Oceanographic Research Papers*, *206*, 104266. https://doi.org/10.1016/j.dsr.2024.104266

CHAPTER 3

Thoughts & Reflections

This thesis is a prime example of CMDR's goals and objectives and highlights the relationship between NIST and HPU. I was able to adapt and apply methods designed prior to my arrival and apply them to real-world environmental samples. The samples proved to behave differently than the spike-recovery trial and gave us insight into how to improve the method, which is quickly becoming a staple in our lab and used across many different projects. When attending the Ocean Sciences Meeting 2024, many were eager to hear about my experience due to the difficulty of trying to develop a density separation method on their own. By demonstrating the DSD's ability to work for different types of sediment we help our goal of creating more standardization across studies, which can be especially difficult in our field.

Some lessons learned throughout the project:

- Subsampling is not ideal mainly due to the fact that plastic particles do not mix homogeneously in solution: to avoid having to do this with my samples we switch to the Py-GC/MS (something that does not rely on visual detection)
- As mentioned throughout the discussion, Py-GC/MS offers both advantages and disadvantages to the analysis
    - The main disadvantage for this study was the fact we could not count the particles, which would allow us to compare against other studies
- Future focus during calibration curve creation should include more points in the smallest size range (for us less than 10µg) with hopes of quantifying more particles

- It is not only the chemicals chosen for digestion, but also the method in which they are applied
    - The samples that underwent the two step process back to back had more organic material left behind compared to the samples that were dried between digestion steps
- The calibration curves surprisingly fit a polynomial curve instead of being linear

Future directions are numerous and suggested as follows:

- Analyzing additional layers of sediment in the same way as the top layer with layers selected based on the Pb210 data, potentially targeting specific decades
- Analyzing the bottom water samples for either microplastics or plastic additives (or both) using the DSD to handle the organic material
- Spending time looking at the thermal desorption chromatograms to understand if plastic additives are in the sediment samples
- Spending time looking for non-targeted polymers in the pyrograms of the top sediment layer samples
- If continuing with the Py-GC/MS, use smaller sieves and filter pore sizes in order to unlock an even smaller size class of microplastics (5 - 20 μm)
- Continue to use and understand the capabilities of the Py-GC/MS
    - Looking further into the creation of calibration curves, especially creating ones that can detect small amounts of polymers
    - Spend more time analyzing the marker compounds for PVC

    - Understanding how Py-GC/MS compares to our other methods of polymer identification (FTIR & Raman), especially looking at the scrape blank which was processed both ways during this study
- Continue to use and improve the density separation device, particularly improving overall fiber recovery

SUPPLEMENTARY INFORMATION

Table S1 from Shaw et al., in Review: Amazon parts List for Accessible and Inexpensive DSD Components (prices as of Dec. 2022).

Part Name	Price	Quantity	Total Price
Vacuum Top	$9.99	1	$9.99
End Caps	$6.59	2	$13.18
Ball Valve	$26.99	1	$26.99
Stainless Steel Balls	$14.99	1	$14.99
Sight Glass	$35.99	2	$71.98
Sieve Top	$17.00	1	$17.00
O-Ring	$13.19	1	$13.19
		Final Price:	**$167.32**

Table S2: The known masses of reference polymers, those denoted with * were used to create external calibration curves for quantification.

Polymer	Mix Number	Weight 1 (µg)	Weight 2 (µg)	Weight 3 (µg)	Weight 4 (µg)	Weight 5 (µg)	Weight 6 (µg)
Nylon-6 - 5-cyano-1-pentene	3	3.9*	21.2*	40.4	60.9*	136.4*	162.9*
Nylon-6 - caprolactam	3	3.9*	21.2*	40.4	60.9*	136.4*	162.9*
Polyacrylonitrile (PAN) - 2-methylenepentanedinitrile	1	4.7*	13.3*	27.6*	45.1*	84.1*	106.7*
Polyacrylonitrile (PAN) - hexane-1,3,5-tricarbonitrile (trimer)	1	4.7*	13.3*	27.6*	45.1*	84.1*	106.7*
Polycarbonate (PC) - p-cresol	2	2.1*	18.0*	29.0*	46.5*	71.2*	130.3*
Polycarbonate (PC) - 4-isopropenylphenol	2	2.1*	18.0*	29.0*	46.5*	71.2*	130.3*
Polyethylene Terephthalate (PET) - benzoic acid	2	6.9*	18.4*	63.7*	83.8*	96.9*	113.1*
Polymethylmethacrylate (PMMA) - methyl methacrylate	3	5.4*	28.7*	66.6*	71.0*	84.7	109.7*
Polypropylene (PP) - 2,4-dimethyl-1-heptene	2	4.9*	20.2*	42.0*	60.5*	74.2*	156.1*
Polystyrene (PS) - Styrene Dimer	3	10.8	15.1*	32.1*	55.2*	87.1*	123.9*

Table S3: Polymer Standards Information

Nylon-6: PA6 CMDR Polykit 1.0, cryomilled courtesy of Scott Gallagher

PAN: Scientific Polymer Products, Polyacrylonitrile, CAS# 25014-41-9

PC: Nanochemazone, Polycarbonate Powder, NCZ-LP-112/23

PE: HDPE.1 CMDR Polykit 1.0, cryomilled courtesy of Scott Gallagher

PET: Goodfellow Cambridge Limits, Polyethylene terephthalate (Polyester, PET, PETP) Powder, ES30-PD-000132

PMMA: Goodfellow Cambridge Limits, Polymethylmethacrylate (PMMA, Acrylic) Powder, ME30-PD-000148

PP: PP CMDR Polykit 1.0, cryomilled courtesy of Scott Gallagher

PS: PS CMDR Polykit 1.0, cryomilled courtesy of Scott Gallagher

PVC: PVC.1 CMDR Polykit 1.0, cryomilled courtesy of Scott Gallagher

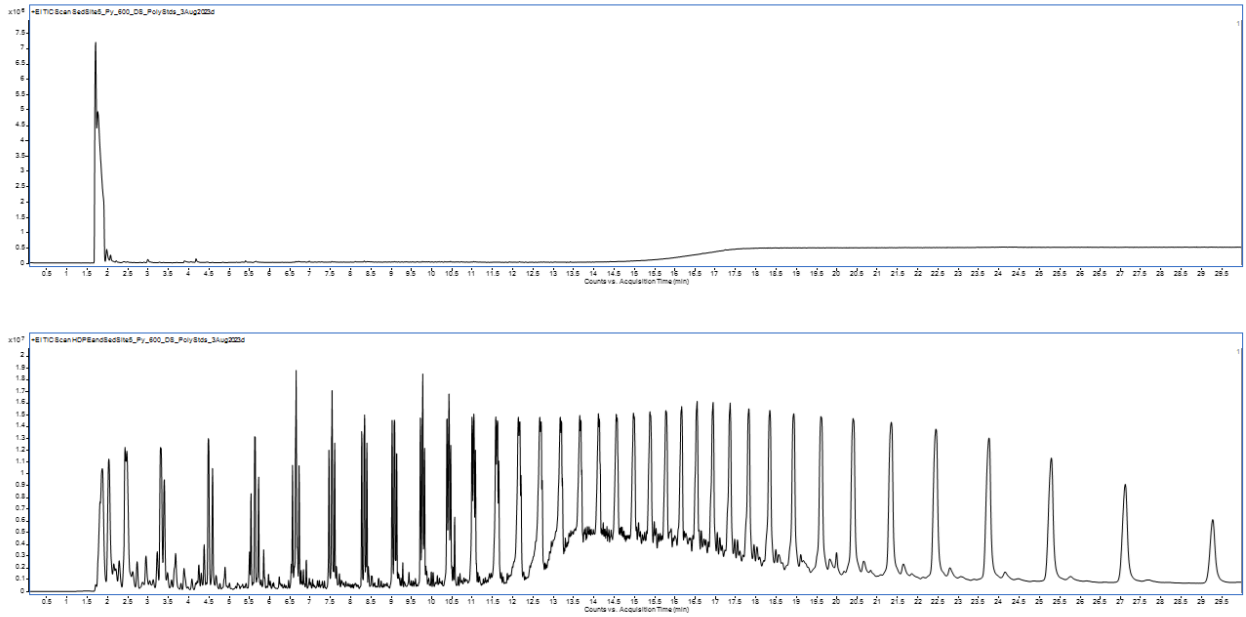

Figure S1: Chromatograms representing some of the sediment collected from the bottom of the density-separation device (Site 5) after use by itself (top) & with a piece of HDPE (bottom).

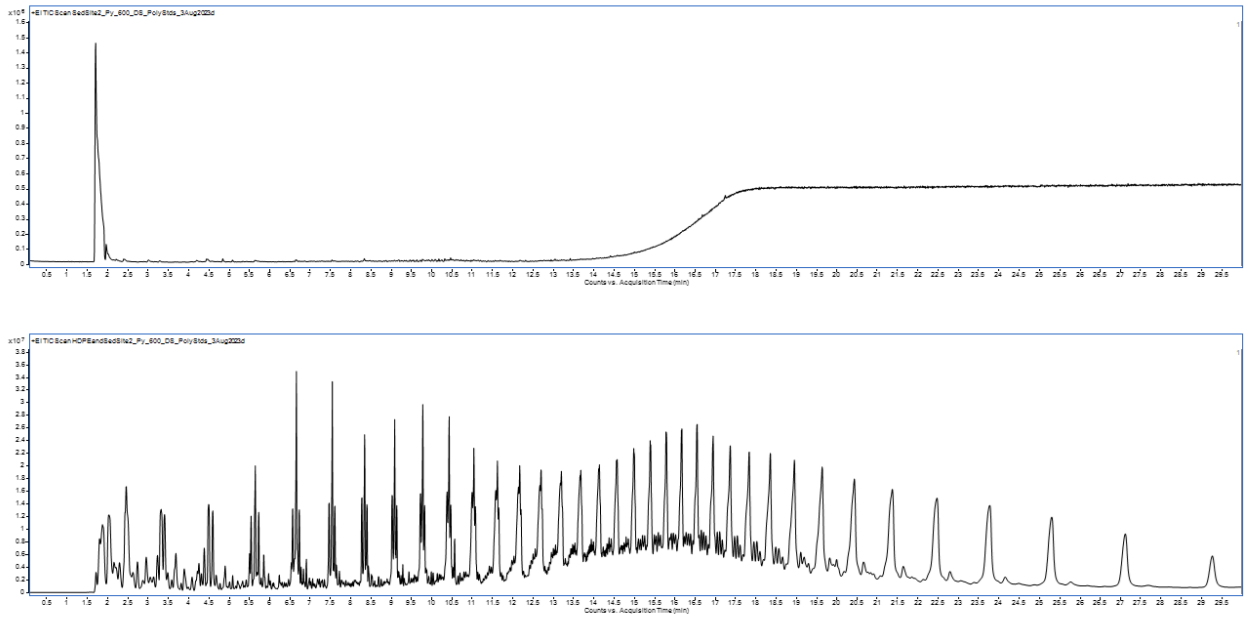

Figure S2: Chromatograms representing some of the sediment collected from the bottom of the density-separation device (Site 2) after use by itself (top) & with a piece of HDPE (bottom).

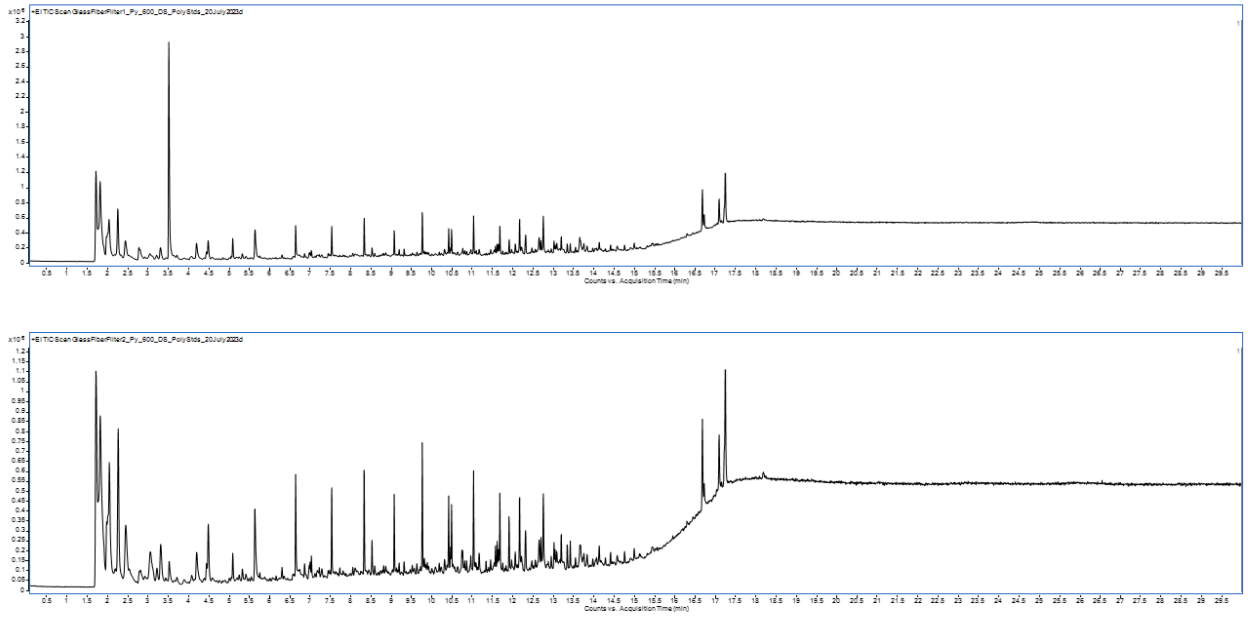

Figure S3: Chromatograms of just the glass fiber filters, demonstrating some of the background noise.

Table S4: A table describing the dry weights of the top layer sediment samples and the weight of the floated particles when it was photographed (the last weight taken of the sample). Average Percent Change = 99.925 +/- 0.0756%.

Site Number	Dry Weight of Sediment added to DSD (g)	Dry Weight of Floated Particles on PC filter (g)	Percent of Original sediment that sank
1	31.382	0.01737	99.94%
2	17.017	0.01551	99.91%
3	17.376	0.00370	99.98%
4	18.031	0.00511	99.97%
5	20.048	0.04341	99.78%
6	24.500	0.00691	99.97%

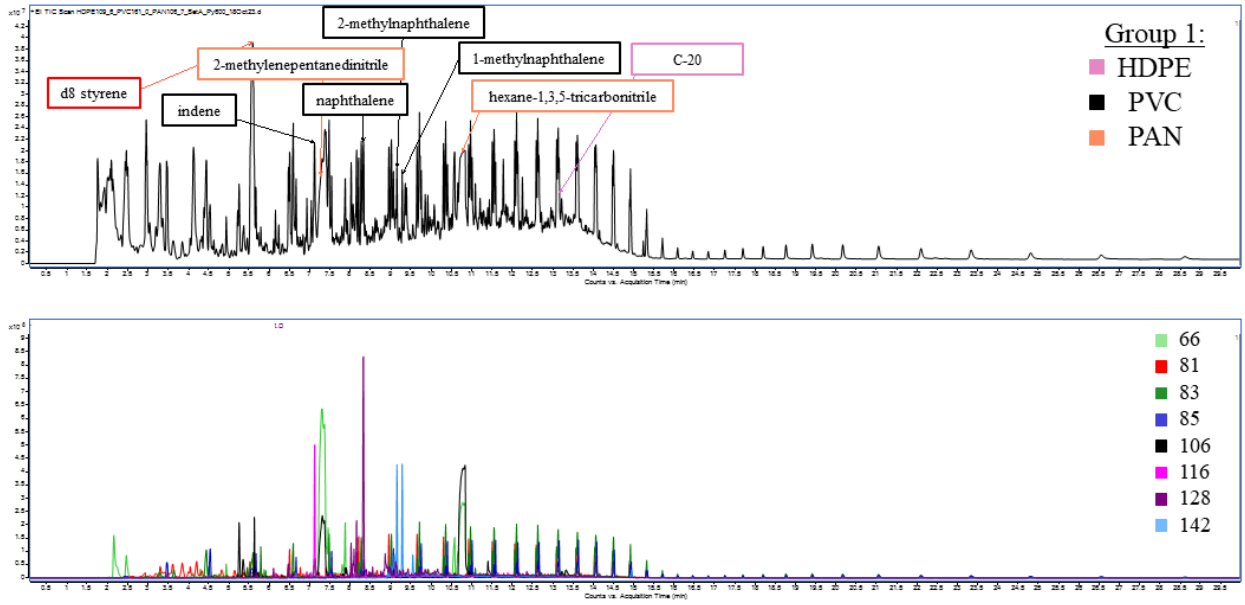

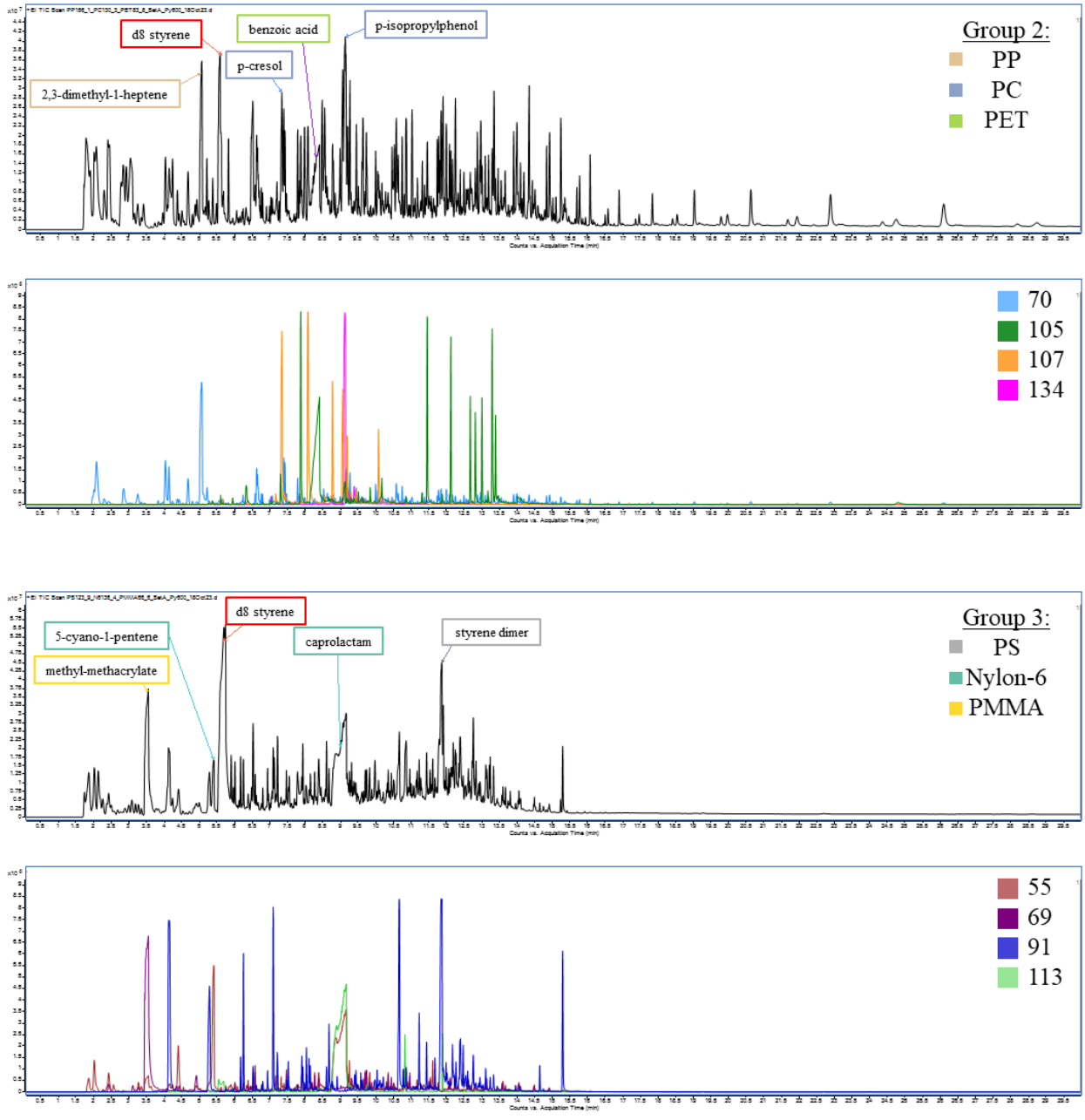

Figure S4: The total ion chromatograms from the three different calibration groups. The marker compounds used for quantification can be seen highlighted for each polymer (colored according to the legend) with the corresponding extracted ion chromatogram (EIC) for each compound.

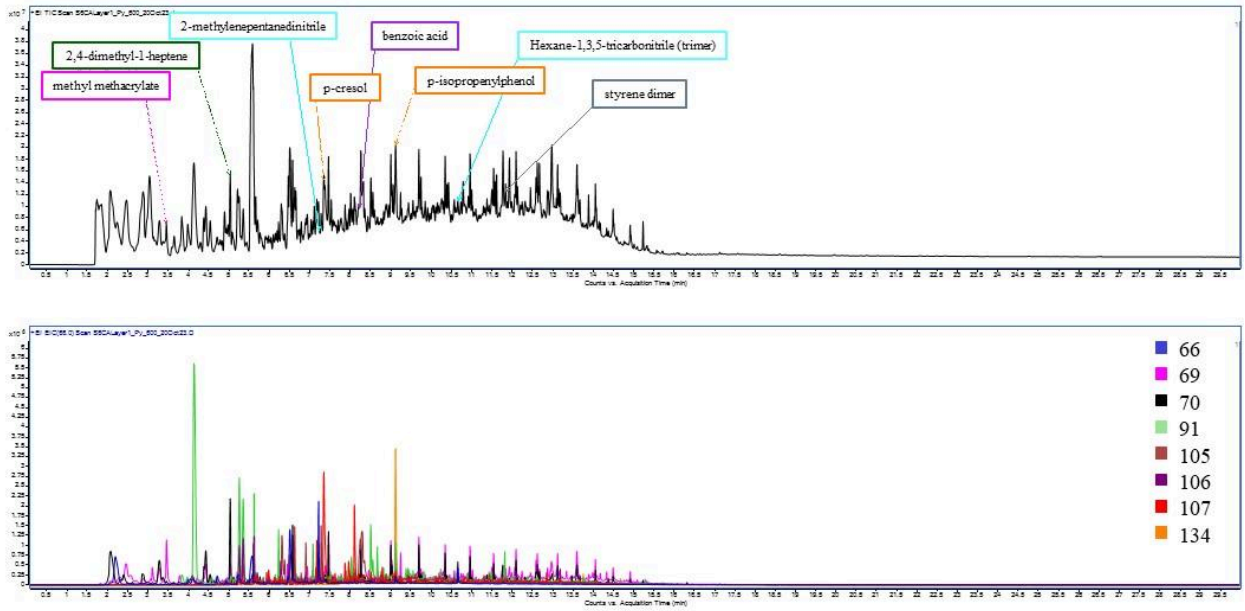

Figure S5: Site 6 chromatogram with the marker compounds used for quantification

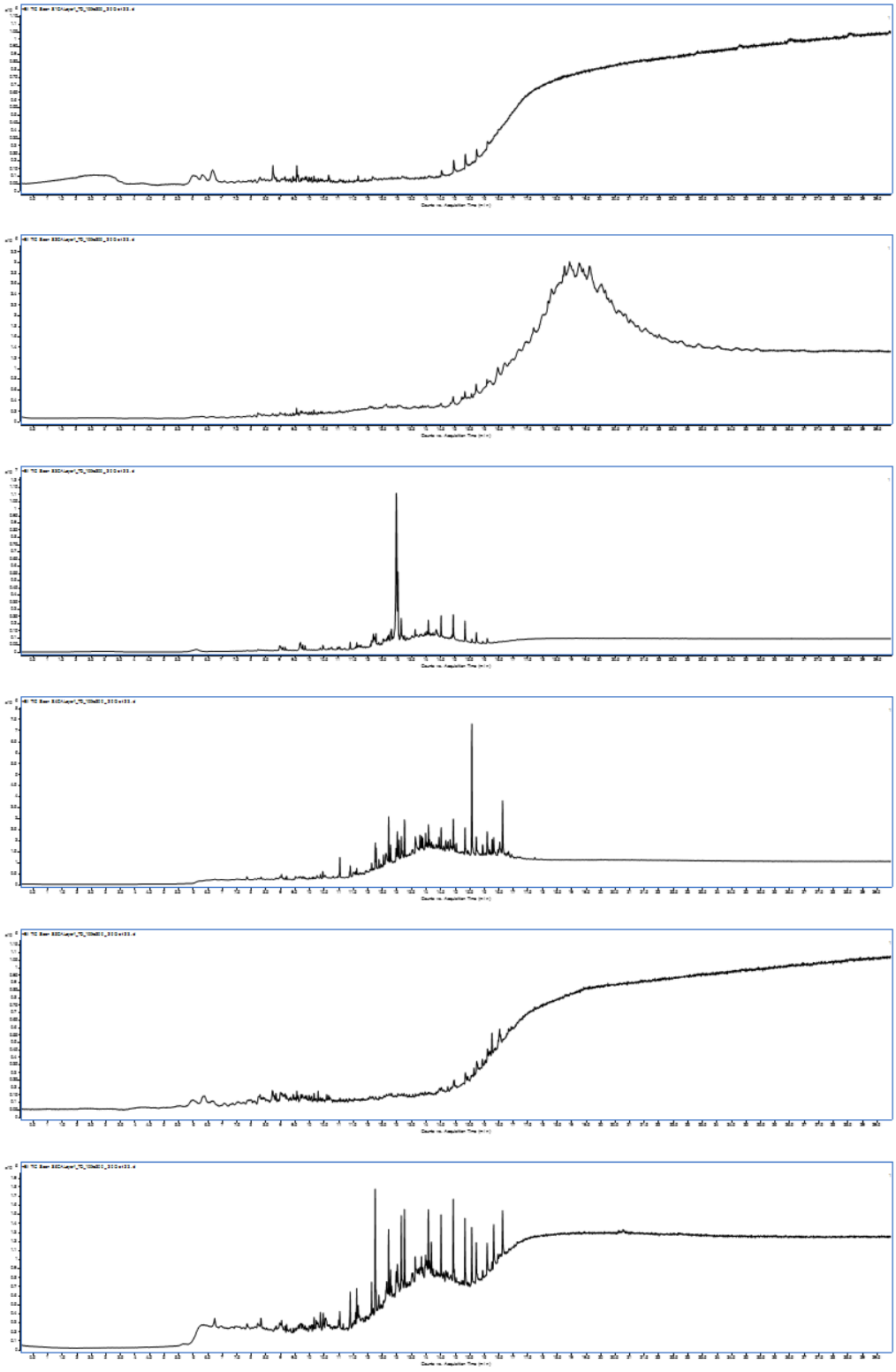

Figure S6: The thermal desorption chromatograms from the six sample sites (top = Site 1, bottom = Site 6). Analysis of these chromatograms was beyond the scope of this thesis.

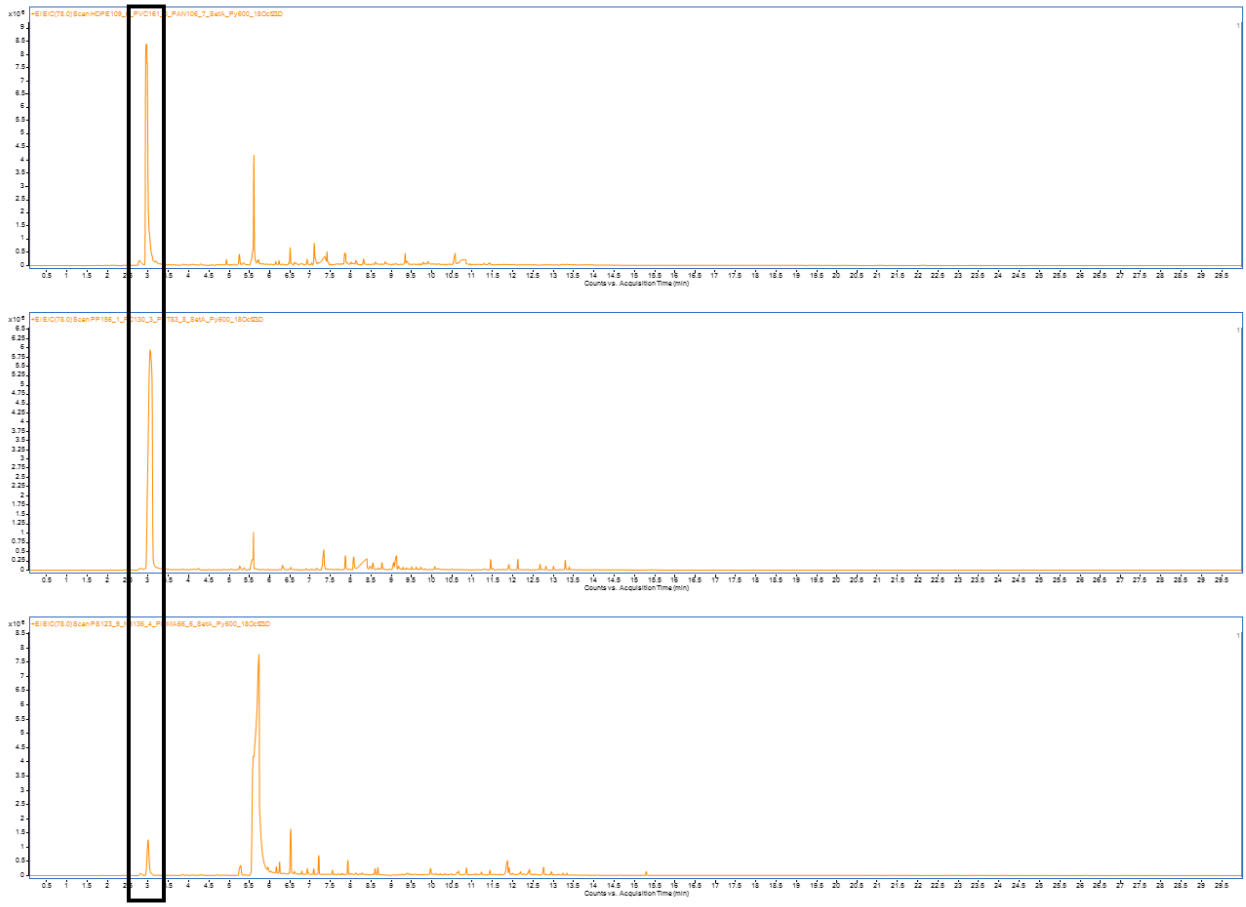

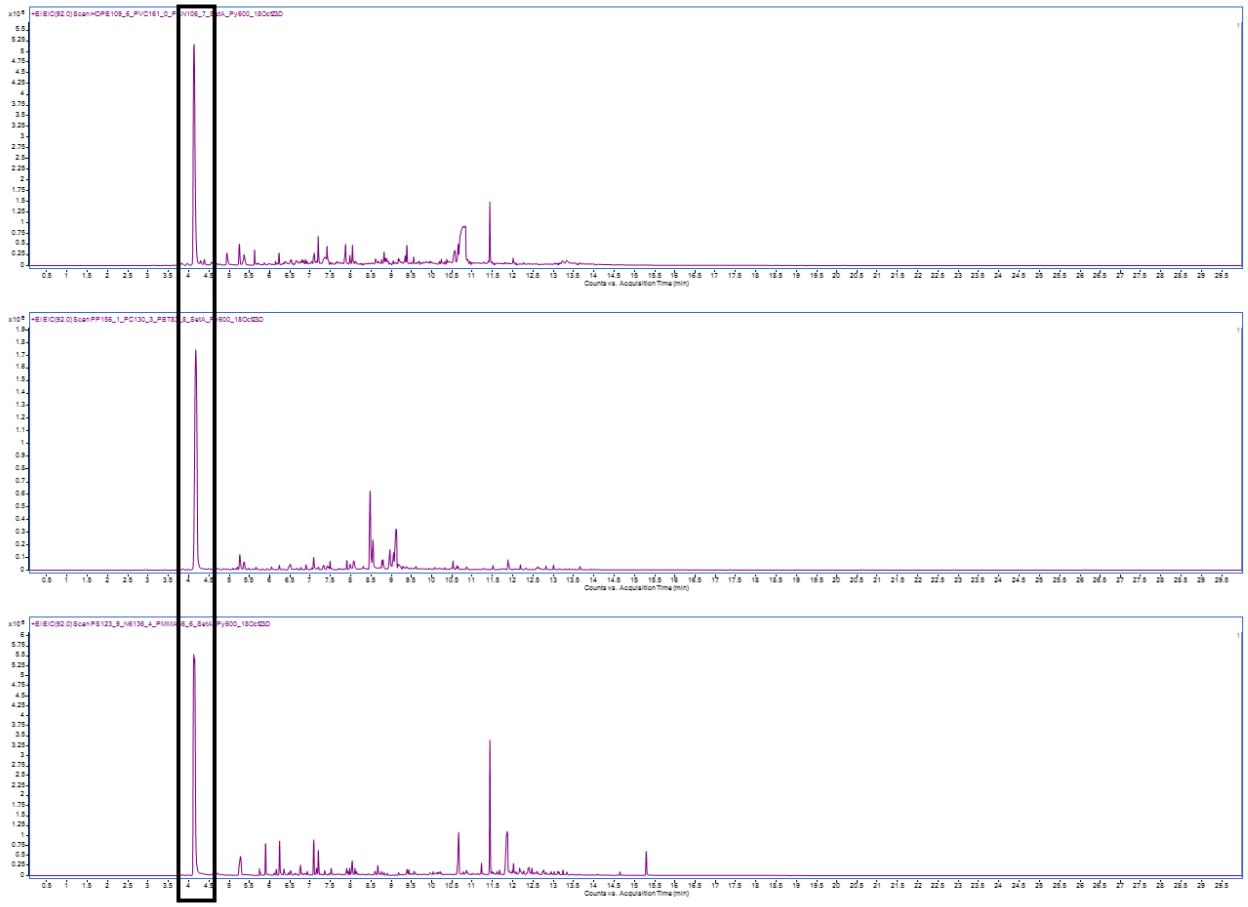

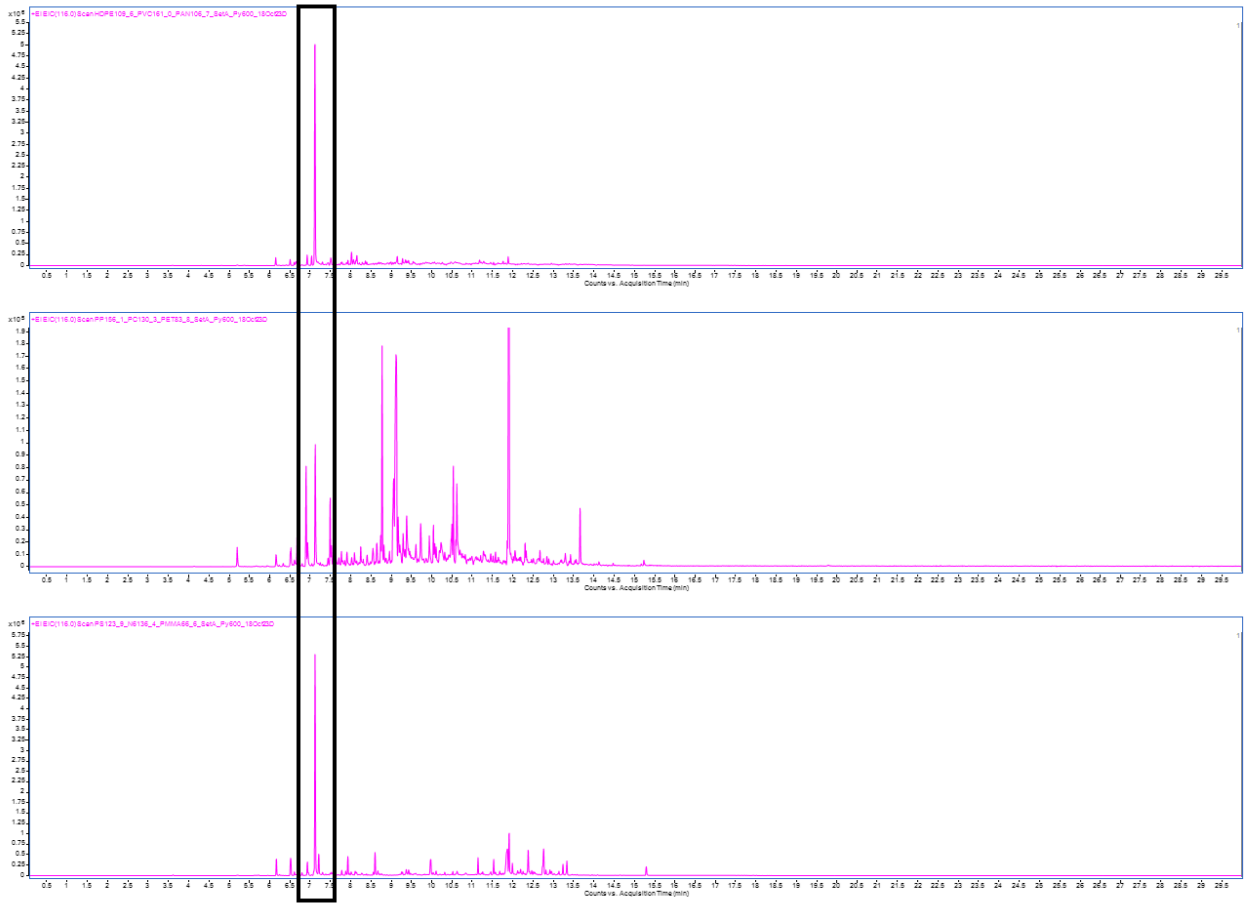

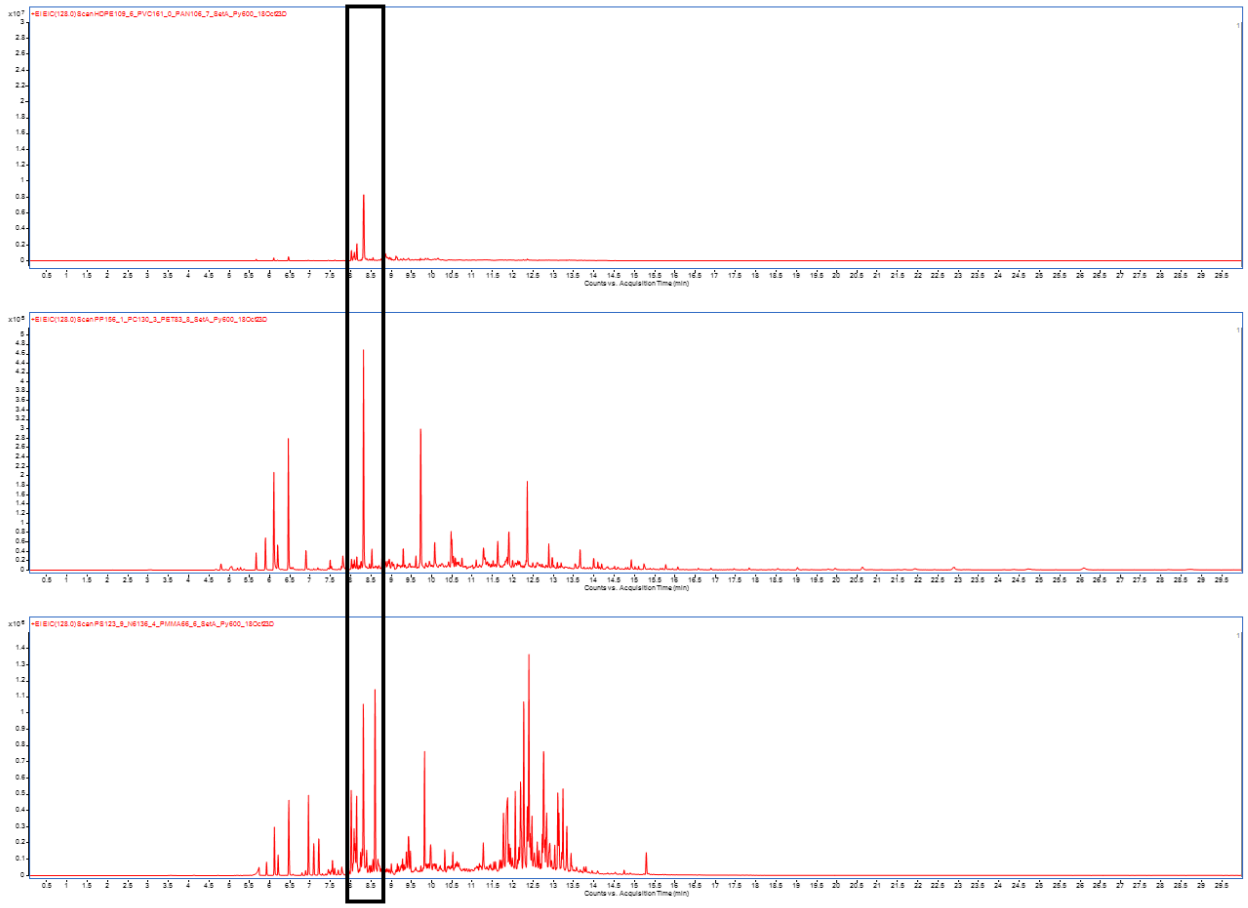

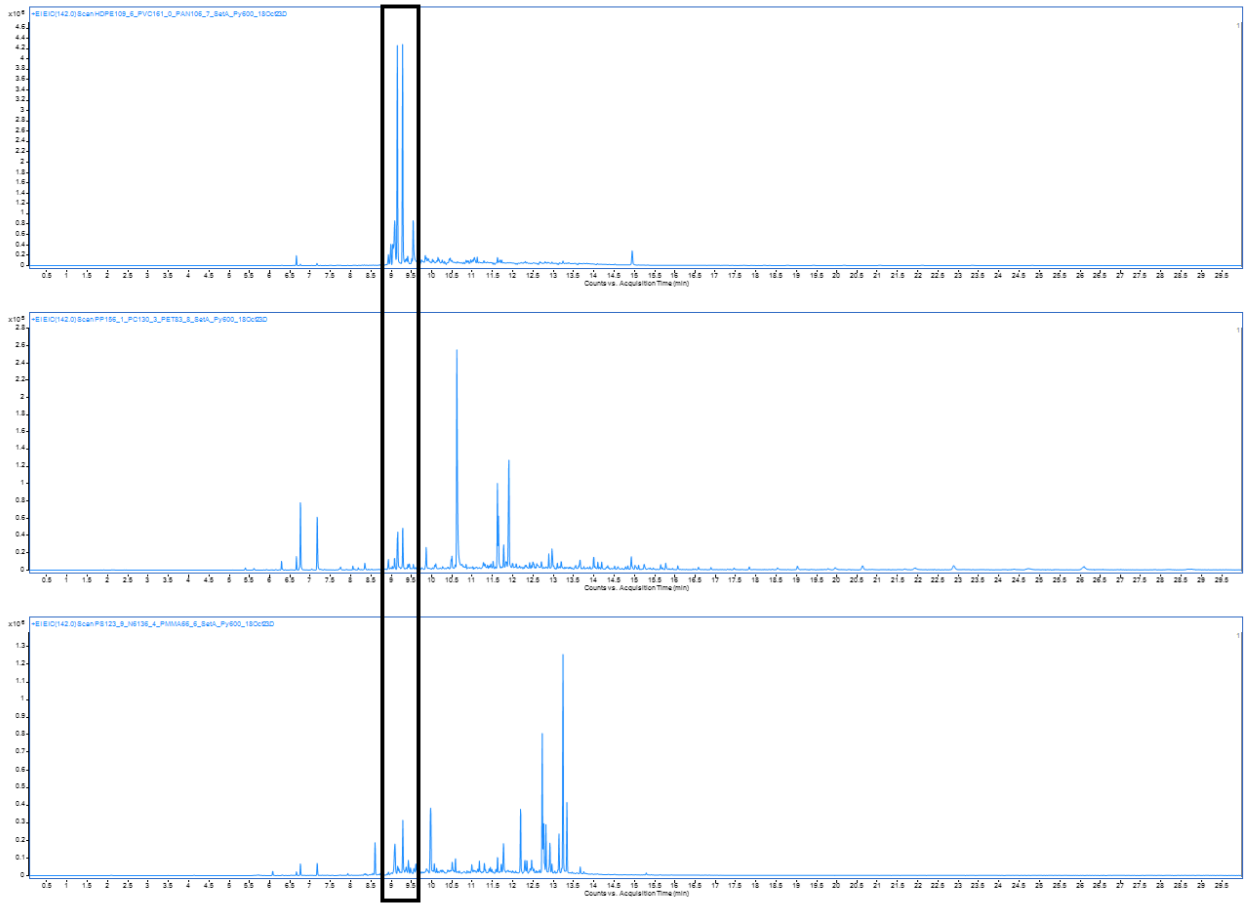

Figure S7: The extracted ion chromatograms (EIC) for each of the PVC marker compounds in order: benzene, toluene, indene, naphthalene, 2-methyl & 1-methylnaphthalene.

Table S5: The polynomial equations created from the calibration curves and used for quantification of PVC in our samples.

Polymer - Marker Compound	Equation	R-squared
PVC - 1-methylnaphthalene	$y = 0.0003x^2 + 0.0285x - 0.0017$	0.999
PVC - 2-methylnaphthalene	$y = 0.0002x^2 + 0.0314x - 0.0015$	0.999
PVC - indene	$y = -0.0027x^2 + 0.0653x + 0.0022$	0.996
PVC - naphthalene	$y = -0.0112x^2 + 0.1738x - 0.0007$	0.998

Figure S8: Mosaic photos of 47 mm polycarbonate filters from some of the lab blank and top layer sediment core samples. The air blanks were on 25 mm gold-plated filters. All photographs were taken with a Thermo Fisher iN10 MX FTIR microscope and stitched together using Canva.

Lab Blank 3

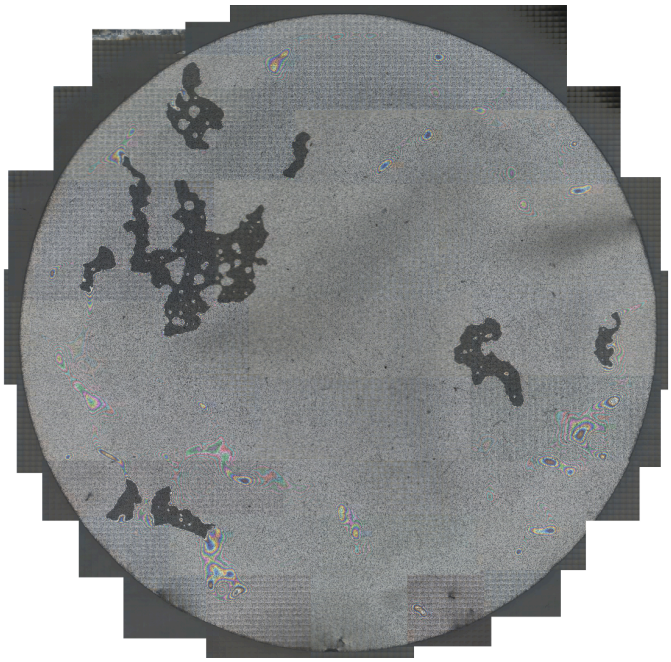

Site 2 Top Layer

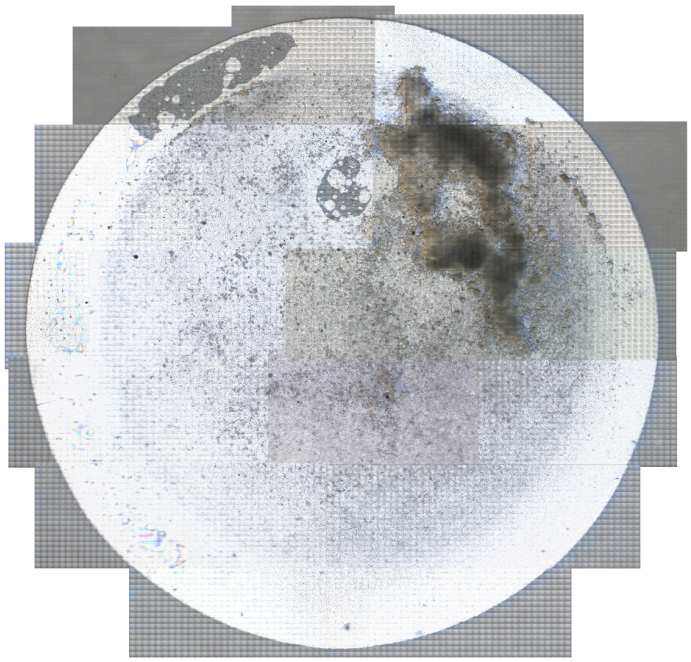

Site 3 Top Layer

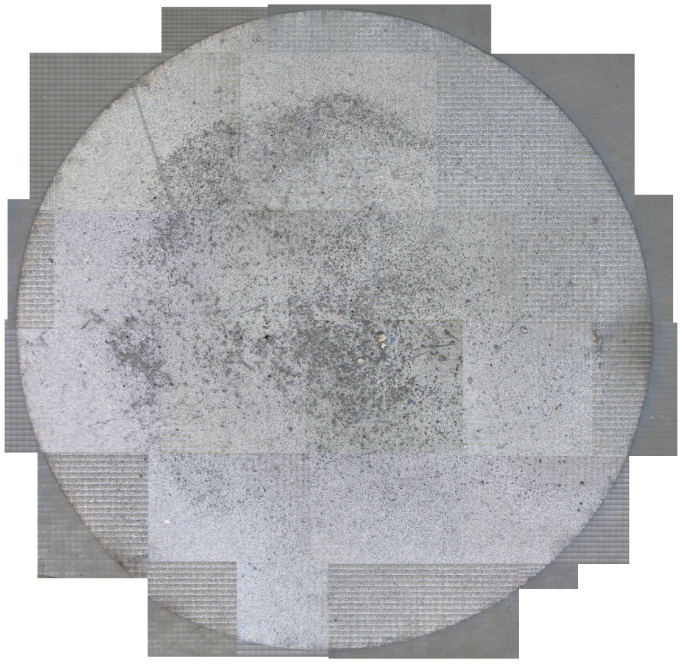

Site 4 Top Layer

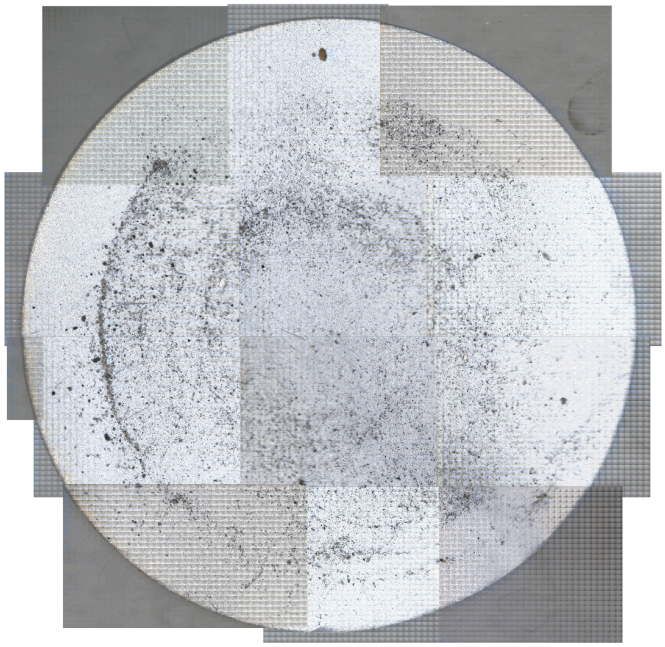

Site 5 Top Layer

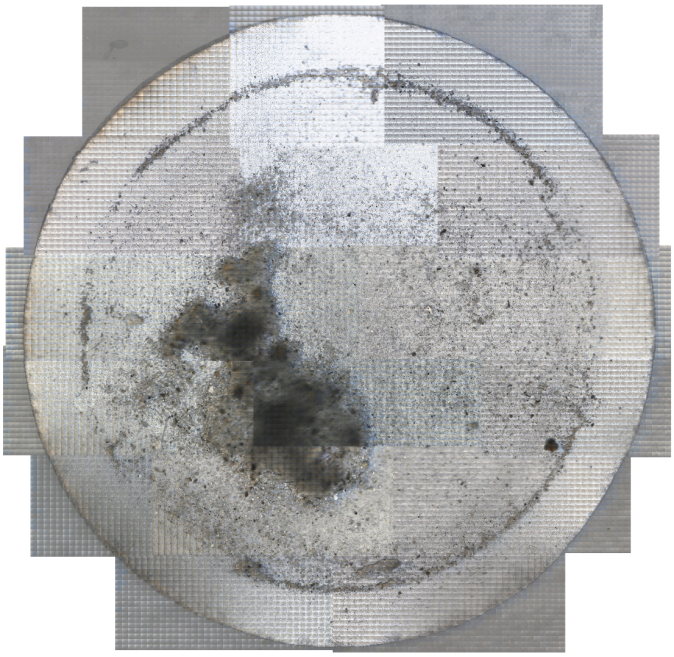

Air Blank Site 1

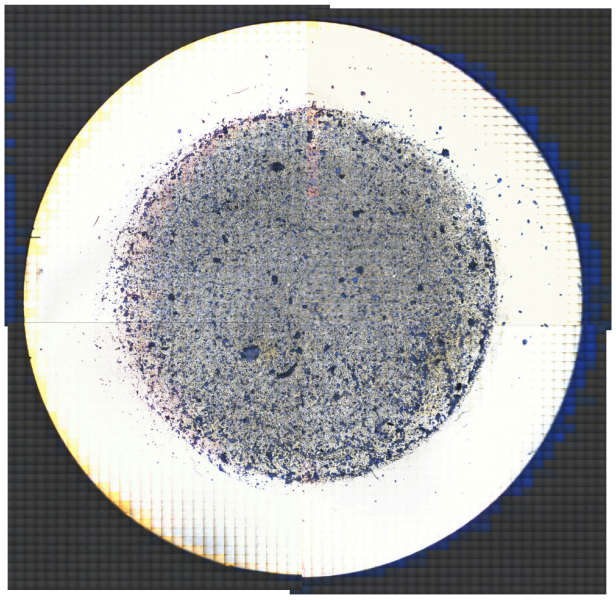

Air Blank Site 2

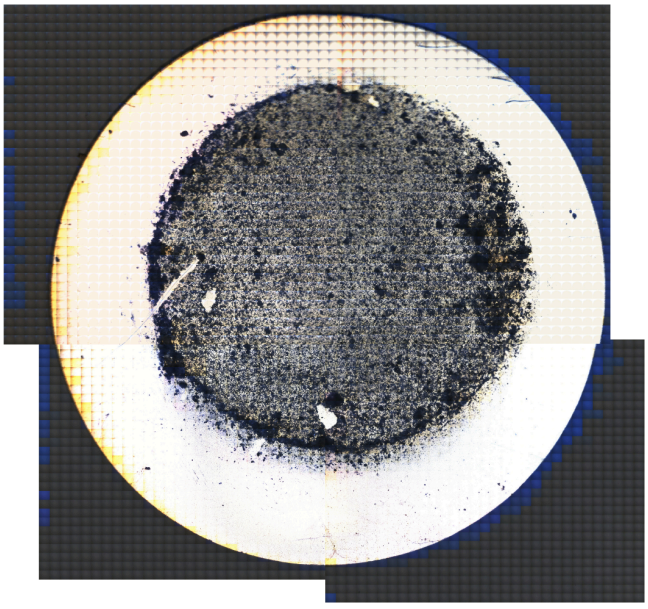

Air Blank Site 4

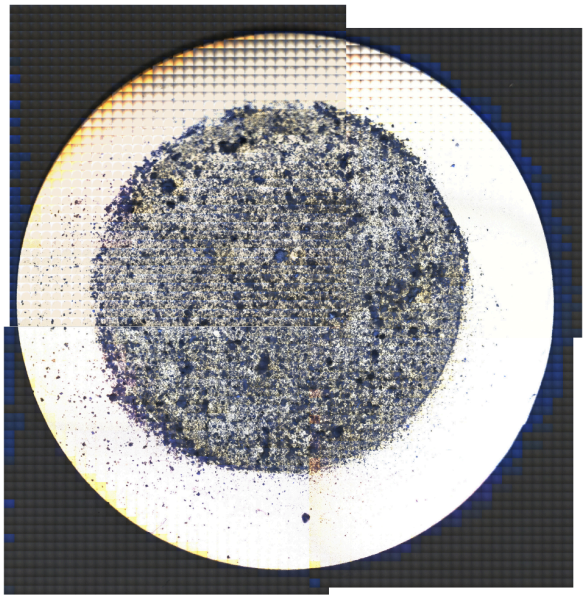

Appendix 1: Report on the Radiometric Dating of a Transect of Marine Sediment Cores in the West Coast of California

Handong Yang
Environmental Change Research Centre
University College London

Rationale and methodology

Lead-210 (half-life is 22.3 year) is a naturally-produced radionuclide, derived from atmospheric fallout (termed unsupported ^{210}Pb). Cesium-137 (half-life is 30 years) and ^{241}Am are artificially produced radionuclides, introduced to the study area by atmospheric fallout from nuclear weapons testing and nuclear reactor accidents. They have been extensively used in the dating of recent sediments. Dried sediment samples from a transect of marine sediment cores taken from west coast of California, were analysed for ^{210}Pb, ^{226}Ra, ^{137}Cs and ^{241}Am by direct gamma assay in the Environmental Radiometric Facility at University College London, using ORTEC HPGe GWL series well-type coaxial low background intrinsic germanium detector. Lead-210 was determined via its gamma emissions at 46.5keV, and ^{226}Ra by the 295keV and 352keV gamma rays emitted by its daughter isotope ^{214}Pb following 3 weeks storage in sealed containers to allow radioactive equilibration. Cesium-137 and ^{241}Am were measured by their emissions at 662keV and 59.5keV (Appleby et al, 1986). The absolute efficiencies of the detector were determined using calibrated sources and sediment samples of known activity. Corrections were made for the effect of self absorption of low energy gamma rays within the sample (Appleby et al, 1992).

Results

HWTS1 from Site 1

Lead-210 Activity

Total ^{210}Pb activity does not reach equilibrium depth with the supported ^{210}Pb activity at the base sample of the core (9 cm, Figure 1a). Unsupported ^{210}Pb activities, calculated by subtracting ^{226}Ra activity (as supported ^{210}Pb) from total ^{210}Pb activity, decline irregularly with depth, showing a decline from sediment surface to 5.5 cm, however, this is followed by an increase from 5.5 to 8.5 cm (Figure 1b). The irregular changes in unsupported ^{210}Pb activities imply an increase in sedimentation rates from 8.5 to 5.5 cm, and then a possible decline from 5.5 cm to the sediment surface.

Artificial Fallout Radionuclides

No ^{137}Cs and ^{241}Am were detected in the samples.

Core Chronology

Because of the irregular changes in unsupported ^{210}Pb activities of the core, the CIC (constant initial concentration) model cannot be used for the sediment chronology calculations. ^{210}Pb chronologies were calculated using the CRS (constant rate of ^{210}Pb supply) dating model (Appleby and Oldfield, 1978; Appleby, 2001). The ^{210}Pb CRS chronologies and sedimentation rates of the core were given in Table 3 and shown in Figure 2. The CRS sedimentation rates suggest that there is an increase in the rates from around 0.014 g cm^{-2} yr^{-1} in the 1950s to 0.71 g cm^{-2} yr^{-1} in the 1970s, and then the rates gradually declined to c. 015 g cm^{-2} yr^{-1} in the present day.

HWTS2 from Site 2

Lead-210 Activity

Equilibrium of total ^{210}Pb activity with the relevant supported ^{210}Pb activity was not reached at the base of the core either (Figure 3a). Unsupported ^{210}Pb activities show a very similar change process with HWTS1: a decline trend from sediment top to 4.5 cm, and an irregular trend of increase with depth from 4.5 to 8.5 cm (Figure 3b), suggesting that sedimentation rates might have an increase from 8.5 to 4.5 cm, when reaching a peak rate at 4.5, there might be a decline in the rates from 4.5 cm to the sediment surface.

Artificial Fallout Radionuclides

No ^{137}Cs and ^{241}Am were detected in the samples.

Core Chronology

The CIC was precluded by the irregular changes in the unsupported ^{210}Pb activities of the core. The CRS chronologies and sedimentation rates of the core were given in Table 6 and shown in Figure 4. As in HWTS1, the ^{210}Pb chronologies have not been validated by any independent time mark. The CRS ^{210}Pb model suggests that there is an increase in sedimentation rates, from c. 0.013 g cm^{-2} yr^{-1} in the 1960s to the 1990s reaching a peak at 0.112 g cm^{-2} yr^{-1} and then declined to 0.019 g cm^{-2} yr^{-1} in the coring time.

HWTS3 from Site 3

Lead-210 Activity

Total ^{210}Pb activity does not reach equilibrium with supported ^{210}Pb activity at the base of the core (10 cm, Figure 5a). Unsupported ^{210}Pb activities decline irregularly with depth (Figure 5b), with reduced decline gradients from core surface to 4.5 cm, implying a decline trend in sedimentation rates from deep to shallow sediments; and with relatively similar level between 5.5 and 9.5 cm, suggesting possible increase in sedimentation rates from deep to shallow sediments within the section.

Artificial Fallout Radionuclides

No ^{137}Cs and ^{241}Am were detected in the samples, maybe due to relatively high sedimentation rates.

Core Chronology

The non-monotonic variation in unsupported ^{210}Pb activities has precluded the use of the CIC model. Chronologies and sedimentation rates of the core were calculated by using the CRS dating model, and they were given in Table 9 and shown in Figure 6. Again, these chronologies have not been validated by any independent time mark. It is suggested that sedimentation rates of the core are relatively high, and show a decline in recent 20 years or so (Figure 6).

HWTS4 from Site 4

Lead-210 Activity

Total ^{210}Pb activity reaches equilibrium with supported ^{210}Pb activity at around 4.5 cm of the core (Figure 7a). Unsupported ^{210}Pb activities in this core decline irregularly with depth. Increase in the decline slops of the unsupported ^{210}Pb activities with depth (Figure 7b) suggests that there is an increase trend in sedimentation rates from deep sediments to the surface of the core.

Artificial Fallout Radionuclides

Very low ^{241}Am and ^{137}Cs activities were detected at 1.5 cm (Table 11) and they were possibly derived from the 1963 maximum fallout of the atmospheric nuclear bomb testing. As both are single and low activity point, they are insufficient for dating.

Core Chronology

The irregular changes in unsupported ^{210}Pb activities of the core have precluded the use of the CIC model. Chronologies and sedimentation rates of the core were calculated by using the CRS dating model, and the CRS model places 1963 between 1.5 and 2.5 cm, which is in reasonable agreement with the ^{241}Am and ^{137}Cs records, although the ^{241}Am and ^{137}Cs records are insufficient

for dating. The dating results were given in Table 12 and shown in Figure 8. Sedimentation rates of the core show an increase process from around 0.002 g cm^{-2} yr^{-1} in the 1860s to 0.022 g cm^{-2} yr^{-1} in the present day.

HWTS5 from Site 5

Lead-210 Activity

This core does not reach equilibrium depth of total ^{210}Pb activity with supported ^{210}Pb activity (Figure 9a). Unsupported ^{210}Pb activities in this core decline irregularly again with depth (Figure 9b). There are dips in unsupported ^{210}Pb activities at 2.5, 6.5, and 8.5 depths (Table 13, Figure 9b), suggesting possible dilution events resulting in increased sedimentation rates at these depths.

Artificial Fallout Radionuclides

There is a relatively high value of ^{137}Cs activity at 4.5 cm of the ^{37}Cs core profile (Figure 9c), it is almost certain that this peak was derived from the 1963 maximum fallout of the atmospheric nuclear bomb testing. ^{241}Am peak at 4.5 cm of the ^{241}Am profile of the core confirms that the ^{137}Cs peak at the same depth was derived from the fallout of the atmospheric nuclear bomb testing.

Core Chronology

The irregular features in unsupported ^{210}Pb activities of the core have also precluded the use of the CIC model. The CRS model chronologies and sedimentation rates of the core were given in Table 15, which shows that the 4.5 cm depth was dated to 1962 +/-6, in very good agreement with the ^{241}Am and ^{137}Cs records. The dating results were given in Table 15 and shown in Figure 10. The ^{210}Pb Sedimentation rates of the core suggest a kind of base rate of c. 0.015 g cm^{-2} yr^{-1} in the core, with some increased peaks, for example the peaks in the 1910s and 1980s, reaching 0.057 and 0.082 g cm^{-2} yr^{-1}, respectively.

HWTS6 from Site 6

Lead-210 Activity

In this core total ^{210}Pb activities do not reach equilibrium with the relevant supported ^{210}Pb activities even at the base of 10 cm in the core (Figure 11a). Unsupported ^{210}Pb activities irregularly with depth, and show a dip at 8.5 cm (Figure 11b), suggesting changes in sedimentation rates, and rate at 8.5 cm should have notably increased that diluted the unsupported ^{210}Pb activity at the depth.

Artificial Fallout Radionuclides

^{137}Cs was detected at the surface (Table 17), which is likely to be derived from in-wash from the shore. Low ^{241}Am activities were detected in some sediments, but the disconnected low activities are insufficient for dating.

Core Chronology

The CIC model was precluded for dating by the irregular ^{210}Pb profile. The CRS model was use for sediment chronologies and sedimentation rates calculations, and the results were given in Table 18 and shown in Figure 12. The CRS ^{210}Pb model suggests that sedimentation rates in the core are normally in a range of 0.02 to 0.045 g cm^{-2} yr^{-1} in the last about 80 years, but there is a notable increase in the rate reaching 0.07 g cm^{-2} yr^{-1} in the 1940s.

Reference

Appleby, P G, 2001. Chronostratigraphic techniques in recent sediments. In W M Last and J P Smol (eds.) *Tracking Environmental Change Using Lake Sediments*. Vol. 1: Basin Analysis, Coring, and Chronological Techniques. Kluwer Academic Publishers, Dordrecht. Pp171-203.

Appleby, P G, Richardson, N, Nolan, P J, 1992. Self-absorption corrections for well-type germanium detectors. *Nucl. Inst. & Methods B*, 71: 228-233.

Appleby, P G, Nolan, P J, Gifford, D W, Godfrey, M J, Oldfield, F, Anderson, N J & Battarbee, R W, 1986. 210Pb dating by low background gamma counting. *Hydrobiologia*, 141: 21-27.

Appleby, P.G. & Oldfield, F., 1978. The calculation of 210Pb dates assuming a constant rate of supply of unsupported 210Pb to the sediment. *Catena*, 5:1-8.

Table 1. ^{210}Pb concentrations in core HWTS1.

Depth	Dry Mass	Pb-210						Cum Unsupported	
		Total		Supported		Unsupp		Pb-210	
cm	g cm^{-2}	Bq Kg^{-1}	±	Bq Kg^{-1}	±	Bq Kg^{-1}	±	Bq m^{-2}	±
0.5	0.0924	1276.16	38.52	198.16	8.55	1078	39.46	1143.9	63.1
1.5	0.3331	604.62	19.96	194.93	7.51	409.69	21.33	2806.6	129
2.5	0.588	416.79	10.45	212.19	2.71	204.6	10.8	3559.5	143.1
3.5	0.8457	353.63	15.49	237.56	7.3	116.07	17.12	3961.9	148.3
4.5	1.2364	330.23	10.54	240.24	2.91	89.99	10.93	4362.3	159.5
5.5	1.5332	340.68	14.17	270.63	4.42	70.05	14.84	4598.6	164.4
6.5	1.8299	393.01	28.14	306.15	8.86	86.86	29.5	4830.5	174.7
7.5	2.1267	461.55	16.52	343.55	4.98	118	17.25	5132.1	192.8
8.5	2.4234	482.5	9.94	336.36	2.99	146.14	10.38	5522.5	199.4

Table 2. Artificial fallout radionuclide concentrations in core HWTS1.

Depth	Cs-137		Am-241	
cm	Bq Kg^{-1}	±	Bq Kg^{-1}	±
0.5	0	0	0	0
1.5	0	0	0	0
2.5	0	0	0	0
3.5	0	0	0	0
4.5	0	0	0	0
5.5	0	0	0	0
6.5	0	0	0	0
7.5	0	0	0	0
8.5	0	0	0	0

Table 3. ^{210}Pb chronologies and sedimentation rates of core HWTS1.

Depth	Drymass	Chronology			Sedimentation Rate		
		Date	Age				
cm	g cm^{-2}	AD	yr	±	g cm^{-2} yr^{-1}	cm yr^{-1}	± %
0	0	2022	0				
0.5	0.0924	2015	7	2	0.0146	0.066	8.4
1.5	0.3331	2003	19	2	0.0258	0.104	12
2.5	0.588	1995	27	3	0.0402	0.157	14.8
3.5	0.8457	1989	33	4	0.06	0.185	21.8
4.5	1.2364	1983	39	5	0.0636	0.185	22.9
5.5	1.5332	1979	43	6	0.0712	0.24	30.6
6.5	1.8299	1974	48	7	0.0491	0.165	42.1
7.5	2.1267	1966	56	9	0.0282	0.095	35
8.5	2.4234	1951	71	15	0.0144	0.049	39.8

Table 4. ^{210}Pb concentrations in core HWTS2.

Depth	Dry Mass	Pb-210						Cum Unsupported	
		Total		Supported		Unsupp		Pb-210	
cm	g cm^{-2}	Bq Kg^{-1}	±	Bq Kg^{-1}	±	Bq Kg^{-1}	±	Bq m^{-2}	±
0.5	0.0518	1243.81	20.35	256.12	3.77	987.69	20.7	544.9	28.3
1.5	0.2005	926.71	21.9	278.31	4.72	648.4	22.4	1743.7	72
2.5	0.4657	535.07	10.84	297.25	2.85	237.82	11.21	2829.3	103.6
3.5	0.822	470.12	14.28	307.34	3.94	162.78	14.81	3534.6	117
4.5	1.1382	386.8	10.31	313.62	3.01	73.18	10.74	3888.9	126.9
5.5	1.4551	408.83	26.13	321.96	7.86	86.87	27.29	4141.9	137.9
6.5	1.7721	446.42	9.33	334.49	2.77	111.93	9.73	4455.3	158.4
7.5	2.089	460.7	16.89	344.5	5.05	116.2	17.63	4816.8	164.1
8.5	2.406	593.68	29.08	332.83	8.94	260.85	30.42	5383.7	180.2

Table 5. Artificial fallout radionuclide concentrations in core HWTS2.

Depth	Cs-137		Am-241	
cm	Bq Kg^{-1}	±	Bq Kg^{-1}	±
0.5	0	0	0	0
1.5	0	0	0	0
2.5	0	0	0	0
3.5	0	0	0	0
4.5	0	0	0	0
5.5	0	0	0	0
6.5	0	0	0	0
7.5	0	0	0	0
8.5	0	0	0	0

Table 6. ^{210}Pb chronologies and sedimentation rates of core HWTS2.

Depth	Drymass	Chronology			Sedimentation Rate		
		Date	Age				
cm	g cm^{-2}	AD	yr	±	g cm^{-2} yr^{-1}	cm yr^{-1}	± %
0	0	2022	0				
0.5	0.0518	2019	3	2	0.0188	0.141	10.1
1.5	0.2005	2012	10	2	0.0229	0.111	12.8
2.5	0.4657	2004	18	3	0.0482	0.155	16.5
3.5	0.822	1997	25	4	0.0569	0.169	21.4
4.5	1.1382	1993	29	5	0.1115	0.352	26.4
5.5	1.4551	1990	32	5	0.0849	0.268	39.5
6.5	1.7721	1985	37	7	0.0572	0.18	29
7.5	2.089	1979	43	8	0.0454	0.143	36.7
8.5	2.406	1966	56	14	0.0134	0.042	38.7

Table 7. ^{210}Pb concentrations in core HWTS3.

Depth	Dry Mass	Pb-210						Cum Unsupported Pb-210	
		Total		Supported		Unsupp			
cm	g cm^{-2}	Bq Kg^{-1}	±	Bq Kg^{-1}	±	Bq Kg^{-1}	±	Bq m^{-2}	±
0.5	0.2556	852.19	18.08	345.95	4.84	506.24	18.72	1422.2	78.9
1.5	0.7405	592.31	18.19	362.12	5.79	230.19	19.09	3120.7	143.4
2.5	1.2814	523.43	10.51	358.29	3.41	165.14	11.05	4180.1	178.2
3.5	1.9318	501.5	13.48	360.4	4.46	141.1	14.2	5173.9	199.5
4.5	2.6192	490.05	10.39	361.3	3.51	128.75	10.97	6100.8	224.2
5.5	3.2479	473.17	15.24	367.3	5.17	105.87	16.09	6835.9	240.8
6.5	3.8765	457.02	27.23	325.15	9.23	131.87	28.75	7580.2	274.3
7.5	4.5051	505.06	14.47	370.81	4.98	134.25	15.3	8416.6	322.2
8.5	5.1338	464.33	16.87	365.59	6.06	98.74	17.93	9143.3	339.5
9.5	5.4119	494.95	15.37	390.35	5.43	104.6	16.3	9425.9	345.5

Table 8. Artificial fallout radionuclide concentrations in core HWTS3.

Depth	Cs-137		Am-241	
cm	Bq Kg^{-1}	±	Bq Kg^{-1}	±
0.5	0	0	0	0
1.5	0	0	0	0
2.5	0	0	0	0
3.5	0	0	0	0
4.5	0	0	0	0
5.5	0	0	0	0
6.5	0	0	0	0
7.5	0	0	0	0
8.5	0	0	0	0
9.5	0	0	0	0

Table 9. ^{210}Pb chronologies and sedimentation rates of core HWTS3.

Depth	Drymass	Chronology			Sedimentation Rate		
		Date	Age				
cm	g cm^{-2}	AD	yr	±	g cm^{-2} yr^{-1}	cm yr^{-1}	± %
0	0	2022	0				
0.5	0.2556	2019	3	2	0.081	0.164	20.1
1.5	0.7405	2014	8	2	0.1553	0.303	24.1
2.5	1.2814	2011	11	3	0.1965	0.33	25.9
3.5	1.9318	2008	14	4	0.208	0.311	29.4
4.5	2.6192	2005	17	5	0.2055	0.312	31.7
5.5	3.2479	2002	20	6	0.2283	0.363	36.7
6.5	3.8765	1998	24	7	0.1657	0.264	42.8
7.5	4.5051	1994	28	8	0.1434	0.228	43.4
8.5	5.1338	1990	32	10	0.172	0.379	50.8
9.5	5.4119	1989	33	11	0.154	0.428	52.4

Table 10. ^{210}Pb concentrations in core HWTS4.

Depth	Dry Mass	Pb-210						Cum Unsupported	
		Total		Supported		Unsupp		Pb-210	
cm	g cm^{-2}	Bq Kg^{-1}	±	Bq Kg^{-1}	±	Bq Kg^{-1}	±	Bq m^{-2}	±
0.5	0.1823	1018.48	19.45	361.74	4.41	656.74	19.94	1439.2	77.1
1.5	0.5351	973.78	11.95	354.94	2.65	618.84	12.24	3688.6	146.9
2.5	0.9058	598.41	12.45	306.77	2.99	291.64	12.8	5300.9	175.4
3.5	1.2916	354.57	9.85	277.97	2.84	76.6	10.25	5921.4	184.9
4.5	1.6469	249.55	7.7	247.57	2.38	1.98	8.06	5994	188.4

Table 11. Artificial fallout radionuclide concentrations in core HWTS4.

Depth	Cs-137		Am-241	
cm	Bq Kg^{-1}	±	Bq Kg^{-1}	±
0.5	0	0	0	0
1.5	1.37	0.58	1.28	0.67
2.5	0	0	0	0
3.5	0	0	0	0
4.5	0	0	0	0

Table 12. ^{210}Pb chronologies and sedimentation rates of core HWTS4.

Depth	Drymass	Chronology			Sedimentation Rate		
		Date	Age				
cm	g cm^{-2}	AD	yr	±	g cm^{-2} yr^{-1}	cm yr^{-1}	± %
0	0	2022	0				
0.5	0.1823	2013	9	2	0.0215	0.06	4.7
1.5	0.5351	1991	31	2	0.0114	0.032	5.3
2.5	0.9058	1951	71	3	0.0071	0.019	9.8
3.5	1.2916	1863	159	19	0.0017	0.005	12.5

Table 13. ^{210}Pb concentrations in core HWTS5.

Depth	Dry Mass	Pb-210						Cum Unsupported	
		Total		Supported		Unsupp		Pb-210	
cm	g cm^{-2}	Bq Kg^{-1}	±	Bq Kg^{-1}	±	Bq Kg^{-1}	±	Bq m^{-2}	±
0.5	0.1791	674.39	15.31	171.66	3.59	502.73	15.73	1062.3	57.2
1.5	0.5416	273.92	7.2	160.72	2.29	113.2	7.56	2009.5	90.5
2.5	0.905	197.72	7.72	155.5	2.55	42.22	8.13	2271	95.7
3.5	1.3529	222.51	8.41	159.87	2.56	62.64	8.79	2502.8	102.8
4.5	1.8608	245.09	7.12	166.06	2.34	79.03	7.49	2861	112.4
5.5	2.3014	179.75	11.01	129.06	3.31	50.69	11.5	3142.1	119.9
6.5	2.7419	127.11	9.71	125.7	3.27	1.41	10.25	3202.7	129.8
7.5	3.1825	118.44	9.36	98.78	2.82	19.66	9.78	3233.2	137.2
8.5	3.623	95.02	8.99	88.47	2.81	6.55	9.42	3285.8	143.8
9.5	3.8258	86.5	7.15	74.08	2.07	12.42	7.44	3304.4	145.6

Table 14. Artificial fallout radionuclide concentrations in core HWTS5.

Depth	Cs-137		Am-241	
cm	Bq Kg^{-1}	±	Bq Kg^{-1}	±
0.5	0	0	3.36	0.91
1.5	0	0	0	0
2.5	0	0	0	0
3.5	0	0	0	0
4.5	7.61	0.9	11.38	0.64
5.5	0	0	0	0
6.5	0	0	1.95	0.9
7.5	0	0	0	0
8.5	0	0	0	0
9.5	0	0	0	0

Table 15. ^{210}Pb chronologies and sedimentation rates of core HWTS5.

Depth	Drymass	Chronology			Sedimentation Rate		
		Date	Age				
cm	g cm^{-2}	AD	yr	±	g cm^{-2} yr^{-1}	cm yr^{-1}	± %
0	0	2022	0				
0.5	0.1791	2010	12	2	0.0143	0.04	6.6
1.5	0.5416	1993	29	2	0.0376	0.104	10.9
2.5	0.905	1986	36	3	0.0815	0.201	21.7
3.5	1.3529	1979	43	3	0.0434	0.091	18.3
4.5	1.8608	1962	60	6	0.0203	0.043	20.8
5.5	2.3014	1936	86	11	0.0144	0.033	41.4
6.5	2.7419	1924	98	12	0.0351	0.08	47.1
7.5	3.1825	1920	102	12	0.0227	0.051	60.5
8.5	3.623	1913	109	14	0.0566	0.176	73
9.5	3.8258	1898	124	16	0.018	0.07	77.2

Table 16. ^{210}Pb concentrations in core HWTS6.

Depth	Dry Mass	Pb-210						Cum Unsupported	
		Total		Supported		Unsupp		Pb-210	
cm	g cm^{-2}	Bq Kg^{-1}	±	Bq Kg^{-1}	±	Bq Kg^{-1}	±	Bq m^{-2}	±
0.5	0.1631	736.36	17.23	138.5	3.25	597.86	17.53	1113	59.5
1.5	0.4842	447.2	14.88	144.93	3.44	302.27	15.27	2504.6	104.7
2.5	0.8163	306.27	9.72	148.64	2.46	157.63	10.03	3242.4	120.8
3.5	1.1191	289.18	8.51	151.63	2.2	137.55	8.79	3688.6	126.5
4.5	1.4283	219	9.2	141.04	2.5	77.96	9.53	4013.1	130.5
5.5	1.7418	224.26	6.74	157.85	2.04	66.41	7.04	4238.9	134
6.5	2.0553	213.96	10.83	148.46	3.12	65.5	11.27	4445.7	136.9
7.5	2.3688	176.81	12.85	147.6	6.61	29.21	14.45	4586.6	142.3
8.5	2.6823	169.69	10.26	147.18	3.12	22.51	10.72	4667.2	148.6
9.5	3.0271	203.98	20.09	144.93	5.99	59.05	20.96	4797.8	156.2

Table 17. Artificial fallout radionuclide concentrations in core HWTS6.

Depth	Cs-137		Am-241	
cm	Bq Kg^{-1}	±	Bq Kg^{-1}	±
0.5	3.42	1.18	1.64	0.95
1.5	0	0	2.17	0.87
2.5	0	0	0	0
3.5	0	0	0	0
4.5	0	0	1.28	0.65
5.5	0	0	0	0
6.5	0	0	0	0
7.5	0	0	1.71	0.97
8.5	0	0	0	0
9.5	0	0	0	0

Table 18. ^{210}Pb chronologies and sedimentation rates of core HWTS6.

Depth	Drymass	Chronology			Sedimentation Rate		
		Date	Age				
cm	g cm^{-2}	AD	yr	±	g cm^{-2} yr^{-1}	cm yr^{-1}	± %
0	0	2022	0				
0.5	0.1631	2014	8	2	0.0212	0.066	6.5
1.5	0.4842	2001	21	2	0.0276	0.084	9.6
2.5	0.8163	1990	32	3	0.0383	0.121	12.7
3.5	1.1191	1982	40	4	0.0338	0.11	15.5
4.5	1.4283	1974	48	5	0.0467	0.15	21.6
5.5	1.7418	1967	55	6	0.0442	0.141	24.4
6.5	2.0553	1959	63	8	0.035	0.112	32.6
7.5	2.3688	1952	70	10	0.0634	0.202	59.5
8.5	2.6823	1948	74	12	0.0711	0.216	60.7
9.5	3.0271	1938	84	15	0.0202	0.06	61.1

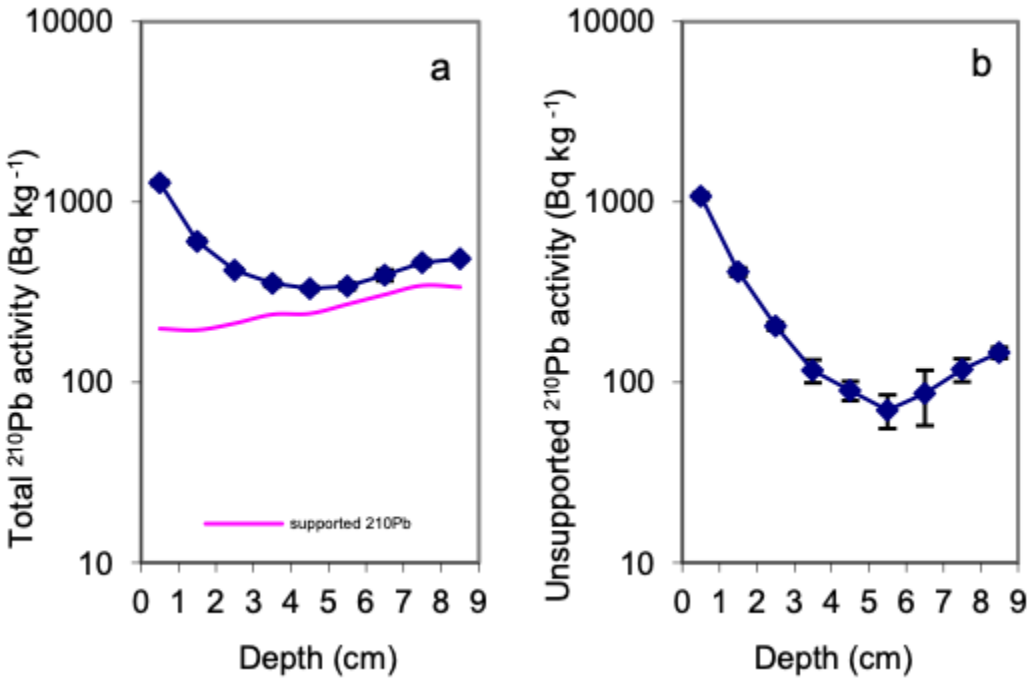

Figure 1. Fallout radionuclide concentrations in core HWTS1 taken from Pacific Ocean, showing (a) total ^{210}Pb, and (b) unsupported ^{210}Pb concentrations versus depth.

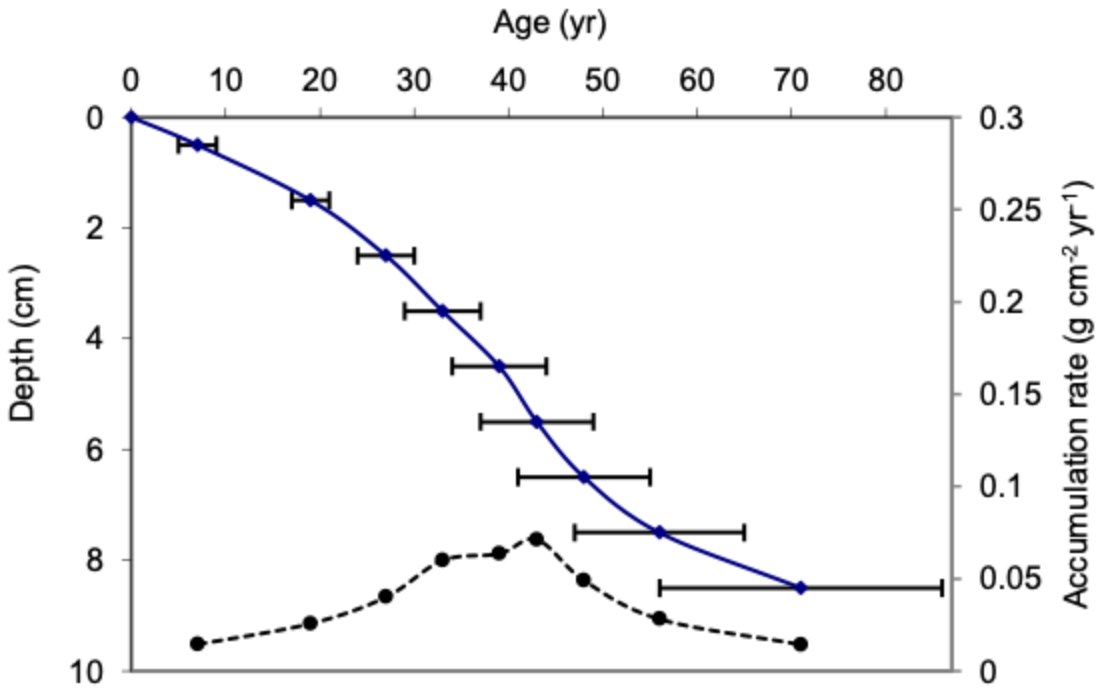

Figure 2. Radiometric chronologies of core HWTS1 taken from Pacific Ocean, showing the CRS model ^{210}Pb dates and sedimentation rates. The solid line shows age while the dashed line indicates sedimentation rate.

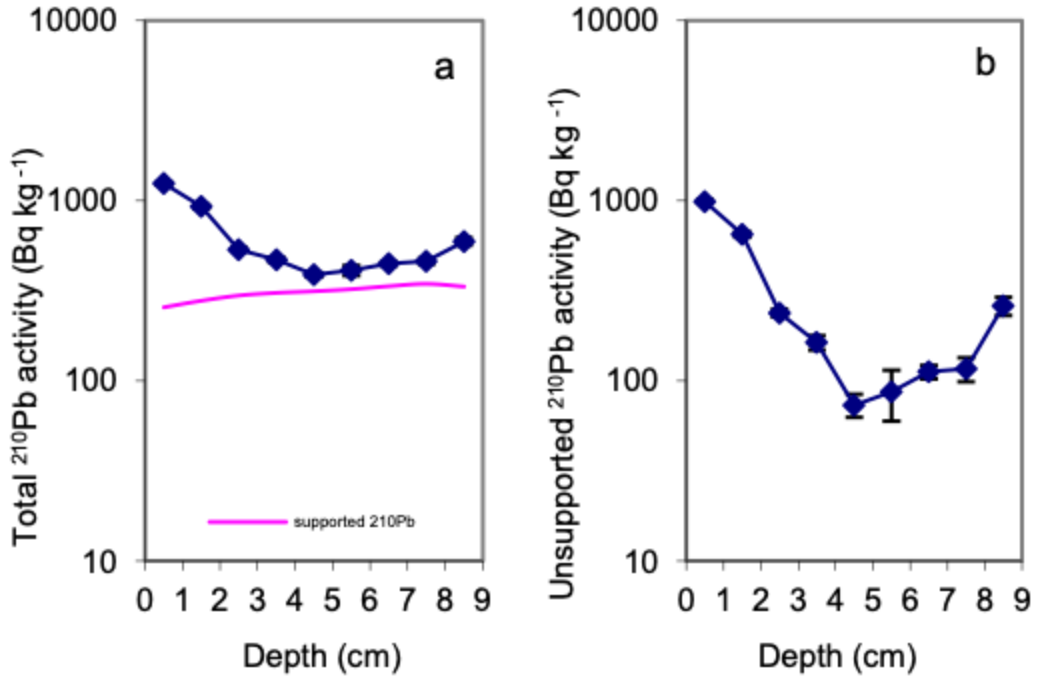

Figure 3. Fallout radionuclide concentrations in core HWTS2 taken from Pacific Ocean, showing (a) total ^{210}Pb, and (b) unsupported ^{210}Pb concentrations versus depth.

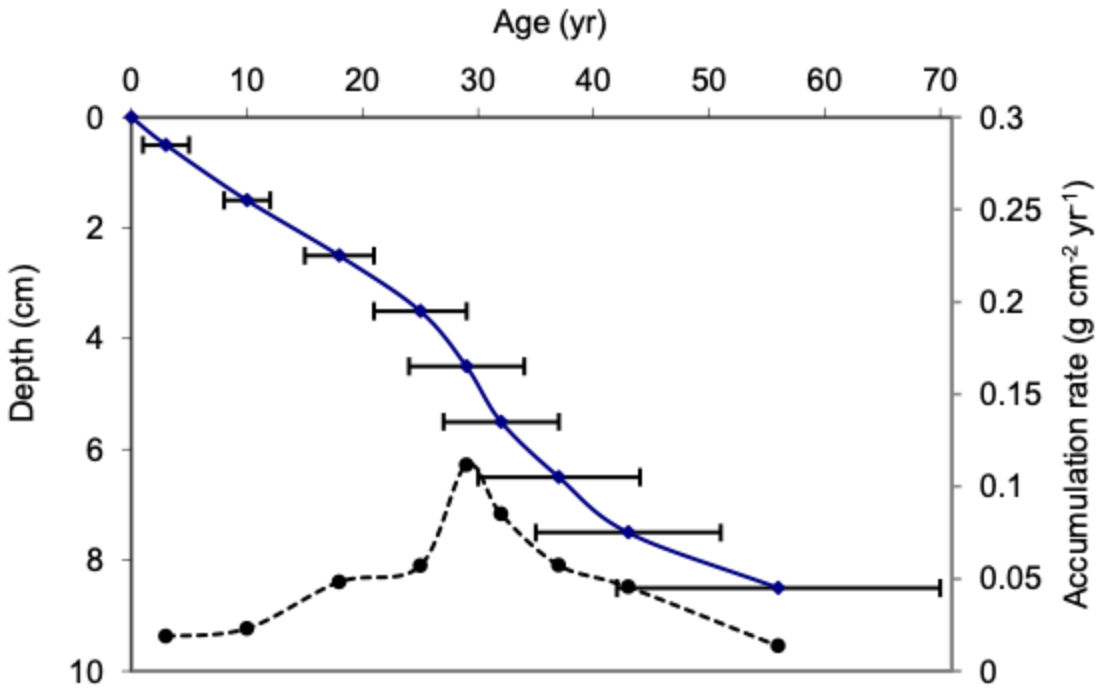

Figure 4. Radiometric chronology of core HWTS2 taken from Pacific Ocean, showing the CRS model 210Pb dates and sedimentation rates. The solid line shows age while the dashed line indicates sedimentation rate.

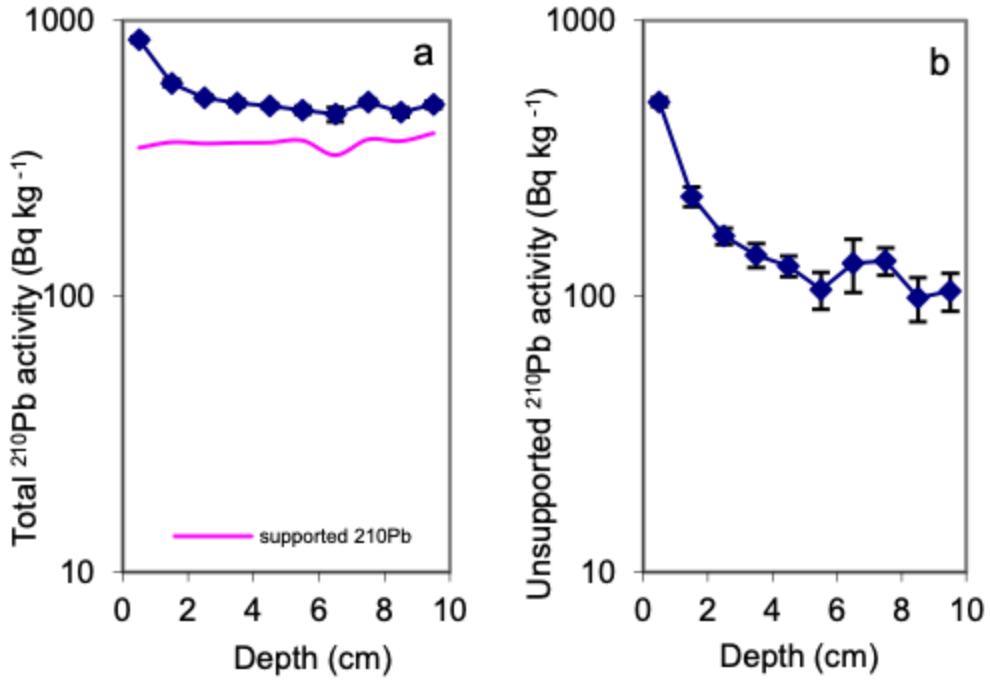

Figure 5. Fallout radionuclide concentrations in core HWTS3 taken from Pacific Ocean, showing (a) total ^{210}Pb, and (b) unsupported ^{210}Pb concentrations versus depth.

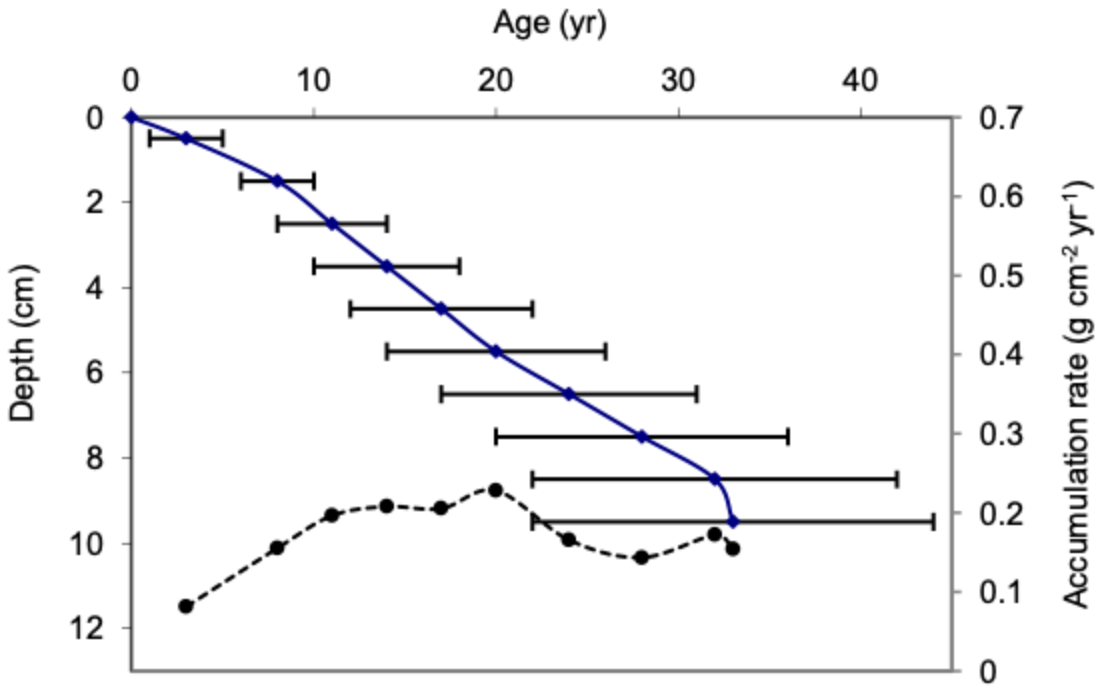

Figure 6. Radiometric chronology of core HWTS3 taken from Pacific Ocean, showing the CRS model ^{210}Pb dates and sedimentation rates. The solid line shows age while the dashed line indicates sedimentation rate.

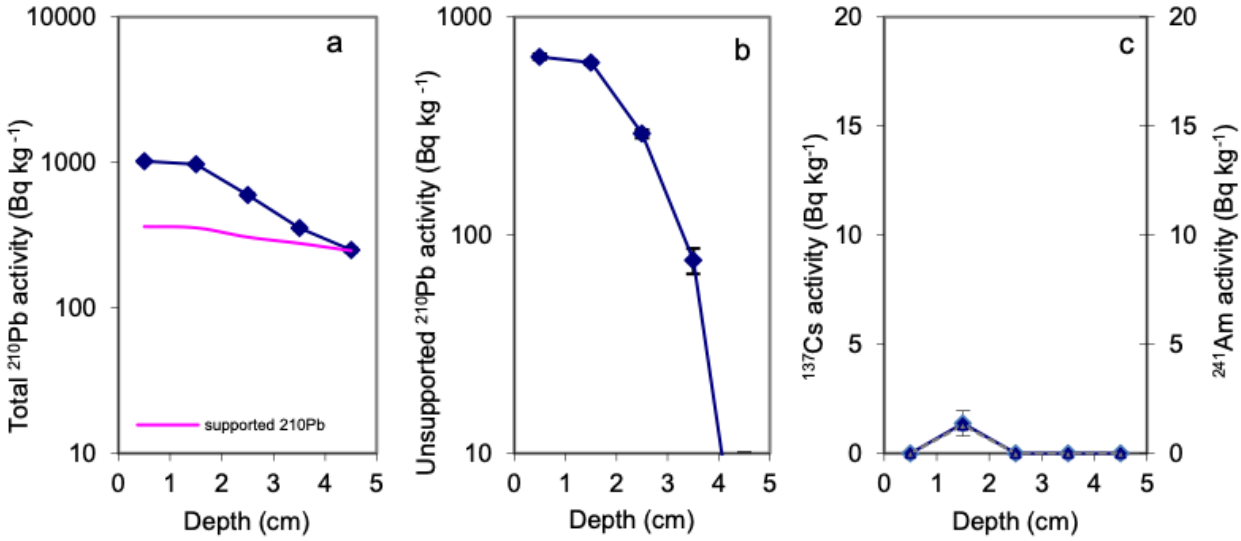

Figure 7. Fallout radionuclide concentrations in marine sediment core HWTS4 taken from Pacific Ocean, showing (a) total ^{210}Pb, (b) unsupported ^{210}Pb, and (c) ^{137}Cs and ^{241}Am concentrations versus depth.

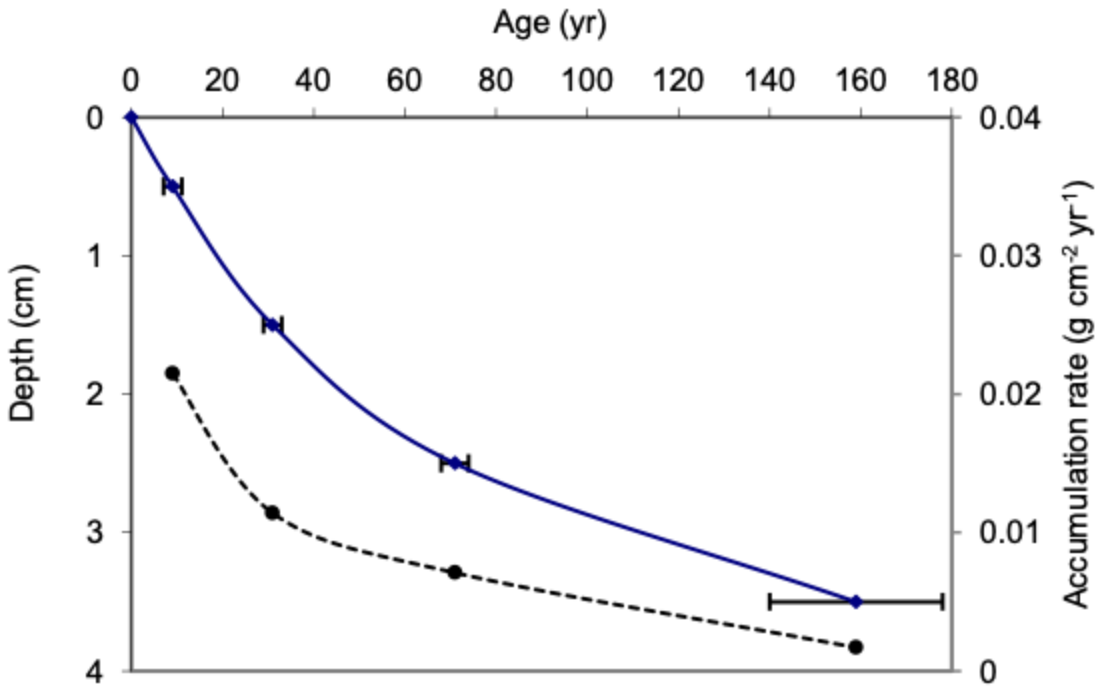

Figure 8. Radiometric chronology of marine sediment core HWTS4 taken from Pacific Ocean, showing the CRS model ^{210}Pb dates and sedimentation rates. The solid line shows age while the dashed line indicates sedimentation rate.

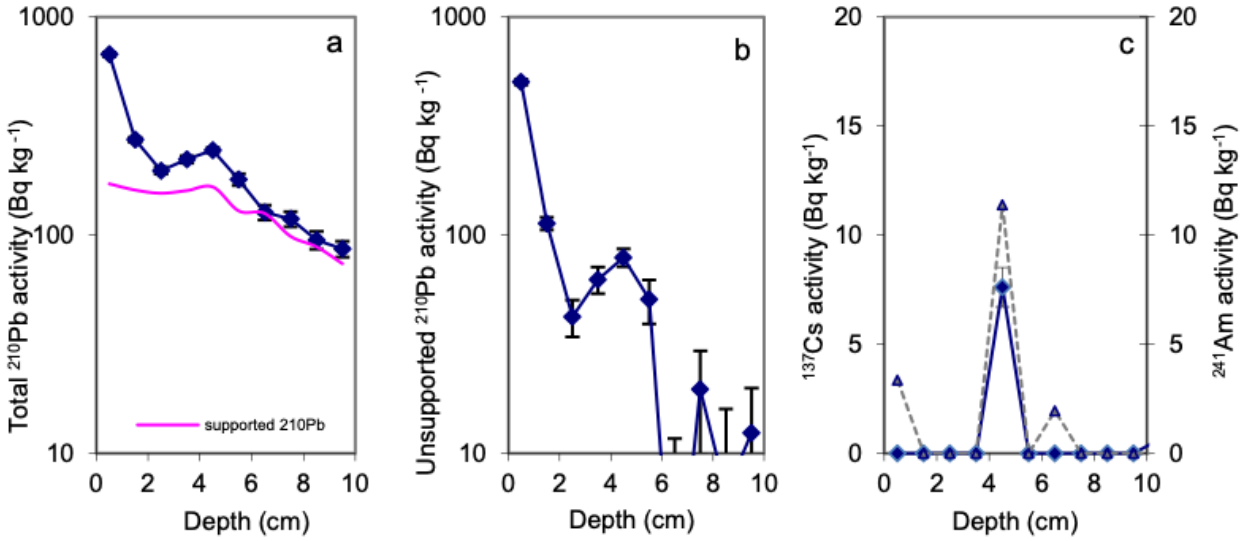

Figure 9. Fallout radionuclide concentrations in marine sediment core HWTS5 taken from Pacific Ocean, showing (a) total ^{210}Pb, (b) unsupported ^{210}Pb, and (c) ^{137}Cs and ^{241}Am concentrations versus depth.

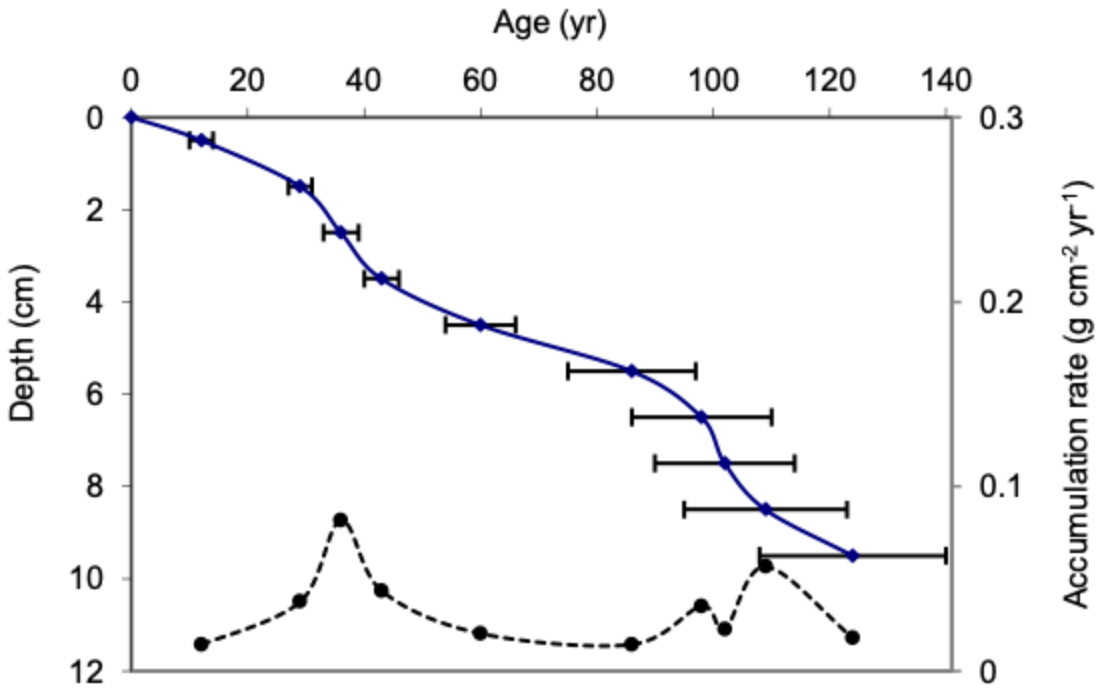

Figure 10. Radiometric chronology of marine sediment core HWTS5 taken from Pacific Ocean, showing the CRS model ^{210}Pb dates and sedimentation rates. The solid line shows age while the dashed line indicates sedimentation rate.

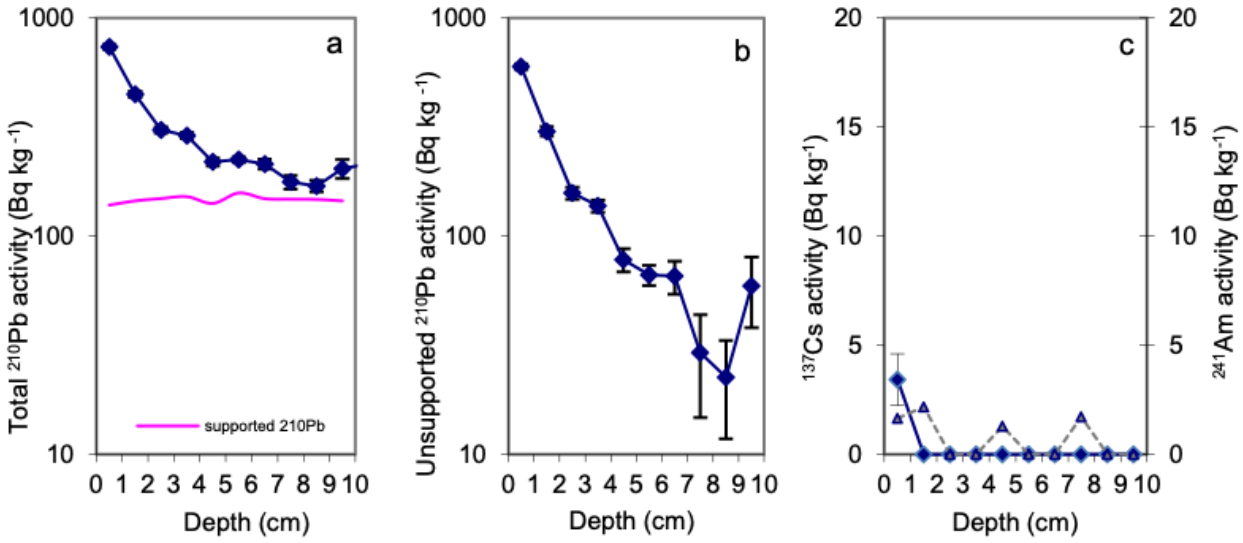

Figure 11. Fallout radionuclide concentrations in marine sediment core HWTS6 taken from Pacific Ocean, showing (a) total ^{210}Pb, (b) unsupported ^{210}Pb, and (c) ^{137}Cs and ^{241}Am concentrations versus depth.

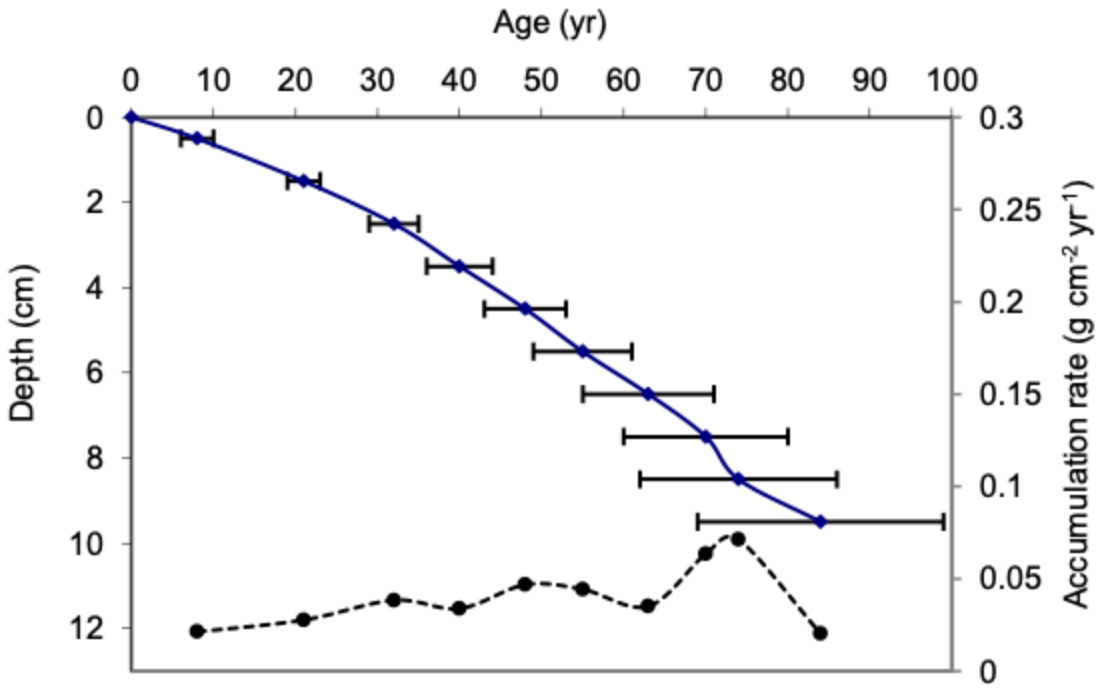

Figure 12. Radiometric chronology of marine sediment core HWTS6 taken from Pacific Ocean, showing the CRS model ^{210}Pb dates and sedimentation rates. The solid line shows age while the dashed line indicates sedimentation rate.